

Copyright
by
Jason Yunhe Lu
2014

**The Report Committee for Jason Yunhe Lu
Certifies that this is the approved version of the following report:**

**Uranus Orbiter and Probe Mission:
Project Upsilon**

**APPROVED BY
SUPERVISING COMMITTEE:**

Supervisor:

Wallace T. Fowler

Srinivas V. Bettadpur

**Uranus Orbiter and Probe Mission:
Project Upsilon**

by

Jason Yunhe Lu, B.S.

Report

Presented to the Faculty of the Graduate School of
The University of Texas at Austin
in Partial Fulfillment
of the Requirements
for the Degree of

Master of Science in Engineering

The University of Texas at Austin

May, 2014

Dedication

To my Mother and Father, who have always believed in me.

Acknowledgements

I would like to thank my supervisor, Dr. Wallace T. Fowler, for his guidance on this report. Dr. Fowler has shown unending enthusiasm for the planning, analysis, and design of space missions throughout his career. I am confident I could ask him about any space mission, and he could spend hours of his time discussing the mission with me. I thank Dr. Fowler for teaching his Mission Analysis and Design course, where the idea of this report was conceived.

Thank you to Dr. Srinivas V. Bettadpur for serving as Co-supervisor / Reader for my Report. I thank Dr. Bettadpur for teaching his Space Systems Engineering Design course, which expanded my knowledge on systems engineering processes and methods as well as mission notion and scope definition. I could not have completed this report without knowledge from Dr. Bettadpur's class.

Thank you to Dr. David L. Akin for serving as senior capstone design project supervisor at the University of Maryland. I first developed interest in the planning, analysis, and design of space missions in Dr. Akin's class. Many fundamental concepts and models for vehicle-level design and spacecraft systems used in this report, come from Dr. Akin's course materials.

Finally, thank you to my Orbital Mechanics classmates at UT-Austin, especially those graduating with M.S.E. at the end of this semester. I wish them all the best of success in their future work.

Jason Yunhe Lu

The University of Texas at Austin

May 2014

Abstract

Uranus Orbiter and Probe Mission: Project Upsilon

Jason Yunhe Lu, M.S.E.

The University of Texas at Austin, 2014

Supervisor: Wallace T. Fowler

Project Upsilon is a proposed NASA Flagship Class, Uranus Orbiter and Probe mission concept to investigate Uranus' planetary magnetic field and atmosphere. Three spacecraft - the Upsilon-0 Propulsion Module, the Upsilon-1 Science Orbiter, and the Upsilon-2 Atmosphere Probe - shall be implemented to meet needs, goals, and objectives as stated by the NASA Solar System Planetary Science Decadal Survey 2013-2022. Upsilon-0 shall be expended in order to complete orbital capture about Uranus. Upsilon-1 shall study Uranus' planetary magnetic field, obtaining real-time measurements for nominally 20 months within the first two years of arrival; and for as long as possible after the first two years, as part of an extended science mission. Upsilon-2 shall be descended into Uranus' cloud tops to obtain physical data and imagery well into the atmosphere's depths.

Chemical propulsion is employed in place of solar-electric propulsion, with regard to the interplanetary system-level trade tree. The interplanetary trajectory requires a single un-powered flyby of Jupiter, selected among several flyby node configurations.

The science orbit produces nearly repeating latitude-longitude tracks over a rotating Uranus. The statistical estimation method combines an orbit determination model with respect to Uranus' flattening, and a simple magnetic dipole model for field line modeling.

A 7-year period is allotted for the technology research and development, and the testing and verification stages of the project life cycle; the interplanetary journey to Uranus requires 21 years; and the nominal in-situ operation lifetime is 2 years. The Project Upsilon spacecraft launch in 2021 to "revolutionize our understanding of ice giant properties and processes, yielding significant insight into their evolutionary history"; contributing to the Planetary Science Decadal Survey's, and NASA's, key planetary science and deep space exploration visions.

Table of Contents

List of Tables	x
List of Figures	xiii
Chapter 1 Mission Scope	1
1.1 Report Scope	2
1.2 Need Statement	4
1.3 Mission Goals and Objectives	5
1.4 Mission Description	7
1.5 Mission Stakeholders	8
1.6 Mission Constraints	9
1.7 Design Assumptions	12
1.8 Concept of Operations	13
1.9 Mission Timeline	19
Chapter 2 Background	22
2.1 The Planet Uranus	23
2.2 Earth's Magnetic Field	32
Chapter 3 Heritage	37
3.1 Voyager-2	38
3.2 Challenging Minisatellite Payload - CHAMP (ESA)	44
3.3 Galileo Atmosphere Probe	49
3.4 New Horizons Telecommunications	53
Chapter 4 Mission Planning Considerations	56
4.1 Definitions	57

4.2 Science Orbit.....	
4.2.1 Concept	61
4.2.2 Candidate Science Orbit - Description and Orbit Evolution	66
4.2.3 Candidate Science Orbit - Spacecraft Tracks and Coverage	71
4.3 Launch Window and Science Window.....	
4.3.1 Concept	81
4.3.2 Trajectory Configuration Tool - TRACT	82
4.3.3 Figures of Merit	83
4.3.4 TRACT Results - Node Configuration Selection	86
4.3.5 TRACT Results - Launch Window and Science Window Selection	93
4.4 Estimation Method.....	
4.4.1 Concept	98
4.4.2 Science Phase I - Locate Magnetic Pole	99
4.4.3 Science Phase II - Model Magnetic Intensity, Inclination, and Declination	110
4.4.4 Nominal Trajectory and <i>Apriori</i> Estimate	123
Chapter 5 Preliminary Spacecraft Design.....	125
5.1 Upsilon-0 Propulsion Module.....	129
5.2 Upsilon-1 Science Orbiter.....	147
5.3 Upsilon-2 Atmosphere Probe.....	164
5.4 Cost Estimation.....	168
Chapter 6 Conclusions	170
Bibliography	173
Vita.....	189

List of Tables

Table 2-1: Selected Bulk Parameters of Uranus.....	24
Table 4-1: Geometric Constraints on the Candidate Science Orbit	64
Table 4-2: Timing Constraints on the Candidate Science Orbit.....	65
Table 4-3: Candidate Science Orbit - Keplerian Orbital Elements	66
Table 4-4: Candidate Science Orbit - Initial Best-fit Evolution Rates (30-day Numerical Integration)	68
Table 4-5: Uranian Satellites Inside the Candidate Science Orbit	77
Table 4-6: Uranian Rings Inside the Candidate Science Orbit.....	78
Table 4-7: J2000 State of Earth and Uranus Relative to the Solar System Barycenter	86
Table 4-8: Keplerian Orbital Elements of the Arrival Trajectory and the Nominal Trajectory	123
Table 5-1: System-level Mass Allocations.....	130
Table 5-2: System-level Size and Volume Constraints.....	132
Table 5-3: Selected Design Parameters of Candidate Engines and Thrusters	134
Table 5-4: Required Mass Distribution to Complete Uranus Arrival Burn	134
Table 5-5: Upsilon-0 Propulsion Structure - Mass Allocation.....	136
Table 5-6: Upsilon-0 Fairing and Shroud - Size Estimation	137
Table 5-7: NASA Minimum Design and Test Factors and Safety.....	138

Table 5-8a: Toray M55J High Modulus Carbon Fiber - Mechanical Properties	140
Table 5-8b: Toray 250°F Epoxy/M55J Composite - Mechanical Properties	140
Table 5-9: Cone Bending Parameters.....	145
Table 5-10: Upsilon-0 Propulsion Module - Mass Allocation	146
Table 5-11a: Deep Space Network Operating Frequency Bands (Frequency) ...	148
Table 5-11b: Deep Space Network Operating Frequency Bands (Wavenumber)	149
Table 5-12a: Spectral Simulation of Planetary Atmospheres - Earth Constituents	149
Table 5-12b: Spectral Simulation of Planetary Atmospheres - Uranus Constituents	149
Table 5-13a: Link Budget - Upsilon-1 (New Horizons) HGA, On-orbit Downlink to DSN 70-m Antenna	151
Table 5-13b: Link Budget - DSN 70-m Antenna, Uplink to On-orbit Upsilon-1 (New Horizons) HGA	152
Table 5-14: Selected Design Parameters of the "18-module" 340-W Modular RTG	155
Table 5-15: Upsilon-1 Thermal Analysis - Equilibrium Temperature for Various On-orbit Thermal Configurations	158
Table 5-16: Al 7075-T6 - Mechanical Properties.....	160
Table 5-17: Upsilon-1 Science Orbiter - Planetary Science Package	162
Table 5-18: Upsilon-1 Science Orbiter - Mass Allocation.....	163
Table 5-19: Upsilon-2 Atmosphere Probe - Mass Distribution.....	165
Table 5-20: Upsilon-2 Atmosphere Probe - Entry Flight Path Angles	166

Table 5-21: Upsilon-2 Atmosphere Probe - Spacecraft Components and Atmosphere Science Package	167
Table 5-22: "Spacecraft / Vehicle Level Costing Model"	168
Table 5-23: Project Upsilon Spacecraft Total R&D and Production Cost.....	169

List of Figures

Figure 1-1: Project Upsilon - Component Map	14
Figure 1-2: DSN Antenna Segment	16
Figure 1-3: DSN Downlink Tracking & Telemetry Segment.....	16
Figure 1-4: Project Upsilon - Data Flow	17
Figure 1-5: Project Upsilon - Minimum Communication Architecture	18
Figure 2-1: "Seasons of Uranus"	23
Figure 2-2: Internal Structure of the Gas Giant, Jupiter	25
Figure 2-3: Internal Structure of the Ice Giant, Uranus	25
Figure 2-4: Uranus' Magnetic Dipole Tilt	27
Figure 2-5a: Uranus Internal Model - Temperature	29
Figure 2-5b: Uranus Internal Model - Pressure	29
Figure 2-5c: Uranus Internal Model - Density	30
Figure 2-6: "Uranus Zonal Wind Profile in 2003"	31
Figure 2-7: Magnetic Intensity, Inclination, and Declination.....	33
Figure 2-8a: NOAA/NGDC US/UK World Magnetic Model - Epoch 2010.0, Main Field Total Intensity (F)	35
Figure 2-8b: NOAA/NGDC US/UK World Magnetic Model - Epoch 2010.0, Main Field Inclination (I)	36
Figure 2-8c: NOAA/NGDC US/UK World Magnetic Model - Epoch 2010.0, Main Field Declination (D)	36

Figure 3-1: "Artist's Rendering of the Voyager Spacecraft"	38
Figure 3-2: "Orbit of the Juno Spacecraft Relative to Jupiter's Main Radiation Belts	40
Figure 3-3: "Voyager-2 Encounter with Uranus"	42
Figure 3-4: "Magnetic Field Intensity at the Earth's Surface, as Predicted by the GRIMM Model for Epoch 2005.0"	45
Figure 3-5: "Distribution of Data Considered in CM4. Local Time (left) and Seasonal (right) Distributions of Scalar Satellite Data"	46
Figure 3-6: "Sampling of Residual Distributions for CHAMP as a Function of Dipole Latitude (left) and Universal Time (right) Rendered as Modified Julian Date (mjd)"	48
Figure 3-7: Galileo Atmosphere Probe Mission - "Event Time Table".....	51
Figure 3-8: "Schematic Diagram of the Gas Inlet System to the Galileo Probe Neutral Mass Spectrometer (NMS)"	52
Figure 3-9: "Forward Antenna Stack on New Horizons"	54
Figure 3-10: "Noncoherent Doppler Tracking"	55
Figure 4-1: Graphical Representation of the Geodetic (Planetodetic) Latitude ..	60
Figure 4-2: Candidate Science Orbit - Uranus-fixed Inertial Position	67
Figure 4-3a: 30-day Orbit Evolution - Semi-major Axis	69
Figure 4-3b: 30-day Orbit Evolution - Eccentricity.....	69
Figure 4-3c: 30-day Orbit Evolution - Inclination.....	70
Figure 4-3d: 30-day Orbit Evolution - Right Ascension of Ascending Node	70
Figure 4-3e: 30-day Orbit Evolution - Argument of Periapse.....	71
Figure 4-4a: Candidate Science Orbit - Longitude.....	72

Figure 4-4b: Candidate Science Orbit - Latitude.....	72
Figure 4-5a: Candidate Science Orbit - Tracks Set 1	74
Figure 4-5b: Candidate Science Orbit - Tracks Set 2	74
Figure 4-5a: Candidate Science Orbit - Tracks Set 3	75
Figure 4-5b: Candidate Science Orbit - Tracks Set 5 (Set 4 Omitted)	75
Figure 4-6: Candidate Science Orbit - Nearly Repeating Tracks	76
Figure 4-7: Candidate Science Orbit - Orbital Radius of Equatorial Plane Crossings	79
Figure 4-8: Candidate Science Orbit - Full Track Coverage	80
Figure 4-9a: Interplanetary Node Configuration Selection - EJU TRACT PI Distribution	88
Figure 4-9b: Interplanetary Node Configuration Selection - ESU TRACT PI Distribution	89
Figure 4-9c: Interplanetary Node Configuration Selection - EJSU TRACT PI Distribution	89
Figure 4-9d: Interplanetary Node Configuration Selection - EEJU TRACT PI Distribution	90
Figure 4-9e: Interplanetary Node Configuration Selection - EESU TRACT PI Distribution	90
Figure 4-10a: Interplanetary Node Configuration Selection - EJU Total PI Distribution	92
Figure 4-10b: Interplanetary Node Configuration Selection - Arrival Orbital Elements	92
Figure 4-11: Launch Window and Science Window Selection - EJU Total PI and Observation Angle, 2020 Launch Window	93

Figure 4-12: Launch Window and Science Window Selection - EJU Total PI and Observation Angle, 2021 Launch Window	95
Figure 4-13: Earth Departure C3 Energy Exceeding Jupiter Hohmann Transfer C3 Energy, 2021 Launch Window	96
Figure 5-1: Project Upsilon Spacecraft Schematic - Launch Configuration	126
Figure 5-2: Project Upsilon Spacecraft Schematic - Upsilon-0 Propulsion Module	127
Figure 5-3: Project Upsilon Spacecraft Schematic - Upsilon-1 Science Orbiter	128
Figure 5-4: "Delta IV-H, C3 Launch Energy Capability (Eastern Range)"	129
Figure 5-5: "Payload Static Envelope, 5-m-dia by 19.1-m Composite Fairing"	131
Figure 5-6: "Delta IV Heavy Design Load Factors"	139
Figure 5-7: Upsilon-0 Fairing and Shroud - Stress and Margin of Safety.....	142
Figure 5-8: "Long Conical Shells with Edge Loads"	144
Figure 5-9: "General Purpose Heat Source - Radioisotope Thermoelectric Generator"	153
Figure 5-10: Single "General Purpose Heat Source" Module	154
Figure 5-11: "Effect of Surface Coating on Temperature"	156
Figure 5-12: Upsilon-1 Structure - Stress and Margin of Safety	161

Chapter 1: Mission Scope

Chapter 1 "Mission Scope" summarizes the notion of Project Upsilon, a proposed Uranus Orbiter and Probe mission. Need statements draw from the National Aeronautics and Space Administration (NASA) and National Academy Space Studies Board, "Vision and Voyages for Planetary Science in the Decade 2013-2022" Decadal Survey. Section 1.1 "Report Scope" summarizes the author's methods taken, and analysis performed to achieve the current state of the mission plan. The mission goals and objectives feature a first orbital capture at an Ice Giant planet, study of Uranus' planetary magnetic field, and an atmosphere probing experiment. The Project Upsilon spacecraft are introduced and described; mission stakeholders, constraints, assumptions, and concept of operations are identified. Finally, a mission timeline allotting for research and development, testing and verification, and launch and operation phases is tentatively outlined. Chapter 1 provides fundamental information from various space mission planning and systems engineering perspectives on the Uranus Orbiter and Probe mission; specific ideas and notions are elaborated upon in subsequent chapters of this report.

1.1 REPORT SCOPE

This report details the methods taken, and analysis performed to achieve the current design of a Uranus Orbiter and Probe mission, named Project Upsilon. The Uranus Orbiter and Probe mission notion is outlined by the "Vision and Voyages for Planetary Science in the Decade 2013-2022" Decadal Survey. Launch opportunities have again arisen for a tour of the outer Solar System, and the most recently defined class of planets - Ice Giant Planets - have yet received a dedicated, in-situ planetary science mission. The Decadal Survey has called for mission proposals investigating Uranus' planetary magnetic field, magnetosphere, atmosphere, satellites, and ring system.

Chapter 1 "Mission Scope" provides the Decadal Survey needs which Project Upsilon aims to fulfill, defines minimum mission goals and measurement objectives, and identifies stakeholders and constraints. Mission planning assumptions focus on launch vehicle selection and numerical model development; while spacecraft design assumptions center on the power and communication subsystems. Current state of the mission plan, on-orbit operations, and spacecraft are described; the Concept of Operations illustrates Project Upsilon from various perspectives. Current state of the mission timeline is tentatively outlined.

Chapter 2 "Background", and Chapter 3 "Heritage" summarizes the existing knowledge in planetary science, magnetism, atmospheric dynamics; as well as interplanetary trajectory planning and spacecraft design; applied in developing the Project Upsilon mission plan.

Chapter 4 "Mission Planning Considerations" details three distinct analyses unique to a Uranus mission. The Candidate Science Orbit is constrained with respect to Voyager-2 results on the size of Uranus' planetary magnetic field; orbital elements are selected for repeating latitude-longitude tracks conducive to statistical estimation (albeit

limiting coverage); and orbital motion is simulated to confirm accommodation of Uranus' satellites and rings.

The Launch Window, and Science Window are defined through leveraging the Trajectory Configuration Tool (TRACT). Figures of Merit are selected to distinguish feasibility of various interplanetary paths to Uranus. The Observation Angle is defined to discern optimal periods of time - Science Windows - during which real-time scientific observations may be collected and relayed back to Earth. Launch Window selection caps payload capability, leading into preliminary spacecraft resource allocation.

The statistical estimation method outlined in this report demonstrates the models and calculations used to process (specifically) magnetic field line observations. Two Science Phases are defined, as results of Science Phase I - presumably achieved during the first Science Window - are used as initial estimates for the Science Phase II. The state vector is defined for spacecraft orbit determination and magnetic field strength (hence referred to as "Intensity", along with a "Scaling Factor" for comparison to Earth's field strength) in the Science Phase I; with addition of magnetic field line angles (hence referred to as "Inclination" and "Declination") to the state in Science Phase II. Observation vectors, combining magnetometer observations and spacecraft attitude observations, are defined for each Science Phase. Matrices for numerical integration are derived via partial derivatives.

Chapter 5 "Preliminary Spacecraft Design" describes nominal resource allocations - mass, propellant, and power - to each of the Project Upsilon spacecraft. A subsystem-to-subsystem, flowing systems engineering method is employed. For instance, orbital mechanics provides propulsion subsystem requirements and propellant selection; propellant-to-inert mass distribution may be used to size the spacecraft; size and volume is then matched for compatibility to heritage components such as the RTG and

communication antennae; the communication link budget provides power subsystem requirements, the power system then incurs thermal stresses on the spacecraft. The above is one simplified perspective among many used to achieve nominal resource allocation. In all, the analysis shown in Chapters 4 and 5 are unique contributions by the author, to planning and design of a Uranus Orbiter and Probe mission. The entire report may serve as a case study in future mission planning and spacecraft design work.

1.2 NEED STATEMENT

The Uranus Orbiter and Probe mission, as outlined by the Planetary Science Decadal Survey, is a priority Flagship Class mission concept to further our understanding of Ice Giant planets, the outer Solar System, and the "workings of solar systems" [Space Studies Board, 2012, pp. 25 of 410] as a whole. The Uranus Orbiter and Probe mission has been recommended for initiation during the decade 2013-2022 alongside two other Flagship concepts - Mars Astrobiology Explorer-Cacher (MAX-C), and Jupiter Europa Orbiter (JEO). Notional design activities on the Uranus Orbiter and Probe mission "should be initiated in the decade 2013-2022 even if both MAX-C and JEO take place" (direct quote) [SSB, pp. 18 of 410]. Certainly, exploration and planetary science conducted at the Ice Giants - Uranus and Neptune - weigh significantly in NASA's overarching mission. This report proposes the design of a Uranus Orbiter and Probe mission, in an effort to contribute to the planetary science research needs, goals, and objectives stated by the Decadal Survey.

How the Giant Planets "serve as laboratories to understand Earth, the solar system, and extrasolar planetary systems" is a leading question in the field of planetary science. The Decadal Survey states that most extrasolar planets discovered may have similar properties as the Gas Giants (Jupiter and Saturn) and Ice Giants (Uranus and

Neptune) in our solar system. Another fundamental question in Giant Planet research is - "how have the myriad chemical and physical processes that shaped the solar system operated, interacted, and evolved over time?" [SSB, pp. 196 of 410]. Uranus' planetary magnetic field has been the subject of much theorization and speculation, but of relatively little study since the Voyager-2 flyby. New observations of unique weather formations in Uranus' atmosphere were obtained with ground-based telescopes [SSB, pp. 25 of 410], which should prompt development of dedicated in-situ study concepts. Uranus' planetary magnetic field and atmosphere are unique environments that hold intriguing opportunities for planetary science research. A Uranus mission "combining an orbiter and a probe will revolutionize our understanding of ice giant properties and processes, yielding significant insight into their evolutionary history" (direct quote) [SSB, pp. 204 of 410].

1.3 MISSION GOALS AND OBJECTIVES

The Uranus Orbiter and Probe mission described in this report - hence referred to as "Project Upsilon" - shall further the accomplishments of the Voyager-2 mission in exploring the outer solar system; achieve the first orbital capture at an Ice Giant planet; refine Uranus gravity models; measure Uranus' planetary magnetic field strength and direction; characterize deviations from the ideal dipole model; and observe the effects of seasonal forcing on Uranus' atmosphere. The scope of this report is limited to study of Uranus' planetary magnetic field, even though the Uranus Orbiter and Probe mission notion may encompass the study of features of Uranus' magnetosphere - the region (which encompasses the planetary magnetic field) where planetary magnetic field particles intermingle with the solar wind, as well as galactic and cosmic charged particles. The key distinction between "magnetic field" and "magnetosphere" in the notional stages (of this individual research and design process) is made at the outset of

this report; in order to avoid over-scoping, inadequate depth and allocation of design effort, insufficient discussion of necessary background and heritage, among many aspects of space mission planning and systems engineering.

Project Upsilon's success hinges on the performance of its science orbiter. The orbiter - hence referred to as "Upsilon-1", stylized "Upsilon-one" or "U-1" - shall enhance our current knowledge of Uranus' planetary magnetic field, atmosphere, and of Ice Giant planets in general. Upsilon-1 shall sustain communications with the ground segment, and provide real-time observations of Uranus' planetary magnetic field and atmosphere for at least 20 months during the first two years following orbital capture; approximate the location of at least one of Uranus' Magnetic Poles; and create a model of Uranus' planetary magnetic field. Characteristic quantities describing the field strength and direction - the magnetic Intensity, Inclination, and Declination - shall be estimated over a large range of latitudes (spanning at least -60 to +60 degrees, for instance) and orbital altitudes (as nominally specified by the Science Orbit periapse and apoapse). Upsilon-1's extended mission shall commence after the nominal 2-year lifetime; as constrained by the spacecraft's remaining propellant supply, power supply, communication function, and instrument function.

Project Upsilon features a first orbital capture at an Ice Giant planet. An expendable propulsion spacecraft - hence referred to as "Upsilon-0", stylized "Upsilon-oh" or "U-0" - shall carry, and assist Upsilon-1 into its Science Orbit about Uranus. Upsilon-0 shall provide orbital transfer capability exceeding nominal estimates governed by the interplanetary trajectory and Science Orbit; provide mid-course maneuver, and attitude adjustment capability; and shield the other spacecraft from radiation, micrometeoroids, and space debris during the interplanetary journey.

Project Upsilon's aims to retrieve new knowledge about Uranus' atmosphere. An atmosphere probe - hence referred to as "Upsilon-2", stylized "Upsilon-two" or "U-2" - shall obtain physical and chemical data below Uranus' cloud tops, as part of the main Uranus science mission. An atmosphere probing opportunity shall be determined within the nominal 2-year lifetime of Upsilon-1. Upsilon-2 shall detach from Upsilon-1 and descend into Uranus' atmosphere; and acquire as much data as possible below Uranus' cloud tops.

1.4 MISSION DESCRIPTION

Project Upsilon is a proposed mission concept dedicated to understanding Uranus' planetary magnetic field, to serve as a NASA Flagship Class, Uranus Orbiter and Probe mission. Project Upsilon aims to provide a model of Uranus' planetary magnetic field at a wide range of latitudes and orbital altitudes, serving as the next state-of-the-art dataset, furthering our knowledge of Ice Giant planets in our solar system and contributing to models for extrasolar Ice Giant planets. Uranus is unique for its axial tilt in our Solar System, providing intriguing opportunities in planetary science and deep space exploration. Uranus is the next stepping stone in NASA's solar system exploration vision after dedicated missions to Jupiter (Juno) and Saturn (Cassini-Huygens). Further information on the Uranus mission environment is detailed in Chapter 2 "Background".

Project Upsilon shall initiate in the decade 2013-2022 with a possible launch window at the end of the decade, a 12-day period between May 2-13, 2021. Three unique spacecraft - the Upsilon-0 Propulsion Module, the Upsilon-1 Science Orbiter, and the Upsilon-2 Atmosphere Probe - shall be implemented. The spacecraft launch on a single NASA-contracted Evolved Expendable Launch Vehicle (EELV) into interplanetary transfer orbit, and flyby Jupiter for gravity assist. The Upsilon-0

Propulsion Module is expended to complete orbital capture about Uranus. The Upsilon-1 Science Orbiter measures Uranus' planetary magnetic field and observes Uranus' atmosphere, for a 2-year nominal period. During this time, ground-based telescopes aid the mission by identifying one of more atmosphere survey opportunities; and the Upsilon-2 Atmosphere Probe will be descended into Uranus' cloud tops, gathering data on unique weather formations, atmospheric constituents, and vital characteristics such as pressure, temperature, and water vapor content. Magnetic field measurement and atmosphere probing during the first two years comprise the main science mission. The choice of a single Jupiter gravity assist is detailed in Chapter 4 "Mission Planning Considerations".

The Science Orbit of Upsilon-1 shall initially implement nearly repeating spacecraft tracks - latitude and longitude location over a rotating Uranus - further defined in Chapter 4 "Mission Planning Considerations". Upsilon-1 shall slowly scan over longitude to approximate the location of one of Uranus' Magnetic Poles. As the spacecraft's orbit evolves over time, groundtrack coverage is extended and Uranus' planetary magnetic field is modeled with respect to three characteristic quantities - the magnetic Intensity, Inclination, and Declination - with respect to spacecraft track location and orbital radius. For the extended science mission, Upsilon-1 shall provide as much data as constrained by the spacecraft's remaining propellant supply, power supply, communication function, and instrument function, before being decommissioned and de-orbited into Uranus.

1.5 MISSION STAKEHOLDERS

National institutions of science and research in the United States - NASA, the National Science Foundation, and the National Academies - have provided the needs to

be accomplished by the mission. The Planetary Science Division (PSD) of NASA's Science Mission Directorate directs Flagship Class missions, conducts technology development activities, and provides support to research infrastructure [SSB, pp. 26 of 410]. The NASA Launch Services Program supplies the launch vehicle and facilities. Domestic as well as international contractors may be responsible for spacecraft bus and instrument package design and integration. The Deep Space Network (DSN) will play a significant role in the Command, Control, and Communications (C3) architecture, and manage incoming science data. Amateur astronomers and civilian observers' works add to in-situ observations made by the spacecraft, and contribute to mission planning and command activities managed by NASA [SSB, pp. 226 of 410]. Finally, planetary science and research institutions such as the NASA Goddard National Space Science Data Center (NSSDC) and National Oceanic and Atmospheric Administration (NOAA); along with universities and schools, shall consume the science data and derive findings which further our knowledge of Uranus, the Ice Giant planets, and our solar system.

1.6 MISSION CONSTRAINTS

The Planetary Science Decadal Survey lists several "key challenges" (direct quotes) [SSB, pp. 22 of 410] to the Uranus Orbiter and Probe mission. "Demanding entry probe mission" refers to not only the complexity of Uranus orbital capture, but also difficulty in identifying atmospheric probe opportunities and execution thereof. The orbiter's lifetime must encompass the journey to Uranus (at least "15.4 years") and subsequent science activities, which brings about selection considerations in the spacecraft's propulsion and power capabilities, shielding accommodations, among others. The Giant Planets' fields greatly stress the spacecraft's magnetic properties. Additionally, establishing communication and maintaining data transfer will be difficult, as a great deal

of signal power and amplification is required to offset space loss over nominally 20 Astronomical Units (AU). Starting efforts in meeting these challenges are described in Chapter 5 "Preliminary Spacecraft Design". The communication pathway between the ground segment and the spacecraft is blocked by the Sun at times during the year, thus the date of arrival at Uranus must be carefully considered and planned. Lastly, the spacecraft's size and mass are limited, due to the energy requirements for an interplanetary trajectory to Uranus. The combination of meeting launch energy and arrival timing requirements is described in Chapter 4.

Launch vehicle selection is limited to the NASA-contracted EELV series. The Delta IV-Heavy was chosen for its launch heritage and interplanetary payload capability. Although the SpaceX Falcon Heavy launch vehicle has greater payload capability, it was not considered due to the limited number of completed tests and missions.

Implementation of nuclear power sources on spacecraft, as a "sun-independent" deep space power source, is a subject of much controversy [Maharik & Fischhoff, 1993; Dawson, 2006]. Nuclear power sources, such as fission reactors and Radioisotope Thermoelectric Generators (RTG) consume radioactive, "highly toxic" Plutonium and Uranium. Significant additional costs are incurred via human factors considerations during development and production, and via disposal and cleanup in event of launch failure. Nuclear power sources are also nearly depleted at this time, with few inexpensive and efficient methods of production. For instance, 1000 kg of Thorium-232 is consumed to obtain 15 kg of Plutonium-238 via nuclear fission;¹ and current estimates place domestic production rates between 1.5 and 5 kg per year.²

¹Thorium Energy Alliance (undated). Pu-238 [*News Bulletin*]
Retrieved From: <http://www.thoriumenergyalliance.com/downloads/plutonium-238.pdf>

²Howe, S. D., Crawford, C., Navarro, J., & Ring, T. (undated).
Economical Production of Pu-238: Feasibility Study. [*Technical Presentation*]
Retrieved From: http://www.nasa.gov/pdf/636900main_Howe_Presentation.pdf

Most importantly, cost and schedule of Project Upsilon's life cycle must satisfy standards set in the Decadal Survey. The notional Uranus Orbiter and Probe mission (without solar-electric propulsion stage) is estimated to incur 2.7 billion USD FY-2015 [SSB, pp. 18 of 410]. If possible, Project Upsilon shall incur less than the nominal estimate of 2.7 billion USD FY-2015.

The project life cycle consists of, in simplest terms, the "technology research and development" (R&D) period and the "mission operations" period. In the scope of this report, the R&D period includes all project life cycle phases up to launch - from Pre-Phase A (Concept Studies) to Phase D (System Assembly, Integration and Test, and Launch). Length of the R&D period varies depending on the amount of heritage applied and Technology Readiness Levels (TRL) of hardware in development. The mission operations period includes all project life cycle phases after launch - Phases E (Operations and Sustainment) and F (Closeout) - whose length varies with mission objectives and the mission setting or destination. Project Upsilon's R&D period is tightly constrained; its mission operations period may at most be optimized.

For instance, the Mars Global Surveyor (MGS) mission utilized entirely inherited engineering and technology - resulting in a 3-year R&D period. The Galileo mission featured a "highly complex payload with new engineering" - resulting in a longer, 8-year R&D cycle (8 years of design effort, but more than 12 years total, including delays brought on by the Challenger Disaster). It would be appropriate to constrain Project Upsilon's R&D phases, from concept study to launch, between that of the MGS and the Galileo mission. Implementation of space-qualified hardware with heritage will help to shorten the R&D phases. Time span of the post-launch life cycle shall be optimized with respect to the other constraints listed here.

1.7 DESIGN ASSUMPTIONS

Mission planning shall operate on several assumptions. First, one launch vehicle shall suffice in placing the spacecraft into interplanetary trajectory to Uranus. The launch facility accommodates the launch vehicle as well as the launch azimuth direction. The ground segment shall maintain communications with the spacecraft, as long as the communications pathway is not blocked by the Sun. "Solar conjunction", then, is assumed to span one month preceding and following the date where Earth, Sun, and Uranus lie on a line (viewed from a direction normal to the Ecliptic plane) in that order - the spacecraft is assumed unable to communicate with the Earth approximately two months every year.

During on-orbit operations, *apriori* estimates of Uranus' gravity field and planetary magnetic field shall be sufficiently accurate within the "differential correction" assumptions of statistical estimation theory. Perturbations to the spacecraft's motion, including but not limited to - third-body gravitation by Uranus' satellites, mean motion resonances with satellites, tidal resonances with Uranus' rotation, planetary and solar radiation, atmospheric drag, momentum transfer from galactic particles, etc. - shall be known to some extent and added to the forcing model as needed. A nearly polar science orbit about Uranus for magnetic field measurement is assumed. Attitude knowledge is assumed to be achieved, where spacecraft measurements may be transformed from the body-fixed frame to an inertial frame, to an acceptable degree of accuracy and precision.

Spacecraft design shall operate on additional assumptions. Spacecraft bus materials, including but not limited to - hull, internal structure, exterior shielding, communication structures, power structures, etc. - shall consist of presently available space-qualified materials. Instrumentation packages shall consist of space-qualified devices and interfaces with heritage. The spacecraft shall implement one or more Pu-238

Radioisotope Thermoelectric Generators (RTG) to produce the power required for the journey to Uranus and subsequent mission operations. Limitations to obtaining Pu-238 have been described in the Mission Constraints, but we assume sufficient amounts of the radioactive material is available for consumption, at this point in the design. Link Budgets are calculated with respect to a certain Link Margin in the design, however, development of Link Budget requirements is beyond the scope of this report.

1.8 CONCEPT OF OPERATIONS

The Concept of Operations (CONOPS) may be described in multiple ways, and each may be interpreted as stand-alone organizational entities providing vital mission information [Bettadpur, 2013].

The "Component Map" CONOPS highlights all elements of the mission's infrastructure at a given time. Perhaps the mission's most critical event is the spacecraft's date of arrival at Uranus. Three spacecraft arrive at Uranus - the Upsilon-0 Propulsion Module, the Upsilon-1 Science Orbiter, and the Upsilon-2 Atmosphere Probe - comprising the space segment. The ground segment includes the DSN ground stations, spacecraft operators, data analysis and distribution teams, all Stakeholders (spacecraft operators, data consumers, etc.) and their respective facilities. The launch segment (though inactive on that day, is still important to note) includes the launch site and facilities, the launch vehicle, and near-Earth control facilities (such as the Mission Control Center in Houston, TX). Figure 1-1 shows the mission infrastructure and their locations on a Component Map. Note that Jupiter has been identified for gravity assist, again, this choice is detailed in Chapter 4. Only the launch vehicle and launch site have been specified as the Delta IV-Heavy, and the Kennedy Space Center at Cape Canaveral

Air Force Base, respectively. DSN has been named the mission's primary communications hub.

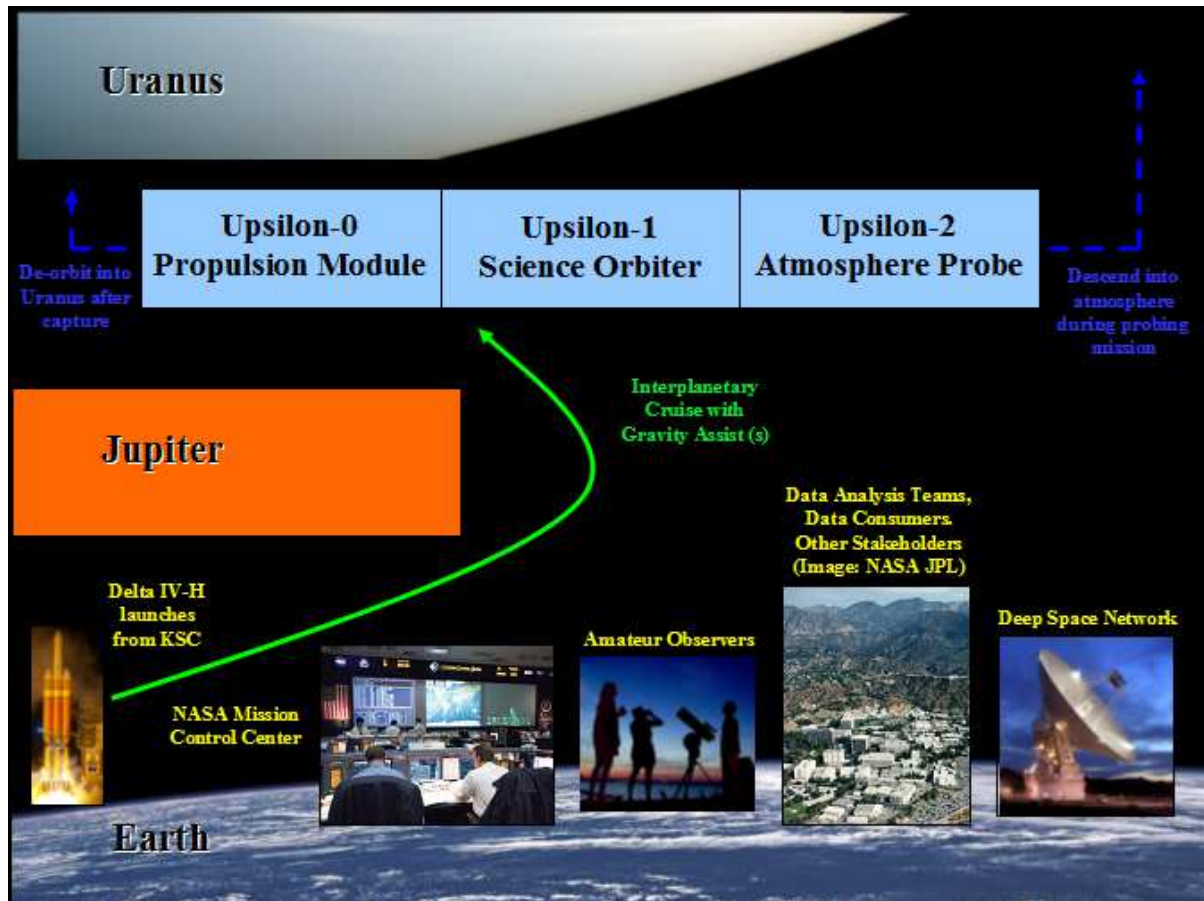


Figure 1-1: Project Upsilon - Component Map. ^{3,4}

³Figure 1-1 Image Sources (bottom, from left to right):

Patrick Air Force Base (2010). 45th Space Wing Successfully Launches Delta IV-Heavy [News Article]. Retrieved From: <http://www.patrick.af.mil/news/story.asp?id=123231921>

NASA Johnson Space Center (2006). Mission Control, Houston: Mission Control Center and Flight Operations [Online Data Sheet]. Retrieved From: http://www.nasa.gov/centers/johnson/pdf/160406main_mission_control_fact_sheet.pdf

Amateur astronomers watch the night sky during the Perseid meteor shower (2006) [Photo]. In Wikipedia, Retrieved March 6, 2014. Retrieved From: http://upload.wikimedia.org/wikipedia/commons/2/22/Astronomy_Amateur_3_V2.jpg

The "Data Flow" CONOPS describes the process in which raw measurements become scientific products, during a particular phase of the mission. Data Flow encounters the maximum number of nodes during the Upsilon-2 Atmosphere Probe mission. U-2 data shall be stored on U-1, as well as relayed towards Earth during the mission. The atmosphere probing mission shall occur during a period where the Earth is in optimal viewing angle to Uranus. Placement of Earth and Uranus during each science mission is discussed in Chapter 4.

First, Upsilon-2 continuously sends measurements of vital characteristics of the atmosphere, to Upsilon-1. Upsilon-1, meanwhile, is engaged in its magnetic field measurement mission, must manage the incoming data from Upsilon-2 until communications break; store the data for backup, and package data for transfer; and send it into deep space towards Earth. The data transfer time depends on the Upsilon-2 instrumentation, and system data transfer rate, discussed in Chapter 5. Notwithstanding,

NASA Jet Propulsion Laboratory (2011).
NASA Facts: Jet Propulsion Laboratory [*Online Data Sheet*].
Retrieved From: http://www.jpl.nasa.gov/news/fact_sheets/jpl.pdf

NASA Jet Propulsion Laboratory (2006).
Deep Space Network: 70-meter Antennas [*Online Data Sheet*].
Retrieved From: <http://deepspace.jpl.nasa.gov/dsn/antennas/70m.html>

⁴Figure 1-1 Image Sources (Earth and Uranus backgrounds):

Sally Ride, Smithsonian Air & Space Magazine (2012).
Single Room, Earth View. America's first woman in space describes the beauty of Earth from orbit [*News Article*].
Retrieved From: <http://www.airspacemag.com/space/single-room-earth-view-5940961/?no-ist=>

The Planetary Society (2010).
The Bruce Murray Space Image Library: Cloud Features Revealed in Voyager 2 Uranus Images [*Online Image Library*].
Retrieved From: <http://www.planetary.org/multimedia/space-images/uranus/uranus-voyager-cloud-features.html>
Additional Notes: Image taken by Voyager-2, January 24, 1986.
Image processing by Czech amateur observer Daniel Machacek, 2010.
Copyright: Daniel Machacek, contact <http://www.planetary.org/about/contact.html>
85 South Grand Avenue, Pasadena, CA 91105 USA
Phone (626) 793-5100, Fax (626) 793-5528, Email: tps@planetary.org

data requires approximately an additional 3 hours to travel from Uranus to Earth (at a nominal distance of 20 AU). The Deep Space Network 70-meter antenna in optimal pointing position (among the Goldstone, United States; Madrid, Spain; and Canberra, Australia complexes) receives the data. The DSN downlink mechanism is represented graphically in Figures 1-2 and 1-3. Data is assumed to arrive at the top of Figure 1-2 (the antenna), progress to the bottom of Figure 1-2 to be treated by Low-Noise Amplifiers (LNA, not pictured), flow through the Downlink Tracking and Telemetry System in Figure 1-3, finally distributed as decoded measurements to data analysis teams, and eventually consumers.

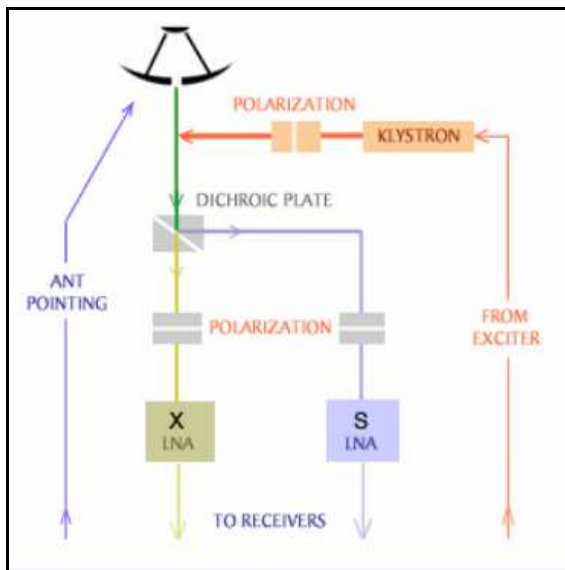


Figure 1-2: DSN Antenna Segment. ⁵

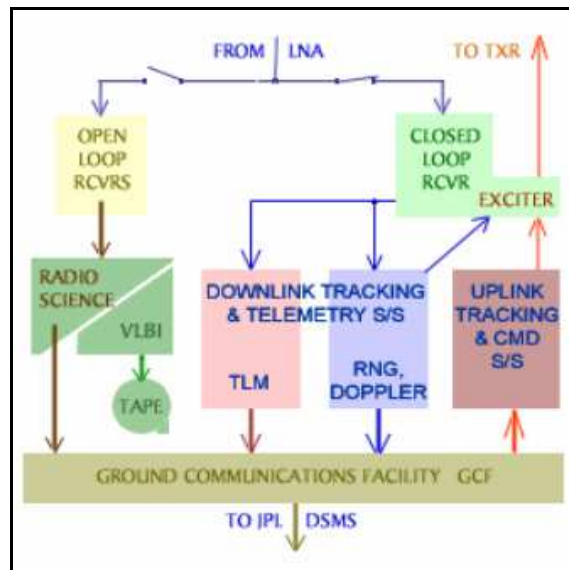


Figure 1-3: DSN Downlink Tracking & Telemetry Segment.

Courtesy of the NASA Jet Propulsion Laboratory.

⁵Figures 1-2 and 1-3 Image Source:

NASA Jet Propulsion Laboratory (undated).
 Basics of Space Flight Section III: Chapter 18. Deep Space Network [Education and Outreach]
 Retrieved From: <http://www2.jpl.nasa.gov/basics/bsf18-3.php>

Figures 1-2 and 1-3 are included to illustrate fundamental understanding of Data Flow within the Deep Space Network infrastructure. Data Flow through the system infrastructure during the Upsilon-2 Atmosphere Probe mission is shown in Figure 1-4.

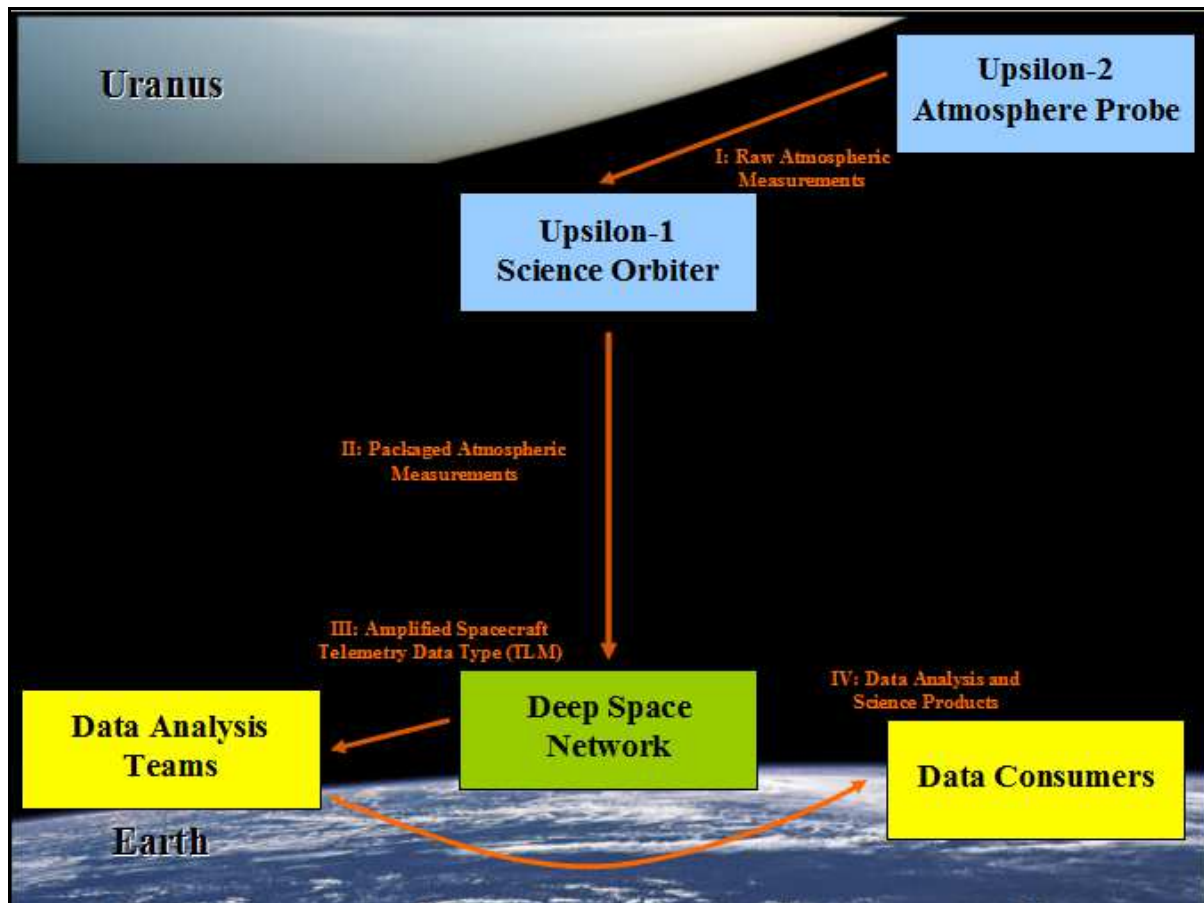


Figure 1-4: Project Upsilon - Data Flow (Upsilon-2 Atmosphere Probe Mission).

The "Communication Link" CONOPS details each connection between mission components (including those listed in the "Component Map" CONOPS), where commands and data may be transferred through space. During interplanetary cruise - U-0, U-1, and U-2 are taken as a single communication entity, with U-1 managing downlink and uplink to the DSN. U-0 is jettisoned upon arrival at Uranus,

communicating with U-1 (while U-2 is attached to U-1) through the insertion burn. During the atmosphere probing mission, U-2 relays data to U-1 for as long as possible, which in turn amplifies the signal for transfer to Earth. Upsilon-1 shall communicate with the DSN during all science phases. The minimum communication infrastructure requires six links. Figure 1-5 shows a "communication web" illustrating the minimum number of links.

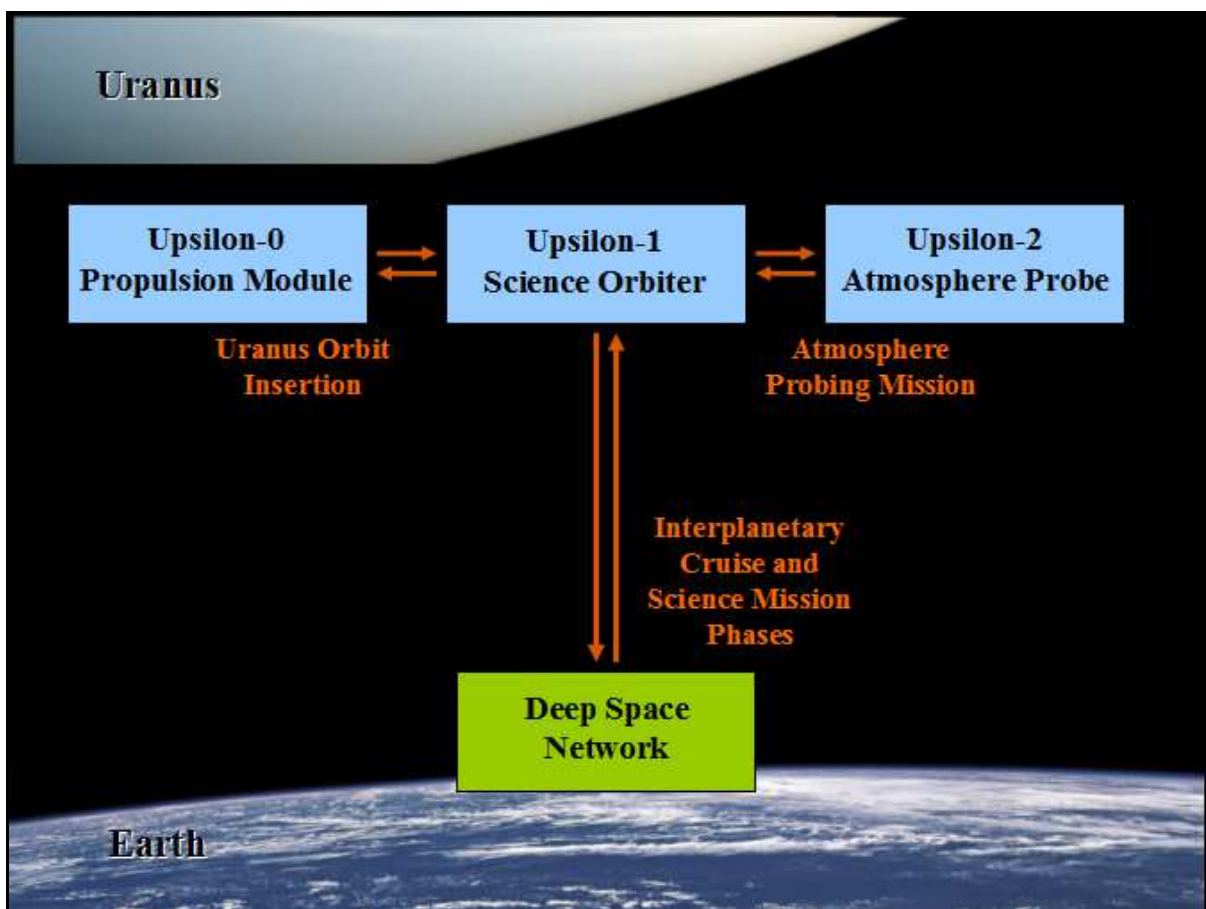


Figure 1-5: Project Upsilon - Minimum Communication Architecture.

1.9 MISSION TIMELINE

The Mission Timeline details the key decision points pertaining to, and critical events during the mission. Key decision points include proposal submission, design reviews, and may be made with respect to mission operations, spacecraft performance, and spacecraft end-of-life. Critical events include spacecraft and hardware Inspection, Analysis, Demonstration, and Test (IADT), launch, orbital transfers, etc. Project Upsilon's projected mission timeline proceeds as follows. Launch, flyby, and arrival times are identified in Chapter 4.

Key Decision Point: May 2014

Project Upsilon proposal submitted.

Key Decision Point: 2017

Project life cycle Pre-Phase A and Phase A, completed - Mission Concept Review (MCR), System Requirements Review (SRR), and System Definition Review (SDR).

Key Decision Point: 2018

Phase B, completed - Preliminary Design Review (PDR). Establish final design solution, complete all design analyses, drawings, and simulations.

Key Decision Point: 2019

Phase C, completed - Critical Design Review (CDR). Demonstrate that the system meets requirements, complete individual component testing and breadboard development. Begin prototype development and interfacing.

Key Decision Point: 2021

Phase D, completed - Flight Readiness Review (FRR). Demonstrate that the system is ready for launch.

Critical Event: 12:00:20 AM, May 5, 2021

Upsilon-0, Upsilon-1, Upsilon-2 launched from NASA's John F. Kennedy Space Center on a Delta IV-Heavy launch vehicle.

Critical Event: Early Morning, May 5, 2021

Launch vehicle expended to insert Upsilon-0, Upsilon-1, Upsilon-2 into interplanetary trajectory to Uranus.

Critical Event: Earth to Jupiter journey.

Conduct instrument tests, review trajectory and perform mid-course maneuvers.

Critical Event: 7:07:14 AM, February 19, 2023

Upsilon-0, Upsilon-1, Upsilon-2 arrive at closest approach of Jupiter during gravity assist, at 32.3 Jupiter Radii. Test cameras and ranging systems.

Critical Event: Jupiter to Uranus journey.

Conduct instrument tests, review trajectory, and perform mid-course maneuvers. Confirm hibernation and re-start capability of spacecraft subsystems.

Critical Event: 5:58:40 AM, December 13, 2041

Closest approach of Uranus, less than 1500 km above Uranus' cloud tops. Upsilon-0 is expended, and de-orbited, to complete orbital capture of Upsilon-1 and Upsilon-2.

Critical Event: July 19, 2042

Earth, Sun, and Uranus lie on a line in approximately one month (assumed 31 days), on August 19, 2042. The first Observation Window, spanning 218 days, has ended.

Critical Event: September 20, 2042

Earth has passed the position, relative to the Sun and Uranus, on August 19, 2042 by one month (assumed 31 days). The synodic period between the Earth and Uranus is approximately 370 days, which yields a second Observation Window spanning 308 days.

Key Decision Point: July 25, 2043

The second Observation Window has ended, the nominal spacecraft lifetime has been achieved. The project life cycle may proceed to Phase F (Closeout), or to the extended magnetic field measurement mission.

Critical Event: September 26, 2043

Upsilon-1 extended magnetic field measurement mission commences for nominally 308 days, or as constrained by the spacecraft's remaining propellant supply, power supply, communication function, and instrument function.

Chapter 2: Background

Chapter 2 "Background" reviews fundamental information pertinent to the mission design. Uranus' bulk parameters, characteristics of its planetary magnetic field, and atmospheric profiles as we currently know are used as starting constraints for the mission design. Distinctions are made between "Ice Giant" and "Gas Giant" among our solar system's Giant Planets. Our current knowledge of the Earth's planetary magnetic field, its properties, and models are discussed. Objective measurement quantities for Uranus' magnetic field - the magnetic Intensity, Inclination, and Declination - are identified.

2.1 THE PLANET URANUS

Uranus is unique in our Solar System for its axial tilt; and provides intriguing opportunities in planetary science and deep space exploration. On average, Uranus orbits 19.2 astronomical units (AU) from the Sun with a period of 84 years [National Space Science Data Center]. Due to its tilt and distance from the Sun, the planet remains in one "season" for 21 years at a time. Uranus will reach its Northern Summer Solstice - where its North Pole is pointed toward the Sun - in 2028, presenting an added opportunity to study the effects of the Sun's heating - solely on - the Northern atmosphere. This section highlights unique characteristics of Uranus pertaining to our mission plan, and is not to be interpreted as a comprehensive description of the planet.

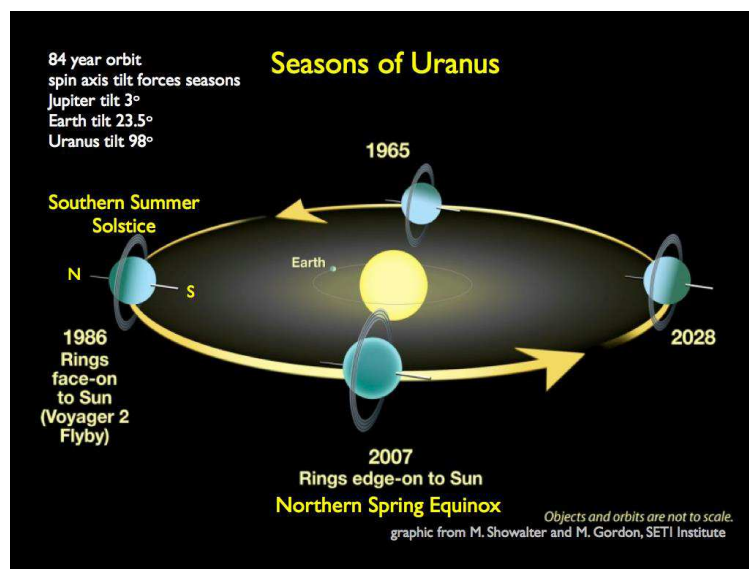


Figure 2-1: "Seasons of Uranus." ⁶

Courtesy of the University of Wisconsin, Space Science Engineering Center.

⁶Figure 2-1 Image Source:

University of Wisconsin, Space Science Engineering Center (2009).
Uranus Atmospheric Research at SSEC - Science [Education and Outreach].
Retrieved From: <http://www.ssec.wisc.edu/planetary/uranus/science>

Uranus, the smallest Giant Planet in our solar system, is just over four times larger than Earth in radius; and over 14 times as massive. Uranus, as a non-rocky planet, is much less dense (0.23 times) as compared to Earth. Combination of its rotation rate and density (due to composition) results in much greater physical bulge near the Equator, as well as bulging of the axisymmetric representation of the gravity field. Uranus' size and distance from the Sun enables a feasible planetary capture; however, its surface gravitational acceleration (measured at one planetary radius, shown in Table 2-1) is lower than Earth's, which places added demand on the spacecraft's propulsion capability. Uranus' oblate gravity field creates further challenges on maintaining the science orbit after capture. Table 2-1 shows Uranus' bulk parameters that are assumed in the Project Upsilon mission design; note the Equatorial Radius is taken as the planetary radius in all subsequent design analyses, and note that the Axial Tilt is the right-hand angle between Uranus' spin axis and its solar orbital plane.

Parameter	Value	Unit
Gravitational Constant	5.749e+06	km ³ /s ²
Gravitational Acceleration	8.80	m/s ²
Gravitational J ₂	3.34343e-03	--
Equatorial Radius	25559	km
Polar Radius	24973	km
Physical Flattening	1/43.616	--
Sidereal Rotation Period	17.24	hour
Axial Tilt	97.77	degree

Table 2-1: Selected Bulk Parameters of Uranus. ⁷

⁷Table 2-1 Reference:

NASA Goddard Space Flight Center, National Space Science Data Center (2010).
 Uranus Data Sheet [*Online Data Sheet*].
 Retrieved From: <http://nssdc.gsfc.nasa.gov/planetary/factsheet/uranusfact.html>

Uranus is an Ice Giant Planet in our solar system along with Neptune. Ice Giants are mainly composed of "ices" such as water vapor, ammonia, and methane; whereas the Gas Giants in our solar system - Jupiter and Saturn - are mainly composed of hydrogen and helium. Ice Giants' core temperatures are thought to be much cooler than that of Gas Giants [Podolak and Cameron, 1974, pp. 22 of 26]. The number of exoplanet candidates steadily increases, with advances in extrasolar observation such as the Kepler Program. The pool of exoplanet candidates consist mostly Giant planets as opposed to Terrestrial ones, and Ice Giants are thought to be more abundant than Gas Giants in that group [SSB, pp. 198 of 410].

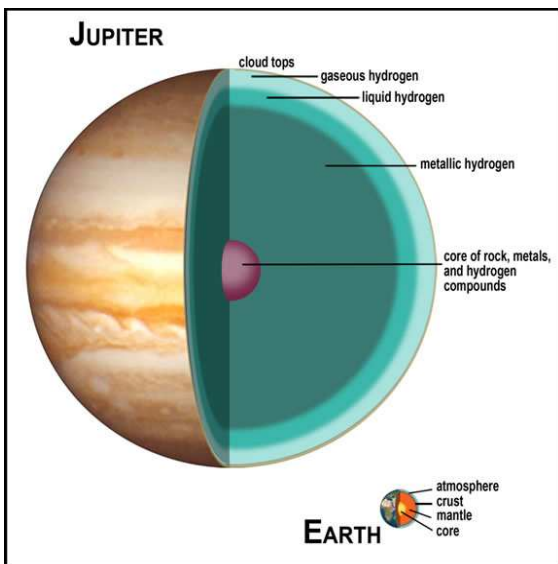


Figure 2-2: Internal Structure of the Gas Giant, Jupiter. ⁸

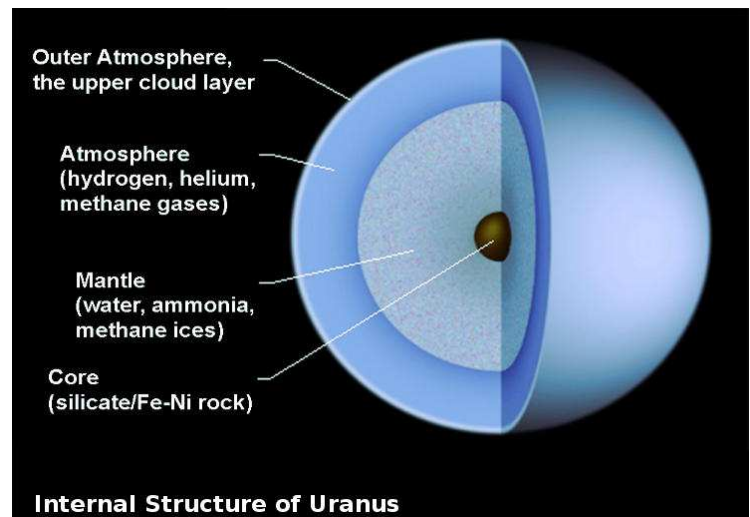


Figure 2-3: Internal Structure of the Ice Giant, Uranus.

Courtesy of the Lunar and Planetary Institute, and Cosmos.

⁸Figures 2-2 and 2-3 Image Sources:

Lunar and Planetary Institute (2013).

Explore! About Jupiter's Family Secrets [Education and Outreach].

Retrieved From: http://www.lpi.usra.edu/education/explore/solar_system/background/

Cosmos (undated). Uranus [Education and Outreach]. Retrieved From: <http://msnlv.com/uranus.html/>

Ice Giants have also been called "water worlds" due to hypothesized icy, liquid mantles below the atmosphere. Figures 2-2 and 2-3 show the theorized composition of Jupiter, and Uranus respectively. Jupiter has several layers composed mainly of hydrogen in different forms - collectively the "hydrogen envelope" [SSB, pp. 16 of 410] above its rocky core; while Uranus has a substantial non-hydrogen, liquid layer above its rocky core. The much thicker liquid layer may account for significant differences between Uranus' planetary magnetic field, and Jupiter's. The different internal structures may also affect processes in each planets' atmospheres.

Voyager-2 revealed aggregate characteristics of Uranus' planetary magnetic field which may be used to constrain a Uranus Orbiter and Probe mission. The magnetosphere, the region included by the outer reaches of the magnetic bow shock interacting with the solar stream and cosmic stream, may be detected as far as 24 planetary radii [Ness et al., 1986]. A Uranus Orbiter and Probe mission with focus on the planetary magnetic field only, may be conducted inside this spatial constraint. Maximum field intensity over the flyby was 413 nanotesla (nT) observed at 4.2 planetary radii [Ness]. The magnetic polar axis is tilted approximately 59 degrees, and offset nearly one-third (1/3) planetary radius from the geographic polar axis [Connerney, 1987]. Uranus' planetary rotation period of approximately 17.24 hours was derived from the rotation rate of the planetary magnetic field.

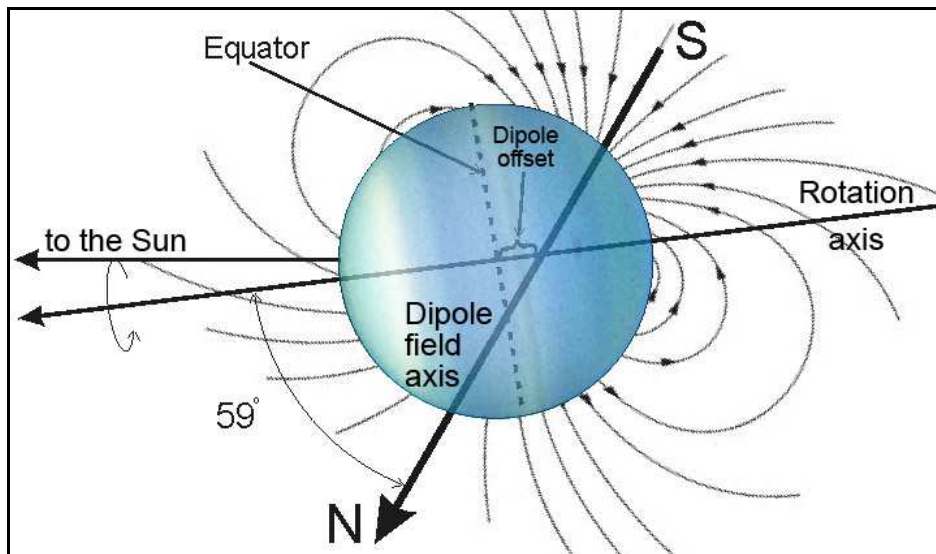


Figure 2-4: Uranus' Magnetic Dipole Tilt. ⁹

Courtesy of Wikipedia and NASA, ESA, L. Sromovsky and P. Fry (University of Wisconsin), H. Hammel (Space Science Institute), and K. Rages (SETI Institute).

Uranus' atmosphere is heated by the Sun, solely in its northern hemisphere, as the planet nears its solstice in 2028. During the southern solstice observed in the mid-1980's, the most recent occurrence of polar heating, temperature difference between the hemispheres may reach upwards of 20% (estimated before the Voyager-2 flyby) [Newburn and Gulkis, 1970, pp. 66 of 93], and 45 K (as inferred from Voyager-2 measurements) [Hofstadter and Butler, 2003]. As for the mission proposed in this report - Project Upsilon, date of arrival of the spacecraft at Uranus should be optimized with respect to the upcoming solstice. The solstice event itself may have passed by the spacecraft's arrival, but the atmosphere will still have undergone an entire season of

⁹Figure 2-4 Image Source:

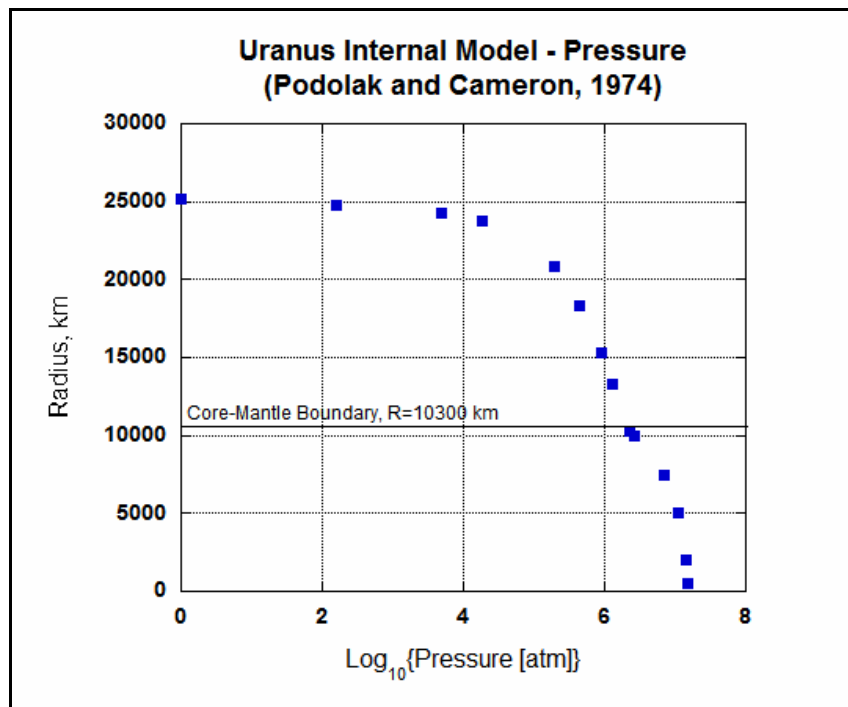
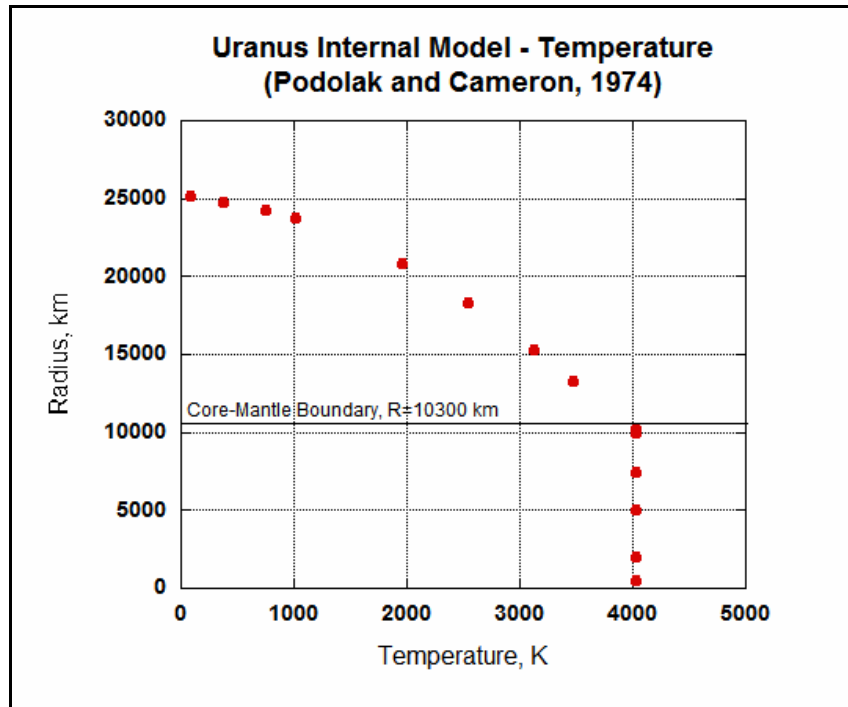
Windows to the Universe (2009).
 The Magnetic Field of Uranus [Education and Outreach].
 Retrieved From: https://www.windows2universe.org/uranus/uranus_magnetic_poles.html

uneven heating. Depending on the flow properties of Uranus' atmosphere, some delay (on the scale of years) exists between the solstice's maximum uneven heating, and the most pronounced occurrences of seasonally forced weather on Uranus. It is possible that atmospheric formations observed 10-15 years after solstice (2038-2043) are even more extreme and unexpected than those observed during the 2028 solstice.

The Upsilon-2 Atmosphere Probe shall be descended into Uranus in order to improve our knowledge of atmospheric constituents and properties such as temperature, pressure density, and wind speed. Limited models of Uranus' atmosphere exist. Figure 2-5a, 2-5b, and 2-5c are reproductions of the simulation by Podolak and Cameron (1974)¹⁰, with the governing assumption that the temperature at 1 atmosphere pressure (atm) equal 84 K. The internal structure was similar to Figure 2-3, with a rocky core, layer of water ice, and an atmosphere of Hydrogen, Helium, and Methane in solar nebula proportions - in that order from innermost to outermost. The overall water to rock mass ratio was set to solar nebula proportions as well. Lastly, the lack of an ice layer (presumably implying an entirely liquid mantle) was assumed. An atmospheric probe will not be able to obtain in-situ measurements deep within Uranus' atmosphere, however, data obtained hundreds of kilometers below Uranus' cloud tops may result in drastic changes to existing models - many of which have not been updated since analysis of the Voyager-2 science return. Chapter 3 includes a heritage mission profile from the Galileo Probe, which provides initial performance expectations for the Upsilon-2 Atmosphere Probe.

¹⁰Figures 2-5a, 2-5b, and 2-5c Reference:

Podolak, M., & Cameron, A. G. W. (1974).
Models of the giant planets.
Icarus, 22 (2), 123-148.



Figures 2-5a and 2-5b: Uranus Internal Model - Temperature and Pressure.

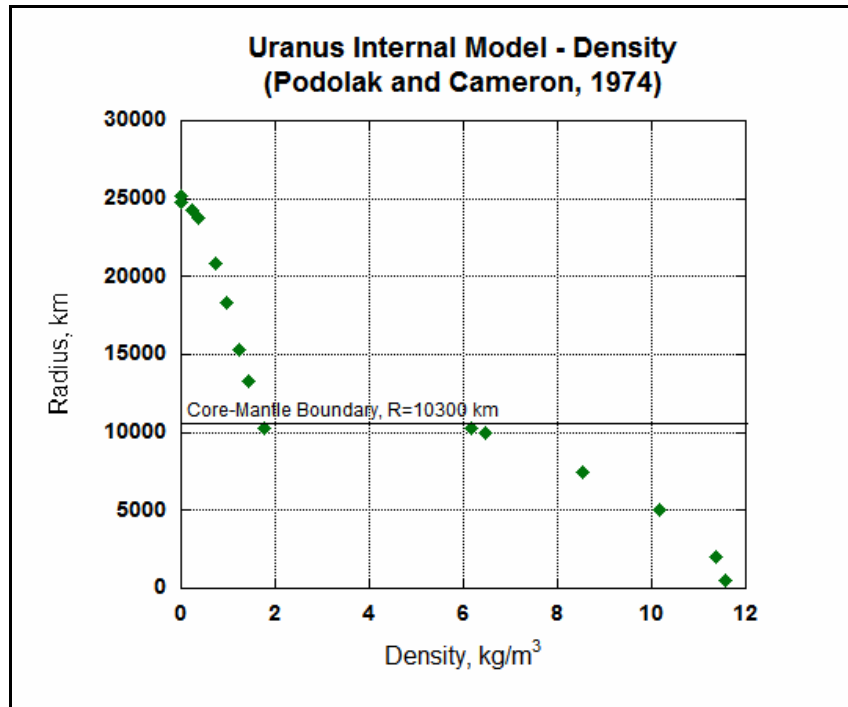


Figure 2-5c: Uranus Internal Models - Density.

Courtesy of M. Podolak (Yeshiva University), and A. G. W. Cameron (Harvard College Observatory and Smithsonian Astrophysical Observatory).

Strong zonal winds exist on Uranus. Observations made by the Keck Observatory in 2003 show wind speeds vary greatly with latitude, following a sinusoidal trend [Hammel et al., 2005]. The time period targeted by Project Upsilon (2038-2043), is in a similar point in Uranus' seasonal cycle, thus any Project Upsilon zonal wind data may be correlated with the Keck Observatory measurements, and works of Hammel et al. (2005). Figure 2-6 shows the wind speed data courtesy of Hammel et al. alongside fits of the latitudinal variation. Many measurements in the equatorial region and middle latitudes exist, but no measurements are available above 50 degrees latitude in either hemisphere. The high latitudes, in either hemisphere, may be appropriate locations to conduct a

probing experiment, providing in-situ wind speed measurements to accompany ground-based observations, ultimately improving the Uranus wind speed model.

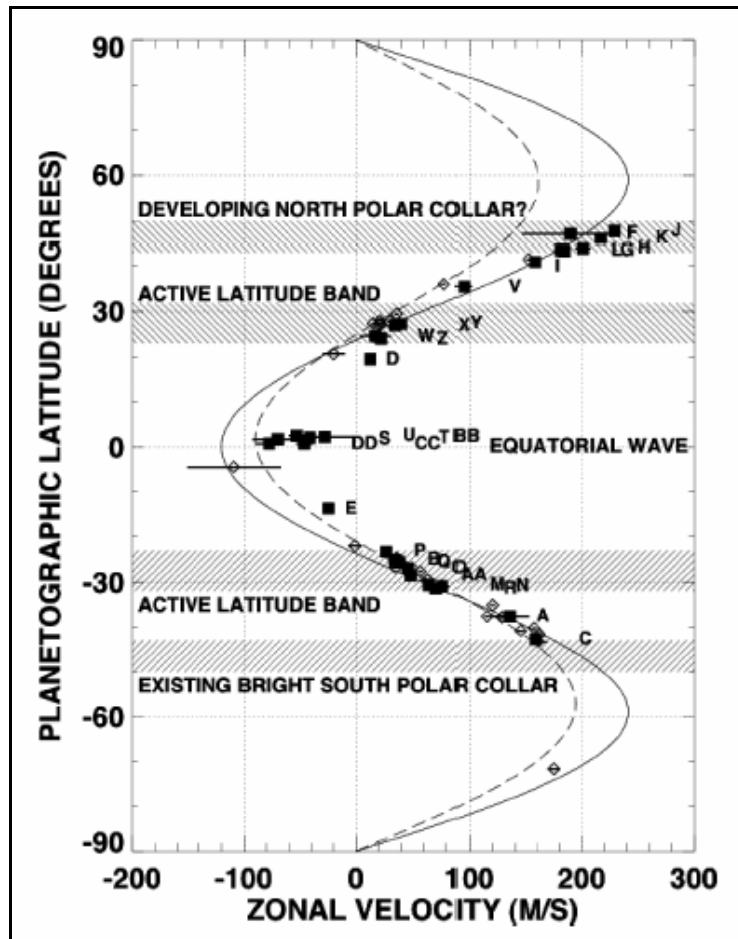


Figure 2-6: "Uranus Zonal Wind Profile in 2003." ¹¹

Courtesy of H.B. Hammel (Space Science Institute), I. de Pater (University of California Berkeley), S. Gibbard (Lawrence Livermore National Laboratory), G.W. Lockwood (Lowell Observatory), and K. Rages (SETI Institute).

¹¹Figure 2-6 Reference:

Hammel, H. B., De Pater, I., Gibbard, S., Lockwood, G. W., & Rages, K. (2005). Uranus in 2003: Zonal winds, banded structure, and discrete features. *Icarus*, 175(2), 534-545.

2.2 EARTH'S MAGNETIC FIELD

Project Upsilon's primary science objective is to model Uranus' planetary magnetic field, and compare its size, density, and interaction with the Sun with those properties of Earth's magnetic field. Knowledge of the Earth's magnetic field is presented as reference, from which we identify the characteristic quantities - magnetic Intensity, Inclination, and Declination - that we hope to measure. The Earth's planetary magnetic field has been well studied, with a host of past, present, and proposed dedicated missions - NOAA's Defense Meteorological Satellite Program (DMSP) [Klein, et al., 1992], ESA's Challenging Minisatellite Payload (CHAMP) [Luhr et al., 2005], ESA's Swarm fleet [Friis-Christensen et al., 2006] etc. The Earth's planetary magnetic field about 10 degrees inclined, and less than 10% offset - both relative to Earth's rotational axis - from an ideal dipole field. In contrast, Uranus' magnetic poles are tilted nearly 60 degrees, and offset as much as 1/3 of the planet's radius. Though the measurement of Uranus' planetary magnetic field presents a great challenge, we may apply our knowledge in measuring the Earth's magnetic field. Fundamental theory and existing models [Maus et al., 2010] may be applied in Project Upsilon's notion and concepts.

The total magnetic field consists of the Main Field, Crustal Field, and External Field. The Earth's geodynamo, principally the spin of Earth's liquid outer core, produces the Main Field; "magnetized rocks and sediments in the [Earth's] crust" produce the Crustal Field; and "electric currents flowing in the [Earth's] ionosphere and magnetosphere" bring about the External Field (direct quotes) [GFZ CHAMP Science Objectives]. The planetary magnetic field at any location may be defined by three characteristic quantities. Intensity is the magnetic field lines' magnitude in the detecting spacecraft's vicinity. Inclination is the magnetic field lines' tilt angle above or below an imaginary spherical surface centered on the planet, with radius equal to the orbital radius.

Declination is the magnetic field lines' azimuth angle relative to the local north - a vector on the imaginary surface, pointing to where the geographic north pole of that surface would be. Definitions and model equations for Intensity, Inclination, and Declination are further detailed in a statistical estimation method applied to the magnetic field measurement. In the scope of this report, the total measured planetary magnetic field at Uranus will be taken as its Main Field.

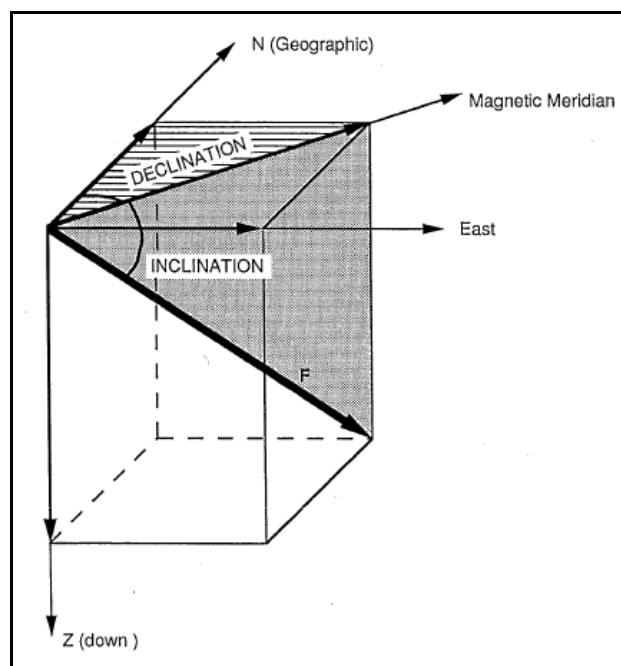


Figure 2-7: Magnetic Intensity, Inclination, and Declination. ¹²

Courtesy of S. P. Grand

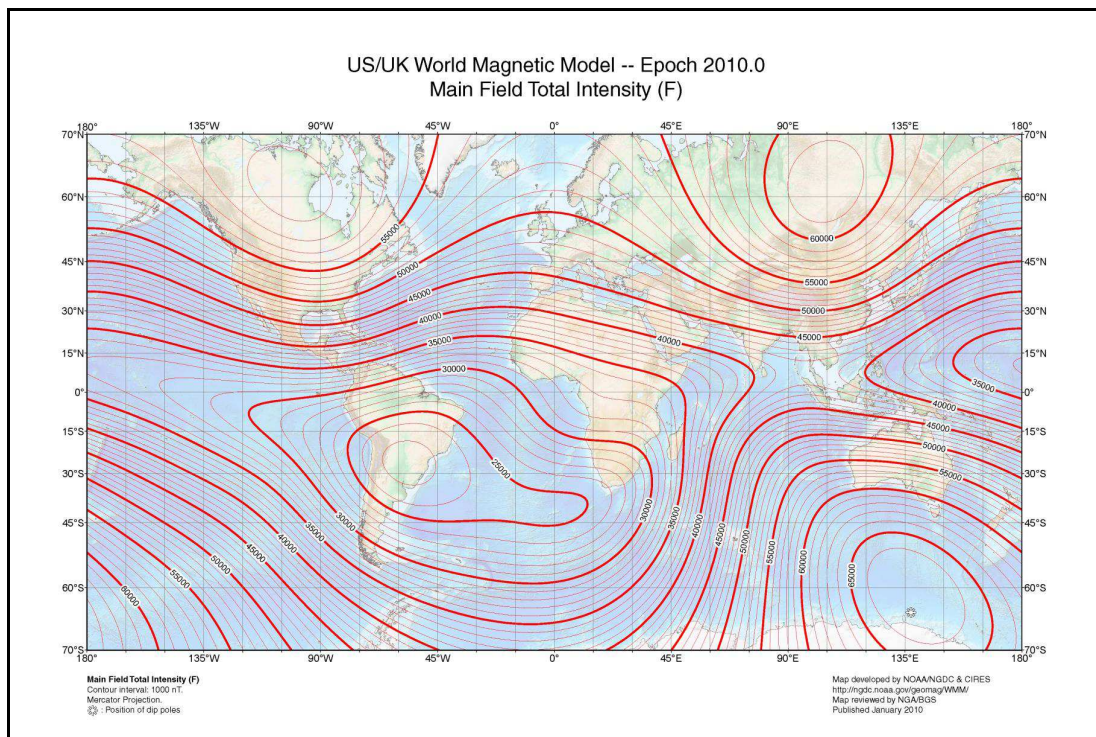
(Jackson School of Geosciences, The University of Texas at Austin).

¹²Figure 2-7 Reference:

Grand, S. P. (2013). GEO384D - Global Geophysics/Physics of Earth. Magnetism, Earth's Magnetic Field. Lecture taught by Dr. Stephen P. Grand, January 30, 2013, Jackson School of Geosciences, The University of Texas at Austin.

The National Oceanic and Atmospheric Administration (NOAA), National Geophysical Data Center (NGDC) "2010 US/UK World Magnetic Model" is a 12-by-12 spherical harmonic representation of Earth's planetary magnetic field [Maus et al., 2010]. Figure 2-8a shows a contour map of the Main Field Total Intensity at sea level. The Intensity variation is close to that expected from an ideal dipole, with the strongest regions near the geographic North and South Poles. The North Magnetic Pole - location in the northern hemisphere of the best-fit north dipole - is approximately 72 degrees West longitude, 80 degrees North latitude; while the South Magnetic Pole is an estimated 108 degrees East longitude, 80 degrees South latitude. Alternate representations of the magnetic poles exist, such as the Dip Pole representation - locations where magnetic field lines point closest to directly down (towards the center of the Earth). The South Dip Pole is marked with a "*" near 135 degrees East longitude, 65 degrees South latitude.

Earth's Main Field Intensity ranges from 23,000 to 66,000 nT near the South Magnetic Pole; in comparison, an ideal dipole model predicts 1/2 Intensity near the magnetic equator as that near the poles. Figure 2-8b shows the Main Field Inclination. The expected Inclination of an ideal dipole field is zero at the Equator, and 90 degrees near the Poles; the Earth's Main Field Inclination follows the theory closely. Figure 2-8c shows the Main Field Declination. Since all ideal field lines point north, the expected Declination of an ideal dipole is zero everywhere. The Earth's Main Field Declination is more irregular than its Inclination, but does not exceed ± 40 degrees in the tropics and mid-latitudes. Examining the Declination shows that field lines converge at the South Dip Pole, where Intensity is greatest; whereas a North Dip Pole is not as well-defined. The capability of generating Earth magnetic field models is demonstrated - Project Upsilon seeks to generate a Uranus magnetic field model, albeit at a reduced level of detail and precision.



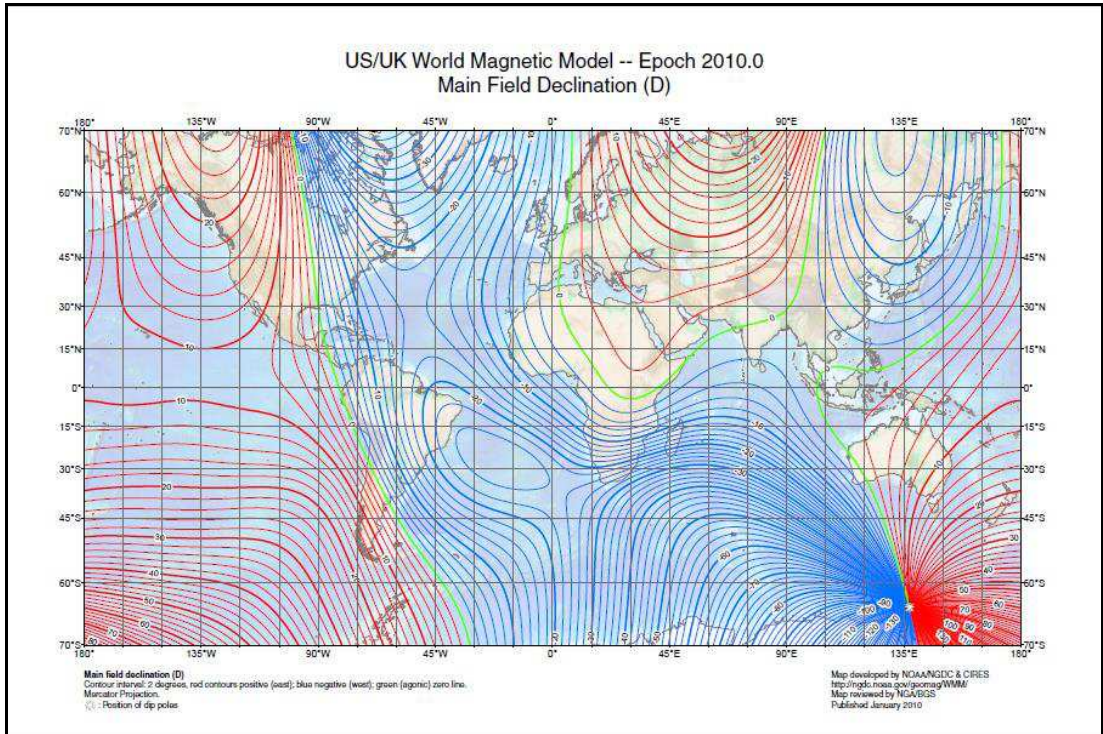
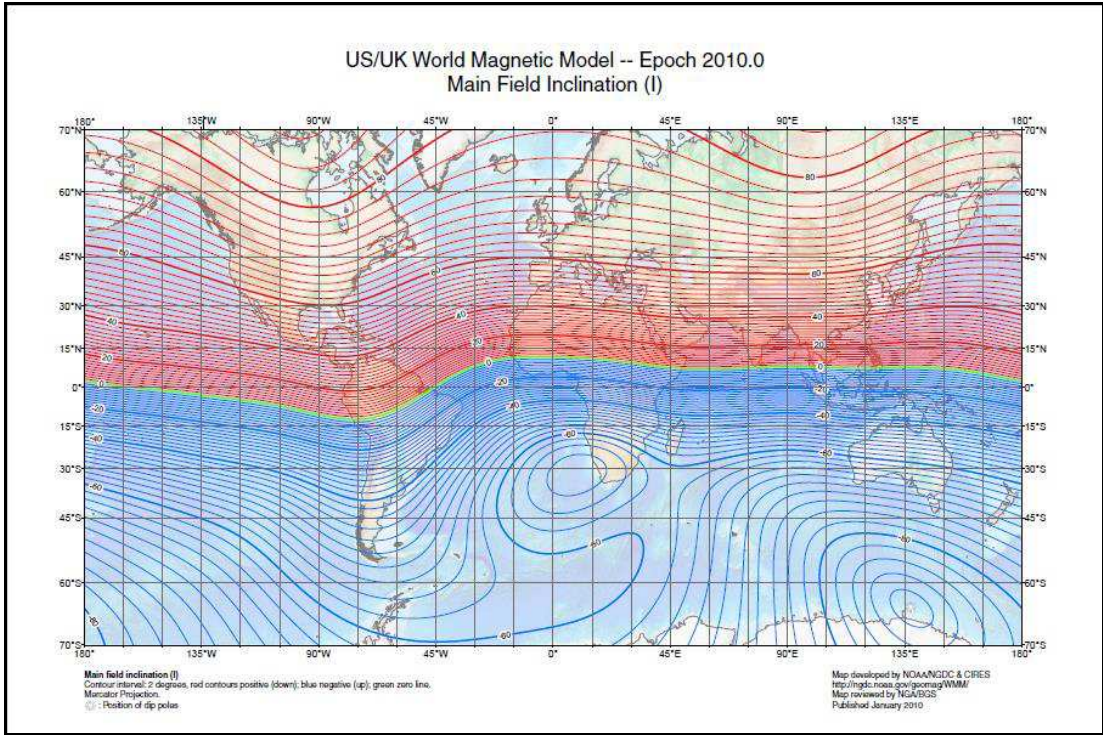
Figures 2-8a, 2-8b, and 2-8c:

**NOAA/NGDC US/UK World Magnetic Model - Epoch 2010.0,
Main Field Total Intensity (F), Inclination (I), and Declination (D). ¹³**

*Maps developed by NOAA/NGDC & CIRES, reviewed by NGA/BGS,
published January 2010.*

¹³Figures 2-8a, 2-8b, and 2-8c Reference:

Maus, S., Macmillan, S., McLean, S., Hamilton, B., Thomson, A., Nair, M., & Rollins, C. (2010).
The US/UK world magnetic model for 2010-2015.
NOAA National Geophysical Data Center.



Chapter 3: Heritage

Chapter 3 "Heritage" provides an initial listing of mission notions and flight hardware that may be verified, or qualified respectively, as heritage to be employed in Project Upsilon. The scope of this report, with respect to heritage, includes elements of Pre-phase A, and Phase A of the design process. As defined by the NASA Goddard Space Flight Center, "Rules for the Design, Development, Verification, and Operation of Flight Systems" design standard. This chapter identifies "heritage hardware to be used" and "makes a cursory assessment of 'use as is' or 'delta-equal'" (direct quotes) [NASA GSFC, 2009].

Most of our knowledge of Uranus come from results of the Voyager-2 mission. More than 40 years, and nearly one-half of Uranus' orbital period about the Sun later, Project Upsilon shall utilize a similar interplanetary trajectory to reach Uranus. The Voyager-2 spacecraft shall serve as a design cornerstone for the Project Upsilon spacecraft. The GFZ Challenging Minisatellite Payload (CHAMP) mission makes a fitting analogue to the single spacecraft, planetary magnetic field measurement notion. The Galileo Atmosphere Probe mission provides an ideal blueprint for the same mission proposed at Uranus. Finally, the New Horizons spacecraft displays state-of-the-art in deep space telecommunications; Project Upsilon may employ elements of this system. The array of available heritage prompts much enthusiasm that Project Upsilon may be ready to launch within the time frame, and cost ceiling, discussed in the mission scope.

3.1 VOYAGER-2

The Voyager spacecraft traveled through a unique planetary alignment opportunity to complete a tour of the Giant Planets - Jupiter, Saturn, Uranus, and Neptune [Kohlcase and Penzo, 1977]. Having completed their solar system exploration mission, the spacecraft continue their journey into interstellar space, while performing science in the Sun's magnetospheric bow shock and beyond [Cesarone et al., 1984]. That both spacecraft have now reached over 100 AU from Earth is a tremendous accomplishment, upon which future deep space missions will build.

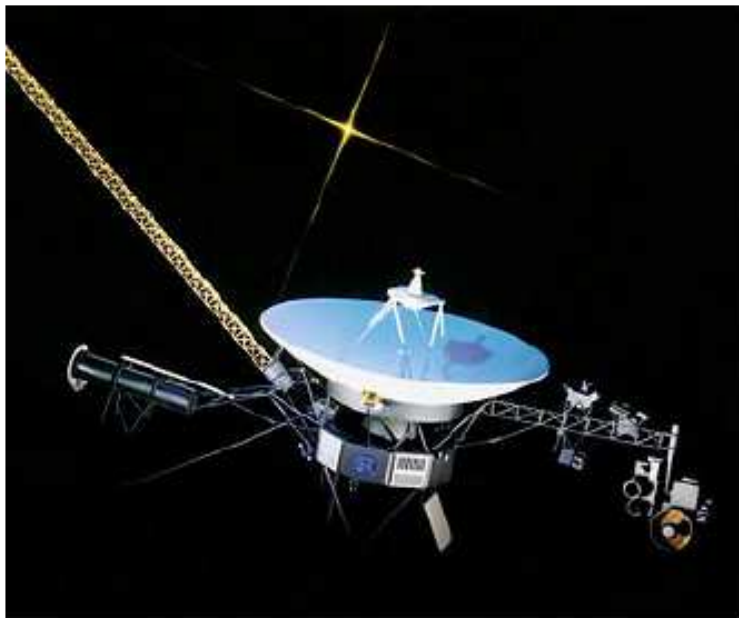


Figure 3-1: "Artist's Rendering of the Voyager Spacecraft." ¹⁴

Courtesy of the Deep Space Communications and Navigation Systems Center of Excellence (DESCANSO), NASA Jet Propulsion Laboratory.

¹⁴Figure 3-1 Image Source:

Ludwig, R., & Taylor, J. (2002).
Voyager telecommunications.
DESCANSO Design and Performance Summary Series.

Project Upsilon's launch timeframe is similar to that of Voyager - the projected launch in 2021 is seven years before Uranus' northern solstice in 2028, while Voyager-2 launched eight years before Uranus' southern solstice in 1986. Although the alignment of Saturn and Neptune is different one-half Uranian year later, the launch opportunity in 2021 still holds significant heritage.

Jupiter is considered the prime gravity assist candidate for missions to the outer solar system, but any passing spacecraft must navigate its intense radiation environment at the risk of electronics malfunction and instrument damage¹⁵. Voyager-2 reached its closest approach of Jupiter on July 9, 1979; at a distance of 721,750 km (approximately 10 Jupiter radii), spending 10 days inside the magnetosphere [NASA, 1979]. The most intense regions at 2-4 planetary radii were avoided [de Pater and Dames, 1979], and later documents from the Juno Mission confirmed that time spent inside the main radiation belt was minimized [Matousek, 2007]. Figure 3-2 shows Jupiter's main radiation belt by differential electron flux; the main belt extends outwards to more than 12 Jupiter radii in the equatorial latitudes, and approximately 6 Jupiter radii in the upper latitudes. Using this heritage, the Upsilon spacecraft should spend minimum time - hours, not exceeding the time scale of days - in the zone indicated on Figure 3-2.

¹⁵Figure 3-2 Image Source:

Matousek, S. (2007).
The Juno new frontiers mission.
Acta Astronautica, 61(10), 932-939.

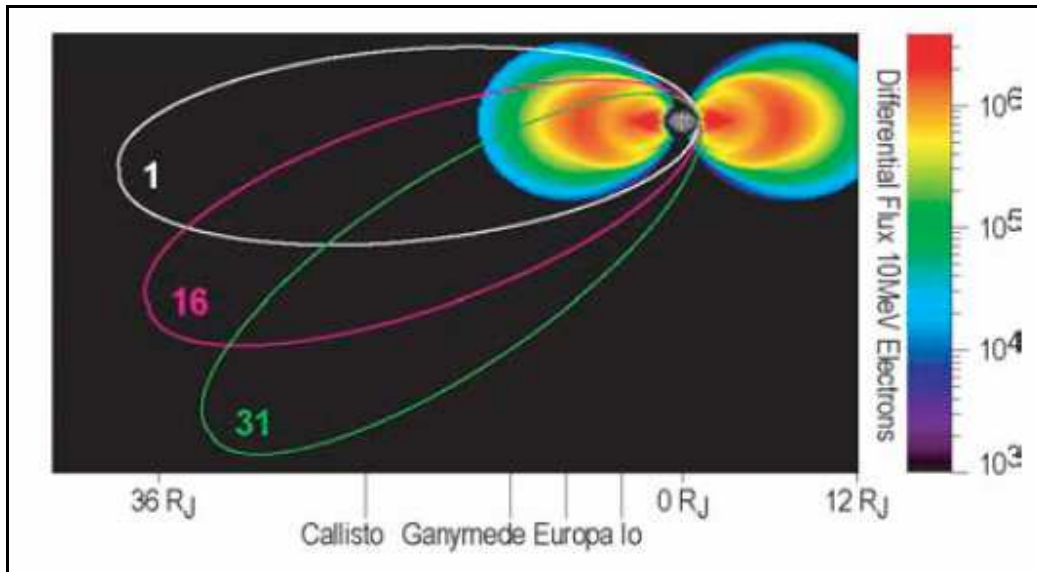


Figure 3-2: "Orbit of the Juno Spacecraft Relative to Jupiter's Main Radiation Belts."

*Courtesy of the NASA Jet Propulsion Laboratory,
and the California Institute of Technology.*

Voyager-2 began a three-month observation tour on November 4, 1985 [NASA, 1985]; and reached its closest approach to Uranus on January 24, 1985; at a distance of 110,000 km (approximately 4 Uranus radii). The Voyager-2 Planetary Radio Astronomy experiment provided our current knowledge of Uranus' rotation rate; the pioneering spacecraft also yielded images of the ring system, views of newly discovered satellites, and fundamental characteristics of the magnetosphere. The spacecraft performed a series of critical checks before its closest approach, which shall serve as heritage in mission scheduling. On-board health checks included the science boom, scanning platform, and attitude control actuators [NASA, 1985]. Rehearsals of the 90-minute communications standby - due to signal occultation by Uranus, shown in Figure 3-3 - were performed.

Such a performance update regimen will be vital for the reliability of all three Project Upsilon spacecraft.

Voyager-2 employed a suite of 10 instruments to complete its science objectives at Uranus. The "Wide and Narrow Angle Cameras, Ultraviolet spectrometer, Infrared Interferometer, and Photo-polarimeter" provided optical viewing of the planet [NASA, 1985]; the Low-field and High-field Magnetometers and the Planetary Radio Astronomy and Plasma Wave Antennae provided state-of-the-art measurements of the magnetic field. Much heritage exists in the power, and propulsion, subsystems. Voyager-2 implemented three (3) Radioisotope Thermoelectric Generators (RTG) and attitude control thrusters operating on space-storable Hydrazine propellant [Kohlcase and Penzo]. Moreover, the Upsilon-1 Science Orbiter shall further the findings of the Voyager-2 "Radio Science" (planetary gravity field); "Magnetic Fields"; and "Imaging Science" (atmospheric dynamics and surface structure) experiments. Voyager-2 provides the notional basis of the proposed Project Upsilon science phases.

The Planetary Radio Astronomy experiment may have revealed the first groundbreaking difference between Uranus, and Jupiter and Saturn. The planetary magnetosphere region was thought to be concurrent with radio emissions, but some other dynamical process was responsible for Uranus' magnetic field - as no radio emissions were detected during the initial approach of Uranus [NASA, 1985]. Voyager-2 entered "solar conjunction" - where the spacecraft and Earth are on opposite sides of the Sun - in December 1985; the three Project Upsilon spacecraft's initial approach must be carefully designed, and length of the initial period before "solar conjunction" may be used as a design Figure of Merit (FOM). When the spacecraft and Earth are on the same side of the Sun, Uranus itself may also block the communication path. Figure 3-3 shows the region where the spacecraft enters "solar conjunction".

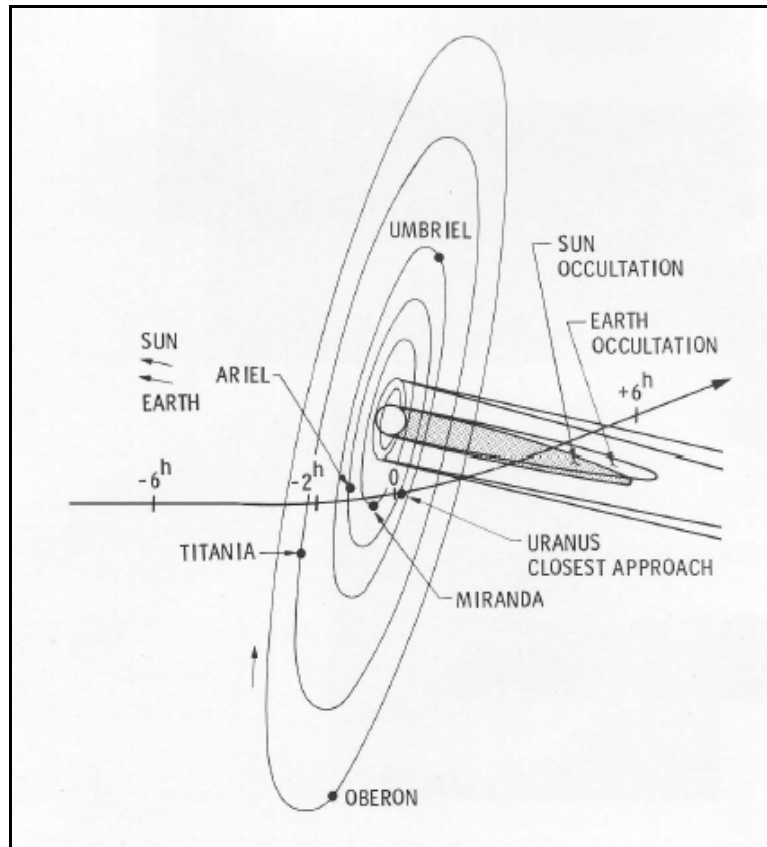


Figure 3-3: "Voyager-2 Encounter with Uranus."¹⁶

Courtesy of the NASA Jet Propulsion Laboratory, and the Planetary Society.

Spacecraft navigation and orbit determination are vital to the mission, especially at such a great distance from the Earth, with no other man-made satellites in orbit of the same planet. In addition, the Voyager-2 team noted Uranus' obliquity as a third challenge in the navigation scheme. Voyager-2 used "optical ranging, Doppler observations, radio ranging, and [a modified] very-long baseline interferometry" methods to determine its

¹⁶Figure 3-3 Image Source:

NASA Jet Propulsion Laboratory (1985).
 Voyager Bulletin. Mission Status Report No. 68. April 10, 1985
 [Voyager Mission Status Bulletins. Courtesy of The Planetary Society].
 Retrieved From: <http://www.planetary.org/explore/resource-library/voyager-mission-status.html>

orbit about Uranus" (direct quote) [NASA, 1986]. A combination of observation types will be vital for the Upsilon-1 Science Orbiter to achieve precision orbit determination. The challenge is magnified as the Upsilon-1 shall insert into a closed science orbit about Uranus.

Most importantly, Voyager-2 made the discovery that inspired the Project Upsilon mission - Uranus' peculiar and tilted magnetic field. In general, "a planet's rotational axis is not necessarily perpendicular to the ecliptic plane, the magnetic axis is not necessarily aligned with the rotational axis, and the magnetic poles do not always correspond to the rotational poles" (direct quote) [NASA, 1986]. Among the Giant Planets Jupiter, Saturn, Uranus, and Neptune, Uranus' magnetic poles are mostly un-aligned with its rotational poles. Voyager-2 also encountered Uranus' magnetospheric bow shock at approximately 170,000 km above the planet; and traveled for three hours inside what the spacecraft observed as Uranus' magnetosheath [NASA, 1986].

Magnetic field experiments make up the crux of the Upsilon-1 Science Orbiter's science operations. Voyager-2 employed both Low-field and High-field Magnetometers, with cooperating redundancy as well as cross-strapping between instruments. "Each system contains two identical Triaxial Fluxgate Magnetometers which measure the magnetic field intensity along three mutually orthogonal axis simultaneously" (direct quote) [Behannon et al., 1977, pp. 13 of 23]. The magnetometers may be deployed on a boom away from the spacecraft, or housed inside the spacecraft - however, out-board deployment is recommended to reduce contamination from the spacecraft's charging. Each magnetometer weighs "5.6 kg", require "2.2 W" power (direct quote), and have been verified with "more than 13 years of satisfactory experience" [Behannon et al., 1977].

In all, the Voyager-2 spacecraft is a design cornerstone for the Upsilon-1 Science Orbiter. It is advisable to employ significant heritage from the spacecraft that has contributed nearly all of our knowledge of Uranus. The Project Upsilon mission may implement the interplanetary trajectory, Jupiter flyby, Uranus arrival, telecommunications, among other elements of the Voyager-2 mission architecture. Upsilon-1's planetary science instrument package draws much heritage from Voyager-2's suite.

3.2 CHALLENGING MINISATELLITE PAYLOAD - CHAMP (ESA)

The Challenging Minisatellite Payload - CHAMP - was a low-Earth orbiting satellite mission managed by the German Research Center for Earth Sciences, launched in 2000 and decommissioned in 2010. The CHAMP mission's magnetic science objectives were to improve the existing field models generated by previous European missions, and to separate Earth's apparent magnetic field into contributions from the three major sources - the Main Field, the Crustal Field, and the External Field. The CHAMP spacecraft would produce precise magnetic field intensity measurements, which were aided by the Danish-manufactured Ørsted satellite's vector measurements [Sabaka et al., 2004] in order to produce a new comprehensive world magnetic model. However, CHAMP's orbit - initially circular at 450 km altitude [Olsen et al., 2006] - yielded magnetic measurements of greater resolution, as compared to Ørsted's orbit of 650x850 km (periapse and apoapse, respectively). The CHAMP mission's primary science result, in the magnetic science domain, is the deviation of Earth's magnetic field intensity, with respect to an ideal dipole field with magnetic poles near the geographic poles, and its variation over time. Figure 3-4 shows the GFZ Reference Internal Magnetic Model (GRIMM), magnetic Intensity derived from CHAMP and Ørsted data [Lesur et al., 2008].

From the GRIMM model and NOAA/NGDC model (Figure 2-8), the expected (total) magnetic field intensity near the Earth's surface varies between 25,000-65,000 nT by location. From the Voyager-2 flyby and maximum intensity measurement (413 nT at 4.2 Uranus radii, near the equatorial plane), the expected magnetic field intensity would be 25,000-50,000 nT at one Uranus radius, assuming a dipole field with inverse-cube law of intensity with orbital radius.

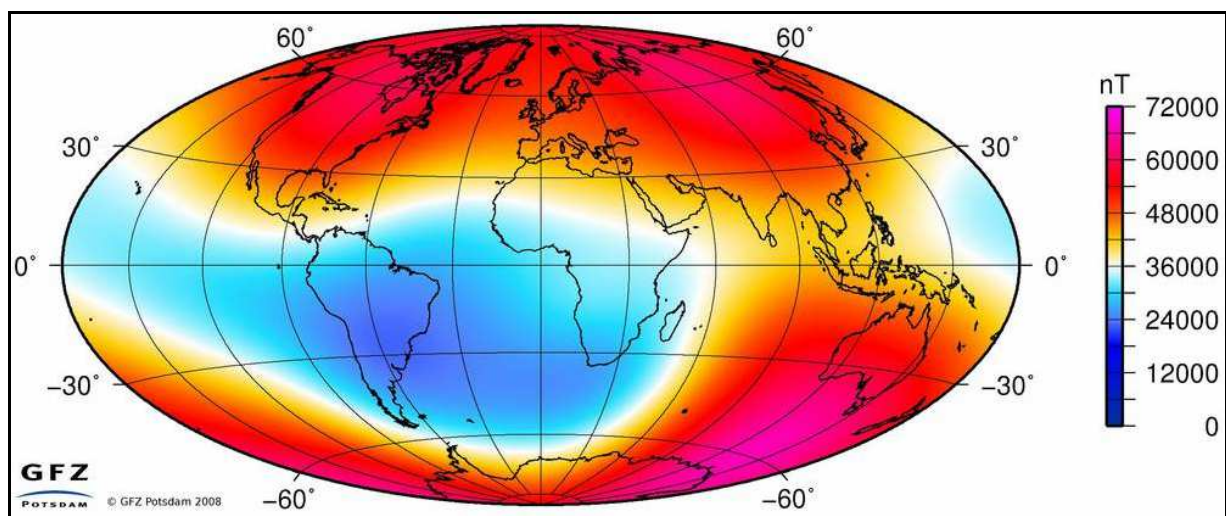


Figure 3-4: "Magnetic Field Intensity at the Earth's Surface, as Predicted by the GRIMM Model for Epoch 2005.0." ¹⁷

*Courtesy of the Helmholtz Centre Potsdam,
GFZ German Research Centre for Geosciences.*

In addition to available models, elements of the CHAMP data analysis may be drawn as heritage. Two years' of CHAMP data from August 2000 to July 2002 were

¹⁷Figure 3-4 Image Source:

Helmholtz Centre Potsdam, GFZ German Research Centre for Geosciences (2013).
The Geomagnetic Core Field [Education and Outreach].
Retrieved From: <http://www.gfz-potsdam.de/en/research/organizational-units/departments-of-the-gfz/department-2/earths-magnetic-field/topics/background/core-field/>

used to construct the Comprehensive Magnetic Model 4 (CM4) [Sabaka et al.]. Figure 3-5, from Sabaka et al. (2004), shows the distribution of CHAMP data over the time of day at its groundtrack location, and the distribution over months of the year. CHAMP data were very evenly spread throughout the temporal domain, and comprised the largest part of the scalar measurement data set (obtained by satellites) considered in CM4. The Ørsted data were not distributed as evenly, and relatively fewer data were available from the previous (and shorter) POGO and MAGSAT missions. The amount of data shown in Figure 3-6, along with data from up to 150 ground observatories at a time, comprised the entire data set considered in CM4.

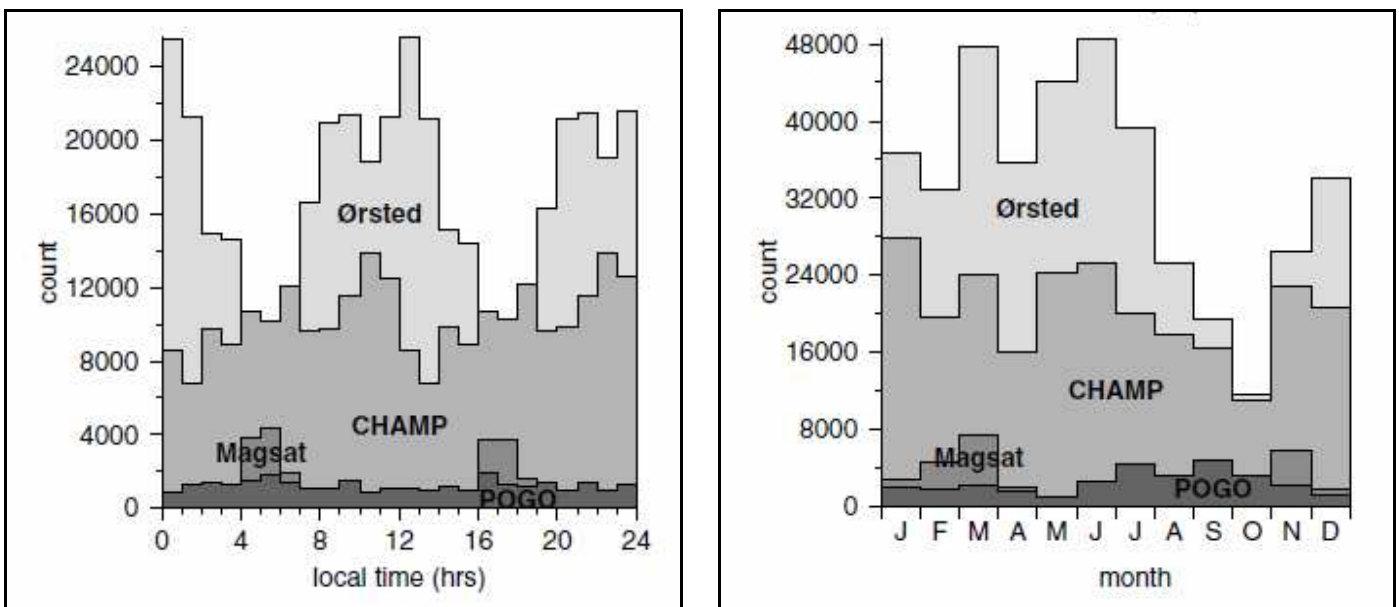


Figure 3-5: "Distribution of Data Considered in CM4.

Local Time (left) and Seasonal (right) Distributions of Scalar Satellite Data." ¹⁸

¹⁸Figure 3-5 Image Source:

Sabaka, T. J., Olsen, N., & Purucker, M. E. (2004).
 Extending comprehensive models of the Earth's magnetic field with Ørsted and CHAMP data.
Geophysical Journal International, 159(2), 521-547.

*Courtesy of Terence Sabaka and Michael Purucker (NASA Goddard Space Flight Center),
and Nils Olsen (Danish Space Research Institute).*

Approximately 200,000 CHAMP data, which were culled from the original raw measurements, were used in CM4. This value corresponds to 100,000 quality-controlled data per year, one quality-controlled data every 300 seconds, and approximately 18.5 quality controlled data per orbit. The raw measurements were obtained at a "sampling rate of 1 min⁻¹" (direct quote) [Sabaka et al., pp. 3 of 27], which corresponds to 95 raw data per orbit. Whether multiple raw data from a one-minute period were averaged before quality control is unknown. The ratio of raw (possibly averaged) to quality-controlled data, of 5-to-1, implies the noisiness of raw magnetic field data. This back-of-the-envelope value should be considered in design of the data transfer scheme for the Project Upsilon mission. Moreover, the science orbit about Uranus presumes to be much larger than CHAMP's about Earth; orbit determination will be much more difficult to achieve. The sampling rate and resolution implemented by CHAMP may not suffice in achieving a rudimentary model of Uranus' planetary magnetic field. The values approximated above may serve as absolute minimum design parameters in the data scheme. Lack of ground observatories at Uranus places further demand on the Upsilon-1 Science Orbiter's data capability.

In the statistical estimation method for CM4, quality-controlled data were weighed by the sine of the geographical co-latitude - measurements near the equator weighed greater than those made near the poles. Figure 3-6, again courtesy of Sabaka et al. (2004), shows the estimation residuals of CHAMP magnetic field intensity data with "dipole latitude" (equivalent to "Magnetic Latitude", a term defined in Chapter 4 of this report), as well as over time. The overall estimation residual of 50 nT may be the best

possible value to be expected for the Uranus magnetic field mission; 100 nT or 200 nT may be more realistic.

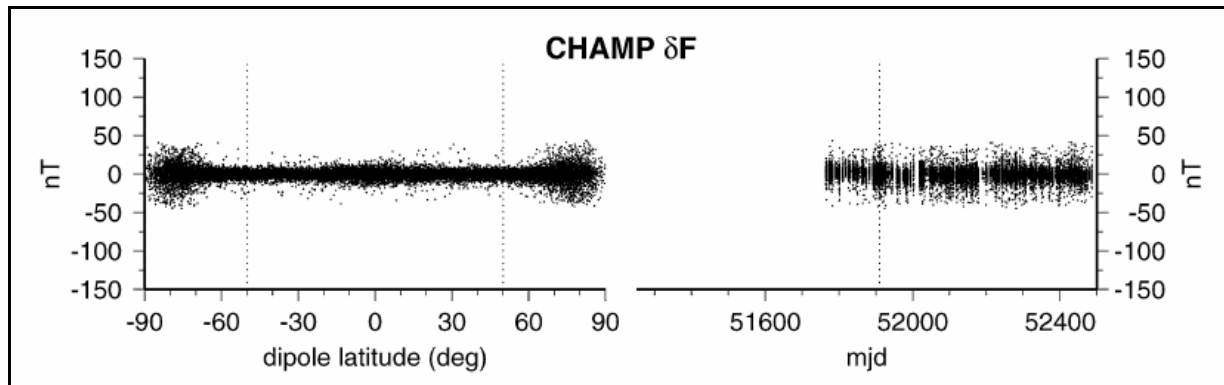


Figure 3-6: "Sampling of Residual Distributions for CHAMP as a Function of Dipole Latitude (left) and Universal Time (right) Rendered as Modified Julian Date (mjd)." ¹⁹

Courtesy of Terence Sabaka and Michael Purucker (NASA Goddard Space Flight Center), and Nils Olsen (Danish Space Research Institute).

Further discussion of the estimation algorithms developed by Sabaka et al. (2004) and Olsen et al. (2006) are outside of this report's scope. Nonetheless, the Project Upsilon mission may derive much heritage from the CHAMP mission in the measurement concept and data analysis scheme. Results from the CHAMP mission offer minimum performance guidelines for the Project Upsilon mission to follow, though much more uncertainty and unknowns exist in performing the same magnetic field measurement at Uranus.

¹⁹Figure 3-6 Image Source:

Sabaka, T. J., Olsen, N., & Purucker, M. E. (2004). Extending comprehensive models of the Earth's magnetic field with Ørsted and CHAMP data. *Geophysical Journal International*, 159(2), 521-547.

3.3 GALILEO ATMOSPHERE PROBE

The Galileo mission to Jupiter presents holds significant heritage for the notion and design of the Upsilon-2 Atmosphere Probe. Galileo's results shed light on the composition Jupiter's upper atmosphere; and Jupiter's atmosphere, on the whole, is believed to most resemble that of the primordial solar nebula [Niemann et al., 1996 and 1998]. The main Galileo spacecraft delivered the Atmosphere Probe (of the same name) into Jupiter's cloud tops, to reveal vital information from "~1000 km above the 1 bar pressure level" to a depth of "22 bars" (direct quote) [Young, 1998]. The atmosphere mission, as a whole, demonstrated "synergy between probe, orbiter, and Earth-based observations" (direct quote) [Young, 1998] for which Project Upsilon mission should strive.

The Galileo Atmosphere Probe entered Jupiter's atmosphere over a "5 μ m hotspot" (direct quote) [Young, 1998] in the southern hemisphere - the length descriptor indicated the approximate wavelength of radiation emitted in the vicinity. These "hotspots" are found in limited regions on the planet's globe - stringent selection of entry opportunities is required. Similar phenomenon on Uranus - though not a scientific analogue - may referred to as "dark spots", which are comparatively rare as well on Uranus, though may become more common as the uneven solar heating during solstice intensifies [Hammel et al., 2009]. Just as "hotspots" more commonly occur in the equatorial latitudes [Showman and Dowling, 2000], specific latitudinal zones exist promoting the formation of "dark spots" [Hammel et al., 2001]. It has also been noted that from Hammel et al. simulations, "dark spots" have a lifetime of approximately 30 days. Since the Upsilon-1 Science Orbiter shall carry the Upsilon-2 Atmosphere Probe, design of the science orbit may consider these latitudinal zones.

The Galileo Atmosphere Probe mission spanned four hours, with the probe spending 58 minutes inside the atmosphere before termination of communications. Figure 3-7 shows the mission timeline in sequence of events. The Neutral Mass Spectrometer (NMS) accounted for large part of the collected data; the Upsilon-2 probe shall employ the NMS as its main science instrument. Maximum drag acceleration of "228 g" was reached "450 km above the 1 bar pressure level" (direct quote) [Young, 1998]; this value would represent a best estimate of greatest stress on the Upsilon-2 probe. Next, the Galileo orbiter "locks onto [the probe's] telemetry signal" at the "0.54 bar" pressure level, presumably tens to hundreds of kilometers inside Jupiter's atmosphere. Selection of radio frequency based on absorption spectroscopy should be considered. Lastly, note the Galileo probe's initial separation from its orbiter at an altitude of more than five (5) Jupiter radii; design estimates of where the Upsilon orbiter and probe separate must accommodate the probe's propulsion, guidance and navigation, and communication capabilities. The Galileo mission timeline provides essential baselines and constraints for design of the Upsilon-2 Atmosphere Probe experiment.

Figure 3-9 shows the schematic diagram of the NMS gas inlet [Niemann et al., 1998]; the NMS unit measures Helium-Hydrogen ratio, detects Deuterium and Tritium isotopes, and isolates noble gases (Ne, Ar, Kr, Xe) and "volatiles" (methane, water vapor, hydrocarbons, and ammonia) from the in-situ environment. The Galileo NMS unit is equally applicable on the Upsilon-2 Atmosphere Probe.

Descent Time, min	Pressure, bars	Event
-187*	...	LRD/EPI data acquired at 5 R_J
-145*	...	LRD/EPI data acquired at 4 R_J
-106*	...	LRD/EPI data acquired at 3 R_J
-68*	...	LRD/EPI data acquired at 2 R_J ; EPI continues until just after entry
-2.8	7×10^{-8}	Entry (450 km above 1 bar pressure level)
-1.82	0.007	Peak deceleration (228 g)
0.0	0.4	Start of descent mode operation
0.058	0.4	Pilot chute deployed
0.079	0.41	Aft heat cover separated; main parachute deployed
0.23	0.43	Start of direct atmospheric measurements
1.0	0.54	Orbiter locks onto probe telemetry signal
3.0	0.88	Begin first NMS sampling of ambient atmosphere composition
3.6	1.0	Passage of 1 bar pressure level
15.4	3.8	End of first NMS sampling of ambient atmosphere composition
29.8	8.6	Begin second NMS sampling of ambient atmosphere composition
33.4	10.0	Passage of 10 bar pressure level
38.5	12.1	End of second NMS sampling of ambient atmosphere composition
46.2	15.6	Begin third NMS sampling of ambient atmosphere composition
58.6	21.7	End of probe signal

Descent time is measured from beginning of probe descent operation (see also text).
*To the nearest minute.

Figure 3-7: Galileo Atmosphere Probe Mission - "Event Time Table." ²⁰

Courtesy of the NASA Ames Research Center.

²⁰Figure 3-7 Image Source:

Young, R. E. (1998).
The Galileo probe mission to Jupiter: Science overview.
Journal of Geophysical Research: Planets (1991–2012), 103(E10), 22775-22790.

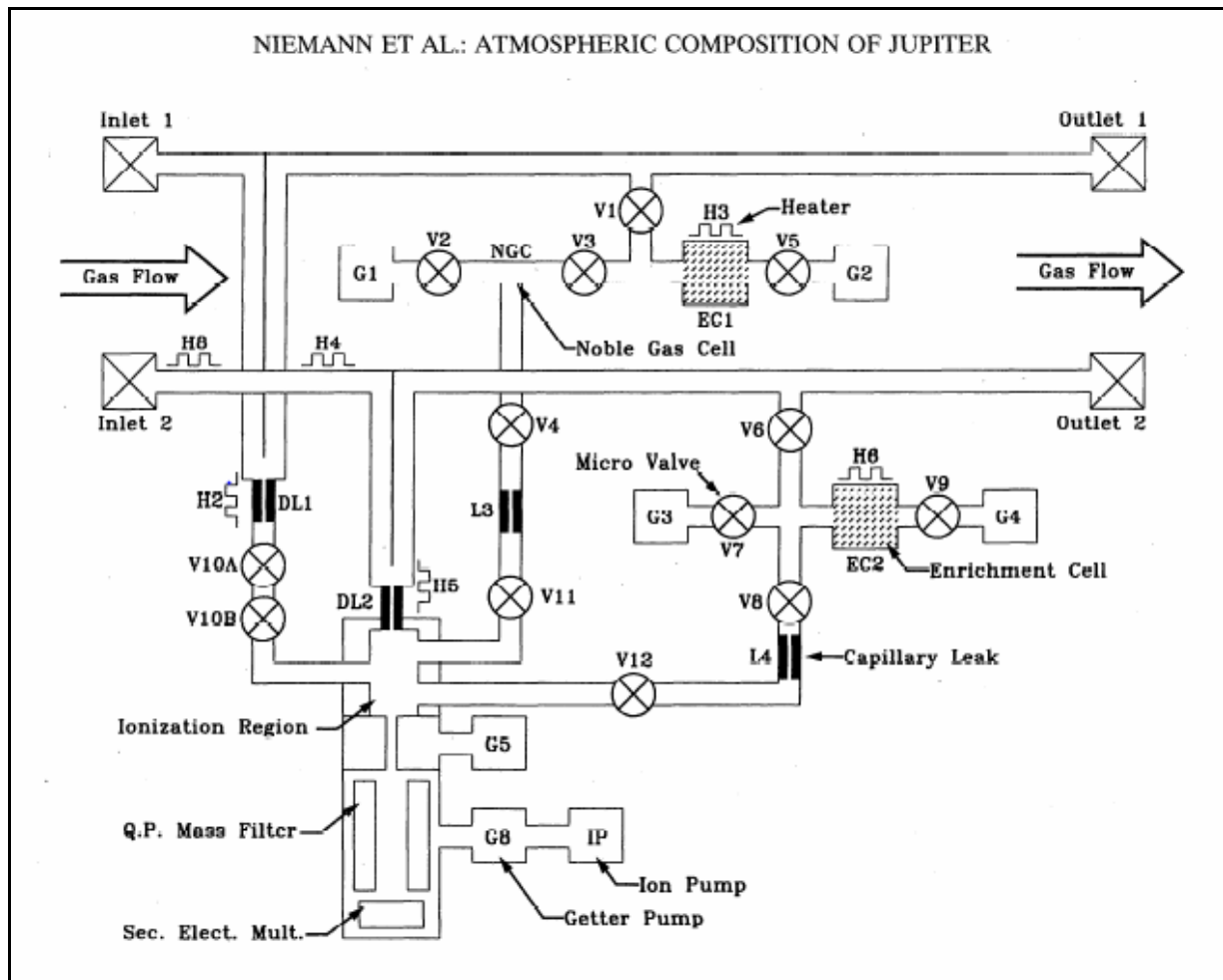


Figure 3-8: "Schematic Diagram of the Gas Inlet System to the Galileo Probe Neutral Mass Spectrometer (NMS)." ²¹

Courtesy of H.B. Niemann et al. (NASA Goddard Space Flight Center),

S.K. Atreya et al. (University of Michigan, Ann Arbor),

D.M. Hunten (University of Arizona, Tuscon),

and T.C. Owen (University of Hawaii, Honolulu).

²¹Figure 3-8 Image Source:

Niemann, H. B., Atreya, S. K., Carignan, G. R., Donahue, T. M., Haberman, J. A., Harpold, D. N., ... & Way, S. H. (1996). The Galileo probe mass spectrometer: Composition of Jupiter's atmosphere. *Science*, 272 (5263), 846-849.

The Galileo Atmosphere Probe provides essential heritage for the Upsilon-2 probe. The Galileo mission timeline may be suitable to follow, and the Neutral Mass Spectrometer serves as a vital part of the subsystems and instrument package design. Science results from Galileo provide background on which elements and compounds should be measured inside Uranus' atmosphere, albeit a different distribution of constituents should be expected. Design of the Upsilon-2 probe and its mission should draw from Galileo.

3.4 NEW HORIZONS TELECOMMUNICATIONS

New Horizons is NASA's contemporary deep space exploration effort, and its telecommunications subsystem - representing the state-of-the-art in deep space C3 architecture - offers critical heritage to be referenced. The New Horizons mission notion, and spacecraft scope as well as size, is likely most analogous to Project Upsilon, albeit New Horizons is in a lower cost class.

New Horizons is NASA's first New Frontiers medium-class mission, dedicated to survey Pluto and the Kuiper Belt [Stern, 2009]. Launched in January 2006, the spacecraft is nearly 30 AU from Earth and 4 AU from Pluto, scheduled to begin its Pluto reconnaissance in 2015 [New Horizons Web Site]. Analogous to Project Upsilon, the spacecraft also utilizes a single Jupiter gravity assist to Pluto, and leverages the Radioisotope Thermoelectric Generator in its power and thermal subsystems. The research and development phases required only four (4) years' time, a remarkable achievement that engenders an optimistic project life cycle projection, given that Project Upsilon is able to employ ample heritage.

The New Horizons telecommunications High Gain Antenna (HGA) quoted at 2.1 meters in diameter in the final design [Stern, 2009]. The HGA, along with Medium- and

Low-Gain Antennae (MGA and LGA) are arranged in a "forward stack" (direct quote) [DeBoy et al., 2004] configuration, shown in Figure 3-9. Advantages of both the HGA - focusing of the signal to enhance power; and the LGA - wide area coverage; were incurred [Christian, 2010]. Note the three-antenna stack is aligned to the spacecraft's spin axis to ensure stable field of view. An additional LGA on the spacecraft's rear is not pictured [DeBoy et al., 2004].

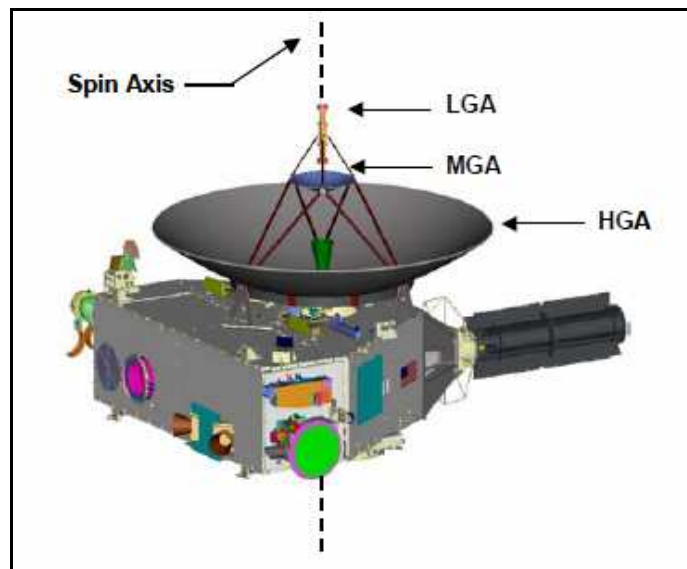


Figure 3-9: "Forward Antenna Stack on New Horizons." ²²

Courtesy of Johns Hopkins Applied Physics Laboratory.

The New Horizons HGA supported a "minimum 600 bps" (bits per second) data rate at "36-AU" distance from Earth, post-Pluto encounter, yielding "42 dB downlink gain" (direct quotes). The total alignment error budget with the Deep Space Network was

²²Figure 3-9 Image Source:

DeBoy, C. C., Haskins, C. B., Brown, T. A., Schulze, R. C., Bernacik, M. A., Jensen, J. R., ... & Hill, S. (2004).

The RF telecommunications system for the New Horizons mission to Pluto. *In Aerospace Conference, 2004. Proceedings. 2004 IEEE (Vol. 3). IEEE.*

"0.3⁰ⁿ" (direct quotes) in order to provide the quoted gain; all of the above are essential starting values in link budget calculations. The antenna's operational temperature range was rated "-200°C to +80°C" to accommodate stresses associated with highest temperatures encountered shortly after Earth departure, and lowest temperatures during mission science operations. The antenna stack support structure leveraged "Voyager and Cassini designs" (direct quote) [DeBoy et al., 2004].

The "Noncoherent Doppler Tracking" method, shown in Figure 3-10 courtesy of DeBoy et al. (2004), used throughout the New Horizons mission, has key applications in the Project Upsilon spacecraft's interplanetary cruise stage. Comparison of the nominal spacecraft downlink frequency with the received telemetry frequency (on the ground segment) yields vital tracking data. It is evident that the Project Upsilon spacecraft should incorporate several aspects of the New Horizons telecommunications subsystem.

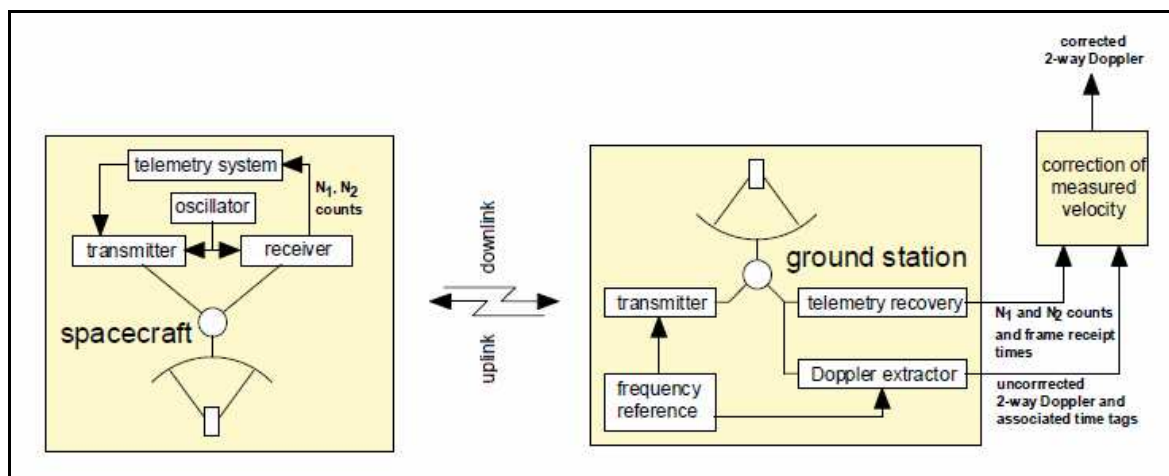


Figure 3-10: "Noncoherent Doppler Tracking." ²³

Courtesy of Johns Hopkins University Applied Physics Laboratory.

²³Figure 3-10 Image Source:

DeBoy, C. C., Haskins, C. B., Brown, T. A., Schulze, R. C., Bernacik, M. A., Jensen, J. R., ... & Hill, S. (2004). The RF telecommunications system for the New Horizons mission to Pluto. *In Aerospace Conference, 2004. Proceedings. 2004 IEEE (Vol. 3). IEEE.*

Chapter 4: Mission Planning Considerations

The Mission Scope - mission needs, goals, objectives, and CONOPS; Background - magnetic fields of Earth and Uranus; and Heritage - Voyager-2, CHAMP (ESA), Galileo Atmosphere Probe, and New Horizons missions, have been presented up to this point in the report. Chapter 4 "Mission Planning Considerations" focuses on various aspects of Project Upsilon that may be implemented as a system baseline for continuing design efforts. Current design activities lie in Pre-Phase A and Phase A of the project life cycle.

The first section presents a possible solution on Upsilon-1's Science Orbit, and to show the method of reaching such a solution that lies within mission constraints and satisfies system-level requirements. Design of the Upsilon-1 Science Orbit presented is recursive between the launch phase (see next section: "Launch Window Determination") and arrival phase (current section). Variables unique to either phase, as well as those common to both phases, must be continually adjusted until a solution is reached. That is, results and knowledge gained from groundtrack design about Uranus; provide information on spacecraft design parameters on departure from Earth; and vice-versa.

The second section examines design trades and figures of merit concerning the launch window, interplanetary journey to Uranus, and arrival insertion into the Science Orbit. As mentioned, the launch window determination is recursive with the Science Orbit design. This section and the previous one may be placed in reverse order in the report, and still achieve the same description of the current design effort. Ordering of this section, and the first section in this chapter is independent.

The final section of this chapter describes a statistical estimation method which may be appropriate to the planetary magnetic field measurement mission. This section

stands independently from the others with respect to mission planning, but has important tie-ins with spacecraft bus design (presented in the Chapter 5 "Preliminary Spacecraft Design"), especially that of the Upsilon-1 Science Orbiter.

4.1 DEFINITIONS

This report section catalogues important mission planning definitions - the various reference frames considered are defined first; definitions and critical science variables are listed thereafter in the order of appearance in this chapter. Design Figures of Merit (FOM) are defined uniquely in Section 4.3 "Launch Window and Science Window". Vectors and matrices used in the statistical estimation method of this chapter are defined in Section 4.4 "Estimation Method. Note that equation numbers return to [1] at the beginning of each section in this chapter.

Planetary Inertial Reference Frame (PIRF): Non-rotating reference frame $\{X_I, Y_I, Z_I\}$ whose origin is fixed to Uranus' planetary center. Let Uranus' equatorial plane be spanned by X_I and Y_I in the convention given by Seidelmann et al. in "Report of the IAU/IAG Working Group on cartographic coordinates and rotational elements: 2006".

Let X_I be the direction from the planetary center, to the intersection of the Equator and Prime Meridian at epoch J2000. The J2000 Prime Meridian is given by the point of intersection of the Great Circle (containing the planetary center and Planetary North Pole), and Equatorial plane; that point of intersection rotated counterclockwise along the Equatorial plane by an angle. That angle is 203.81 degrees for Uranus (direct quote) [Seidelmann et al., 2007].

Let Y_I be the direction of X_I , rotated counterclockwise by 90 degrees. Let Z_I coincide with the unit direction vector from the planetary center to the Planetary North

Pole, equal to the cross product of X_I and Y_I . Keplerian orbital elements - the Semi-major Axis, Eccentricity, (orbital) Inclination, Right Ascension of Ascending Node, and Argument of Periapse - are defined with respect to this reference frame.

Planetary Magnetic Reference Frame (PMRF): Rotating reference frame $\{X_M, Y_M, Z_M\}$ whose origin coincides with Uranus' planetary center. The PMRF rotates at the same rate as Uranus' rotation rate of approximately 17.2 hours per revolution. Thus, positions of the Magnetic Poles shall remain constant in the PMRF, while a rotation matrix about the Z_I -axis (and therefore Z_M -axis) that varies with time will be used to translate the spacecraft's position in PIRF to a position in PMRF. Spacecraft Planet Centric Longitude and Planet Centric Latitude are calculated from PMRF positions; zero longitude is defined in the convention given by Seidelmann et al. (2007), and the equatorial plane corresponds to zero latitude.

Spacecraft Body Reference Frame (SBRF): Body-fixed reference frame $\{S_1, S_2, S_3\}$ whose origin coincides with the spacecraft's center of mass. The unit direction vectors are aligned with the principal moment of inertia axes of the spacecraft.

Spacecraft Track: Spacecraft position over a rotating Uranus' cloud tops, defined by the Planet Centric Longitude and Planetodetic Latitude (corrected from Planet Centric Latitude).

Synodic Period: The period of time required for two objects orbiting a common center, to reach the same point in their individual orbits, and to reach the same point relative to each other as viewed from an inertial reference frame. The discussion in Section 4.2 "Science Orbit" utilizes the Synodic Period between Uranus' planetary rotational period (a fixed longitude-latitude point at Uranus' planetary radius orbiting the planetary center), and the spacecraft's orbital period. Another instance is the Synodic

Period between Uranus' and Earth's orbits about the Sun, approximately 370 Earth sidereal days.

Un-powered Gravity Assist: Interplanetary flyby where the assisting planet supplies all of the momentum and energy change required to reach the next interplanetary node. As opposed to a Powered Gravity Assist, where spacecraft propellant is consumed in a maneuver simultaneously with the momentum change incurred during interplanetary flyby.

Magnetic Intensity: Strength of the planetary magnetic field as detected by the Science Orbiter - from this point on referred to as the "spacecraft" - in its immediate vicinity. Suppose the magnetic field line vector is decomposed into components in any three-dimensional coordinate system - PIRF, PMRF, SBRF etc. - Intensity is the magnitude of the vector form of components.

Magnetic Inclination: Angle between the magnetic field line vector, and the tangent plane to an imaginary spherical surface whose radius is equal to the orbital radius. The spacecraft's location is where the tangent plane meets the spherical surface. Sign convention is upward from the tangent plane. Inclination ranges from -90 to 90 degrees.

Magnetic Declination: Angle between the projection of the magnetic field line vector onto the tangent plane - which is the Magnetic Meridian in Fig. 1, and the unit vector pointing to the Planetary North Pole on the tangent plane - the Local North vector. Angle convention is counterclockwise from the Local North vector. Declination ranges from -180 to 180 degrees.

Scaling Factor: Estimated best-fit Intensity at one Uranus radius as a ratio of the same quantity at one Earth radius.

4.2 SCIENCE ORBIT

4.2.1 Concept

The Upsilon-1 Science Orbiter's planetary magnetic field measurement mission requires coverage over a large range of latitudes and orbital altitudes. Therefore, Upsilon-1 shall operate in a polar, highly eccentric orbit, while minimizing risks associated with Uranus' satellites and ring system. At the same time, design of the Science Orbit is highly influenced by Spacecraft Tracks (analogous to groundtracks of Earth-orbiting satellites) - tracks must propagate over longitude to, again, ensure effective coverage. All of the necessary conditions and constraints for a Candidate Science Orbit are described in this section; confirming analyses with the chosen Candidate Science Orbit (and its associated orbital elements) are presented in Section 4.2.2.

However, little *apriori* information exists on Uranus' planetary magnetic field and gravity field, aside from measurements obtained from the Voyager-2 flyby in 1986. Obtaining many measurements over the same location, relative to a rotating Uranus, mitigates estimation errors in order to produce a more precise model. Presence of these two major constraints - planet coverage and estimation precision - calls for compromise between precessing tracks (former constraint) and strictly repeating tracks (latter constraint). This report section examines a candidate Science Orbit with nearly repeating tracks which may facilitate proper measurement of Uranus' planetary magnetic field.

Conditions required for repeating tracks are examined. The spacecraft must reach the same point in the orbit, as well as the same point over a rotating Uranus, in order for tracks to repeat. Location of the Ascending Node - the direction in a non-rotating planet centric reference frame, of the line from the center of the planet to the point in space where the spacecraft crosses the planet's equatorial plane most recently after reaching periapse - "must repeat with respect to the rotating [planet]" (direct quote) [Fowler,

2013]. The repetition must occur at an integer number of orbital periods after the spacecraft reaching the initial Ascending Node. Equation [1] gives the orbital period, where (a) is the orbit semi-major axis. So, the time between track repetitions is an integer (m) multiplied to the orbital period, shown in equation [2]. Equations [1] and [2] describe the time required for the spacecraft to reach the same point in the orbit.

$$T_p = 2\pi \sqrt{\frac{a^3}{\mu}} \quad [1]$$

$$T_{rep} = mT_p \quad [2]$$

Uranus has an oblate gravity field, and the second-degree zonal harmonic term (J_2) accounts for the largest contribution of that deviation. Oblateness of the gravity field causes the spacecraft's orbit to precess in inertial space. Precession rate due to (J_2) depends on the size of the orbit and its orbital inclination, shown in equation [3]; where (e) is the orbital eccentricity and (i) is the orbital inclination. The precession rate due to (J_2) is negative for prograde orbits ($0 \leq i < 90^\circ$), and positive for retrograde orbits ($90 < i < 180^\circ$). That is, Uranus' oblate gravity field forces orbiting spacecraft to cross the equatorial plane *earlier* than it would in a perfectly symmetrical, spherical gravity field.

$$\omega_{J_2} = -\frac{3}{2} \frac{R^2}{a^2(1-e^2)^2} J_2 \sqrt{\frac{\mu}{a^3}} \cos(i) \quad [3]$$

Uranus' planetary rotation rate affects the spacecraft's tracks. The best estimate for one Uranian day is approximately **62060 seconds** [NSSDC], which corresponds to a rotation rate (ω_u) of **1.0124e-04 rad/s**. Consider a stationary point in inertial space, the longitude of this point precesses over time with the planet's rotation. Precession rate due

to (J_2) has the same effect (of decreasing longitude) as planetary rotation. Thus, the difference of the two rates may be used to design repeating tracks. Time for the spacecraft to reach the same longitude, while traveling over a rotating Uranus, is given by the Synodic Period (equation [4]) of the rates. Finally, the time required for repeating tracks may equal an integer (k) number of Synodic Periods. Time for the spacecraft to reach the same point in the orbit, and time for the spacecraft to reach the same longitude over a rotation Uranus, are set equal in equation [5].

$$T_{syn} = \frac{2\pi}{\omega_{J_2} - \omega_u} \quad [4]$$

$$T_{rep} = kT_{syn} = mT_p \quad [5]$$

The semi-major axis, orbital eccentricity, and orbital inclination must be constrained in order to set the design space for this problem. As defined in Chapter 1 "Mission Scope", a critical design assumption is the ability to access a Uranus polar orbit through the Ecliptic plane. From Chapter 3 "Heritage", Voyager-2 encountered Uranus' magnetospheric bow shock at approximately 170,000 km above the planet (corresponding to an orbital radius of about **195,600 km**); thereby bounding the maximum apoapse of the Science Orbit. The minimum apoapse may be determined such that the Science Orbit is super-synchronous - where the orbital period is greater than Uranus' rotational period. Exchange of angular momentum between the oblate Uranus and a sub-synchronous spacecraft in resonance, results in amplified orbit decay of the spacecraft [Hahn, 2013]. Finally, periapse of the Science Orbit must be low enough to facilitate the Upsilon-2 Atmosphere Probe experiment - where a slight ΔV performed at apoapse lowers the periapse below Uranus' planetary radius - but not so low that atmospheric drag and planetary radiation contribute sizeable perturbations. Section 4.4

"Estimation Method" implements a purely gravitational force model for statistical estimation.

The above simply serve as earliest qualitative estimates of the Science Orbit's properties. Table 4-1 quantitatively shows the constraints described in the previous paragraph. Uranus' planetary (equatorial) radius is taken as the mathematical minimum periapse distance, although it is not recommended for the current iteration of design to approach that value. The "Minimum Apoapse Radius" corresponds to a circular synchronous orbit whose periapse is the Minimum Periapse Radius, calculated with equation [6]. Minimum and maximum orbital eccentricities correspond to the combinations of periapse and apoapse radii. The orbital inclination is quoted from above. Constraints on the node precession rate, orbital period, and Synodic Period were also calculated in Table 4-2. One extra significant digit is given for the Synodic Period to distinguish their minute difference.

$$r_a^* = \frac{2\mu^{\frac{1}{3}}}{(\omega_u)^{\frac{2}{3}}} - r_p^* \quad [6]$$

Parameter	Value	Unit
Minimum Periapse Radius	25600	km
Minimum Apoapse Radius	139,800	km
Maximum Apoapse Radius	195,600	km
Minimum Eccentricity	0.6904	--
Maximum Eccentricity	0.7685	--

Table 4-1: Geometric Constraints on the Candidate Science Orbit.

Parameter	Value	Unit
Minimum Orbital Period	62080	s
Maximum Orbital Period	96010	s
Minimum Node Precession	1.419e-08	rad/s
Maximum Node Precession	2.402e-08	rad/s
Minimum Synodic Period	62069	s
Maximum Synodic Period	62075	s

Table 4-2: Timing Constraints on the Candidate Science Orbit.

First, the periapse radius was fixed at the minimum, and the apoapse radius was allowed to vary within constraints. The orbital period and Synodic Period were calculated and matched to the nearest possible integer values (k) and (m). Then, the process was repeated for increasing periapse radii. Whether both the geometric parameters and timing parameters remain within the constraints given in Tables 4-1 and 4-2, respectively, were verified. Table 4-3 shows the chosen candidate Science Orbit at the current iteration of design. The periapse radius is adjusted to **26880 km**, the orbital period is **81023 seconds**, the node precession rate is **1.598e-08 rad/s**, and the Synodic period is **62070 seconds**. These values correspond closest to a **17-to-13** (k,m) pairing, for (k) and (m) less than 20. Since the current selection of parameters yield nearly repeating tracks, the objective of the Science Orbit design was achieved.

4.2.2 Candidate Science Orbit - Description and Orbit Evolution

Table 4-3 shows all orbital elements, periapse and apoapse radii, and period of the Candidate Science Orbit. The Right Ascension of Ascending Node and Argument of Periapse were obtained via optimization of the interplanetary flight path with the Trajectory Configuration Tool (TRACT). The TRACT-based optimization method is discussed in Section 4.3, "Launch Window and Science Window". The author sincerely acknowledges Marty Brennan for providing the TRACT code, as well as providing guidance on modifying the code to fit the needs of this work.

Orbital Element	Value	Unit
Semi-major Axis	98770	km
(Periapse Radius)	26880	km
(Apoapse Radius)	170670	km
(Orbital Period)	81023	s
Eccentricity	0.7279	--
Inclination	99.25	degree
Right Ascension of A.N.	-5.928	degree
Argument of Periapse	298.2	degree

Table 4-3: Candidate Science Orbit - Keplerian Orbital Elements.

Figure 4-2 shows the candidate Science Orbit in a Uranus-fixed non-rotating inertial reference frame, which the Upsilon-1 shall traverse during its planetary magnetic field measurement mission. Periapse capture was assumed, and the orbit was numerically integrated, in MATLAB, for 90 initial orbital periods (which changes as the orbit evolves over time) to approximately the first three (3) months' propagation after arrival. The J_2 and J_4 gravitational perturbations, taken from Hubbard and Marley (1989; J_6 is given as zero), are included in the numerical integration. The "ode45" algorithm was used;

absolute and relative tolerances were set to the minimum possible values allowed. The approach trajectory, in green, is discussed in "Launch Window and Science Window".

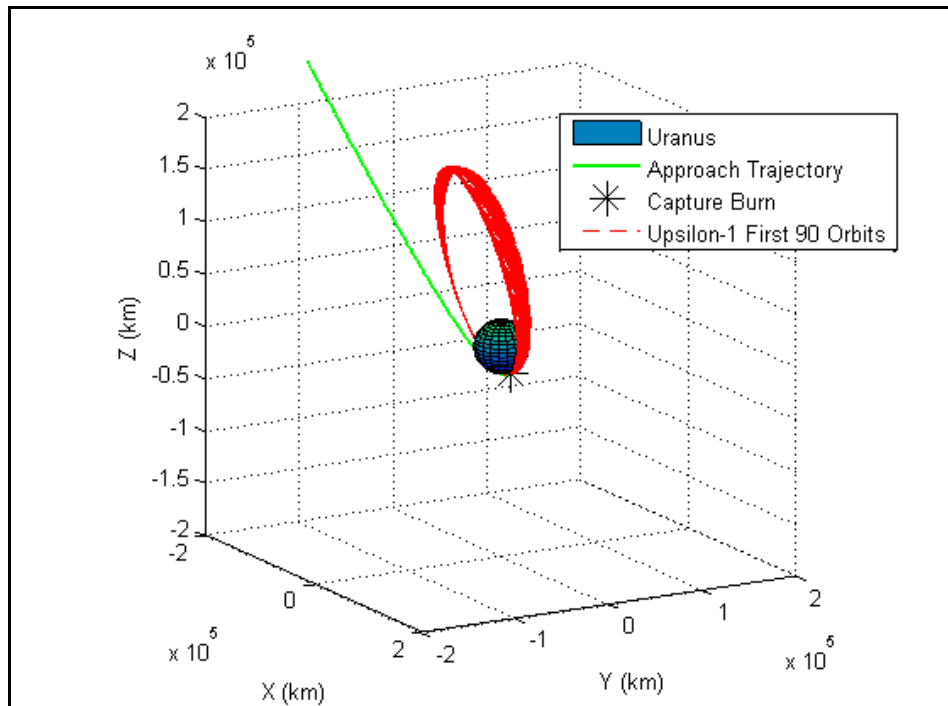


Figure 4-2: Candidate Science Orbit - Uranus-fixed Inertial Position (PIRF).

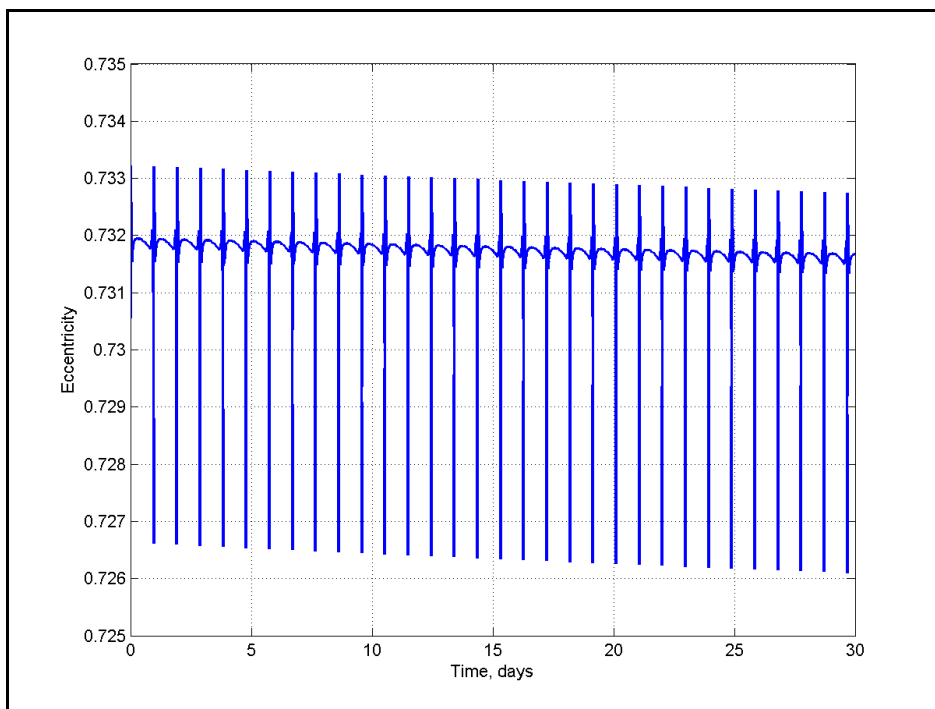
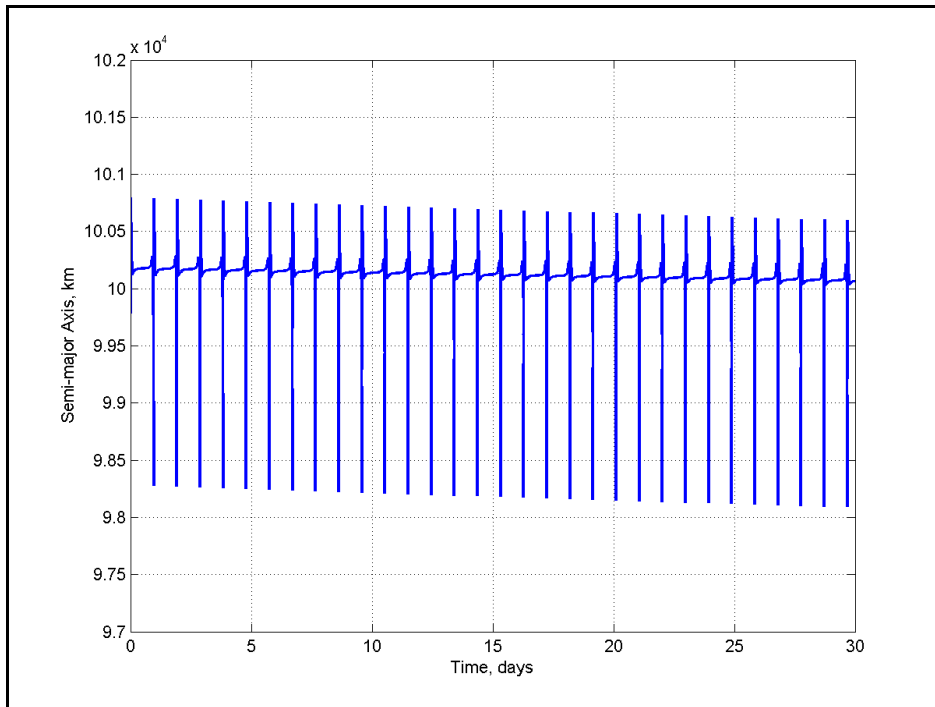
Inertial positions obtained in the numerical integration were converted to orbital elements. Examining the orbit evolution, especially the Semi-major Axis rate of change within the time span of our mission, leads to initial estimates on the spacecraft's propulsion capability for orbit maintenance and upkeep. Table 4-4 shows the best-fit orbital evolution rates over the first **30 days** in the numerical integration - note that one "year" is taken as **365.25 days**, and that one "day" as **86400 seconds**. Theoretical rates for the Right Ascension of Ascending Node and argument of periapse are calculated with the Lagrange Planetary Equations [Kaula, 2000, pp. 29 of 124]. The J_4 contribution is included in the general form of the "disturbing potential" defined by Kaula. The

Ascending Node rate is **9.29e-02 deg/day**; while the periaipse rate is **-2.52e-01 deg/day** - the Lagrange Planetary Equations result agrees well with the numerical simulation.

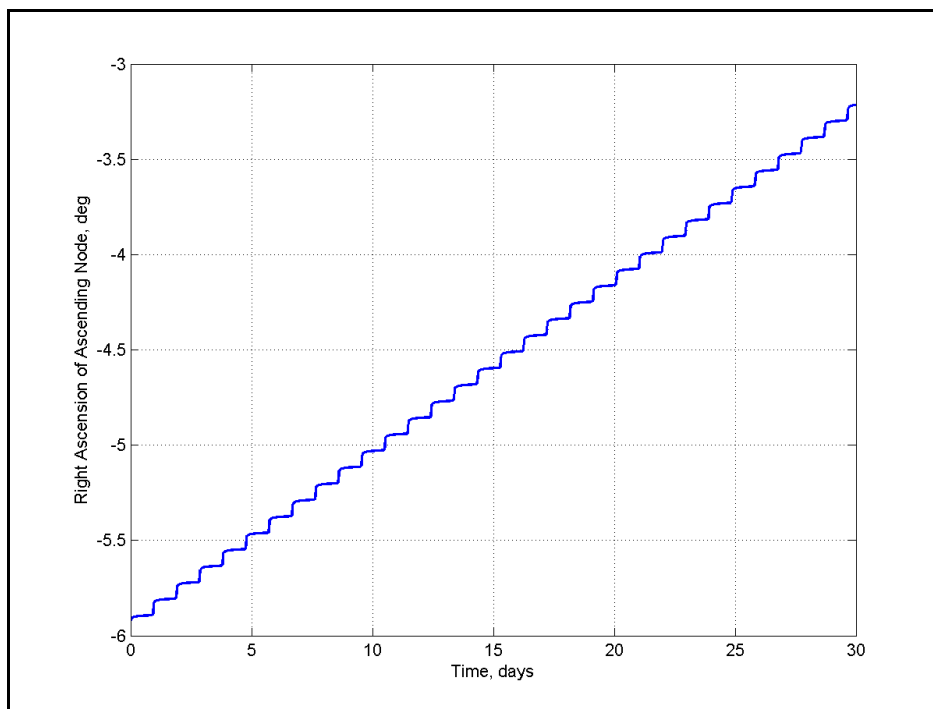
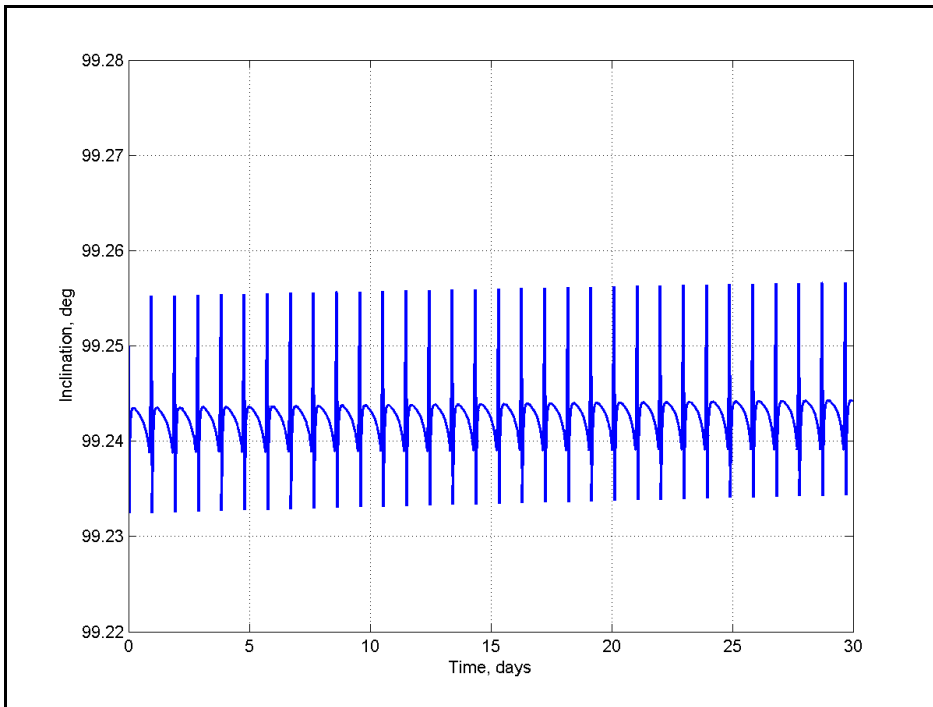
Orbital Element, Rate of Change	Numerical Integration	Unit
Semi-major Axis	-970	km/year
Eccentricity	-0.00258	(year) ⁻¹
Inclination	2.65e-05	deg/day
Right Ascension of A.N.	9.04e-02	deg/day
Argument of Periaipse	-2.49e-01	deg/day

**Table 4-4: Candidate Science Orbit -
Initial Best-fit Evolution Rates (30-day Numerical Integration).**

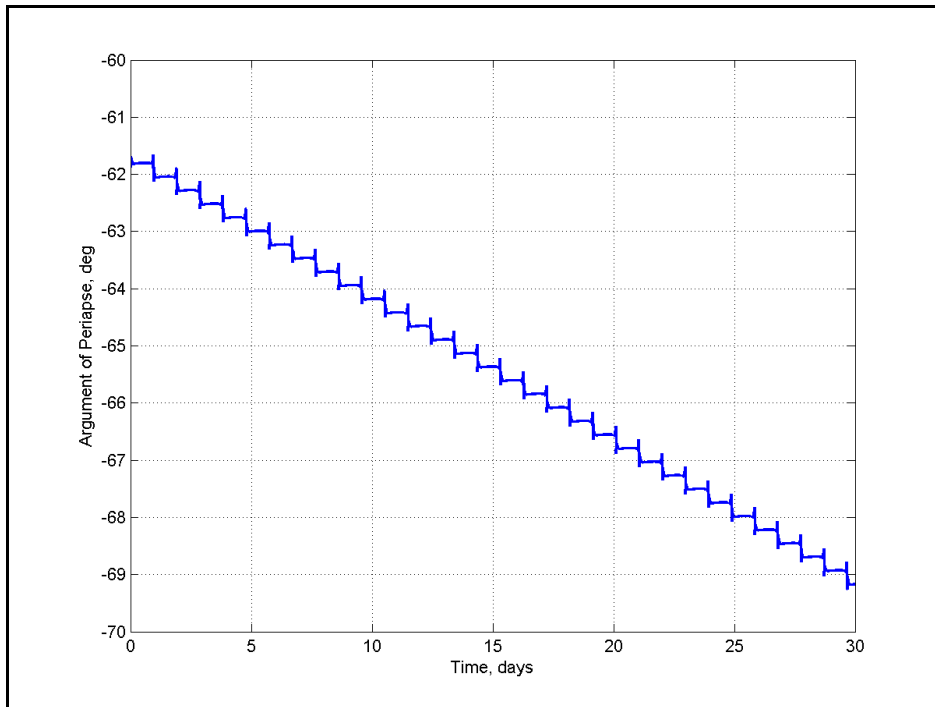
The 30-day numerical integration is limited, in the inability to visualize long-period perturbations to the spacecraft's orbit. A longer integration time would not produce an accurate simulation, as numerical errors accumulate longer time spans. However, the simulation provided enough information on semi-major axis - that it decreases initially - to initialize mitigating design efforts. Although eccentricity decreases initially, lack of atmospheric drag or gas nebula drag in the operating environment ensures that the orbit will not circularize. As long as the inclination remains in the near-polar regime, no drastic corrections are necessary. Figures 4-3a to 4-3e on the following pages show change in each orbital element over the first 30 days after arrival.



Figures 4-3a and 4-3b: 30-day Orbit Evolution - Semi-major Axis and Eccentricity.



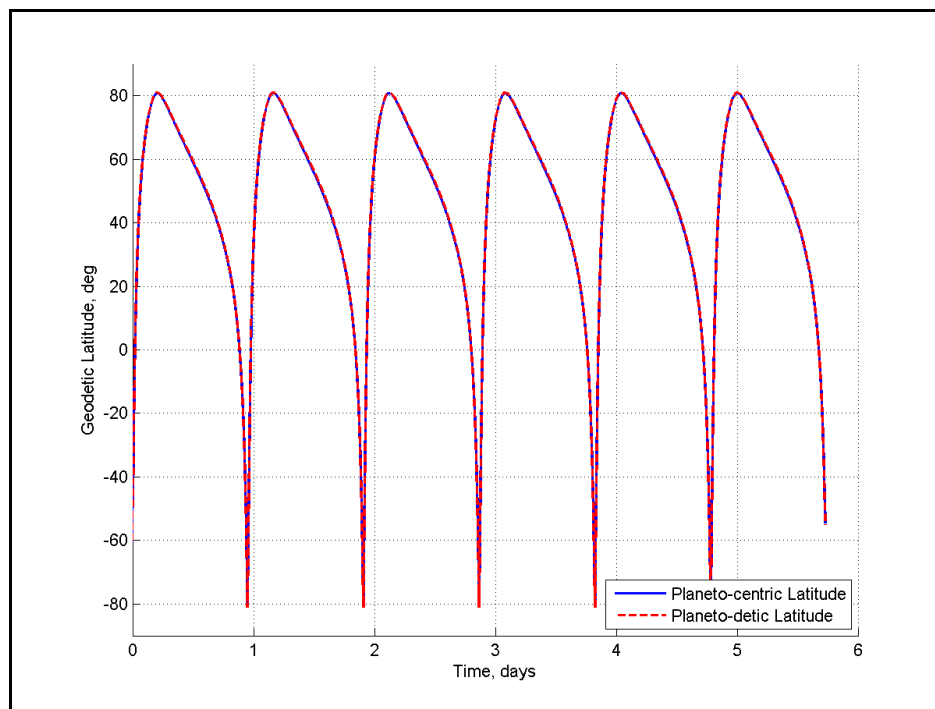
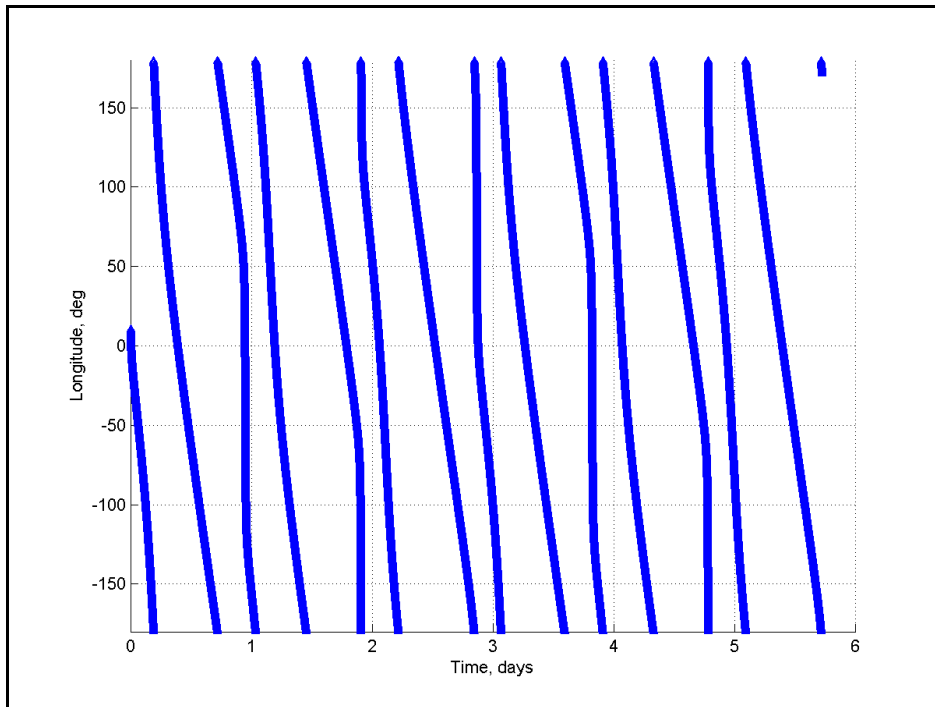
Figures 4-3c and 4-3d: 30-day Orbit Evolution - Inclination and R.A.A.N.



Figures 4-3c and 4-3d: 30-day Orbit Evolution - Argument of Periapsis.

4.2.3 Candidate Science Orbit - Spacecraft Tracks and Coverage

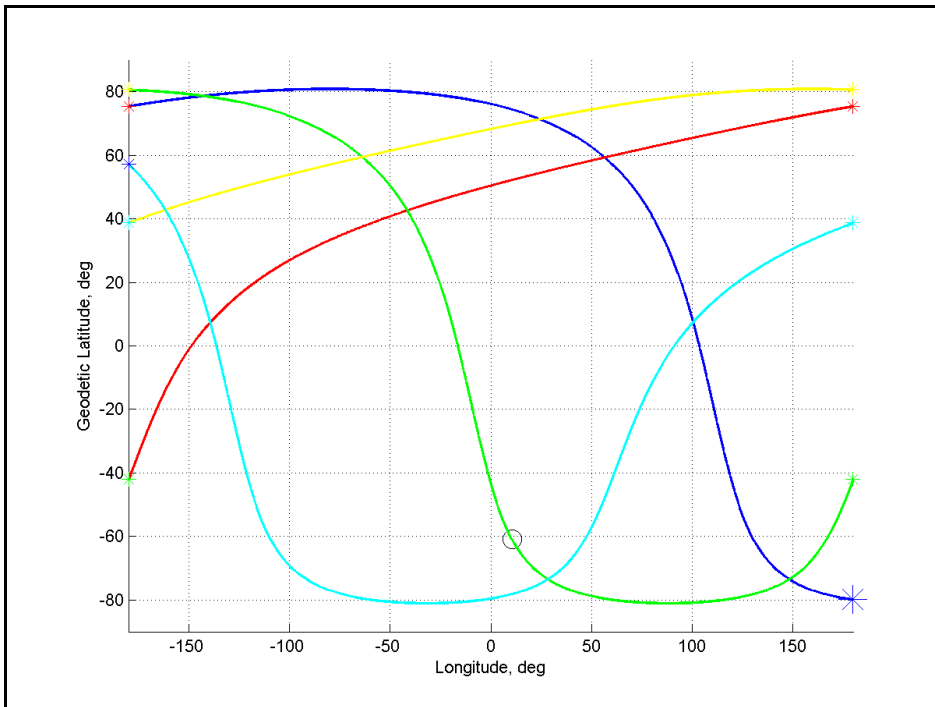
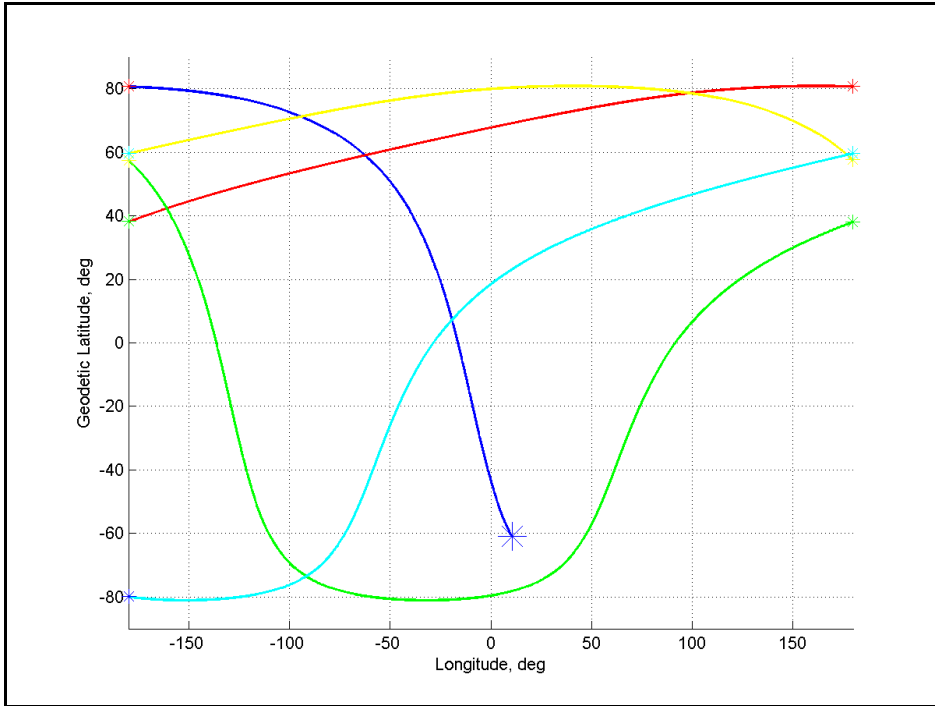
Next, we model the spacecraft's tracks - which describe the longitude and latitude position over Uranus. The spacecraft's inertial position is transformed to position in a planet centric rotating reference frame. Uranus' rotation affects the spacecraft's longitude over time. Planet Centric Latitude is determined from the spacecraft's inertial position, but is corrected to Planetodetic latitude - analogous to geodetic latitude for Earth-orbiting satellites. From the numerical simulation, the largest difference between Planet Centric and Planetodetic latitude for the candidate Science Orbit is 0.7 degrees. Figures 4-4a and 4-4b show the spacecraft's Planet Centric Longitude, Planet Centric Latitude, and Planetodetic Latitude over the first six days after arrival. Time period represented was kept adequately short in order to distinguish variations within a single orbit.



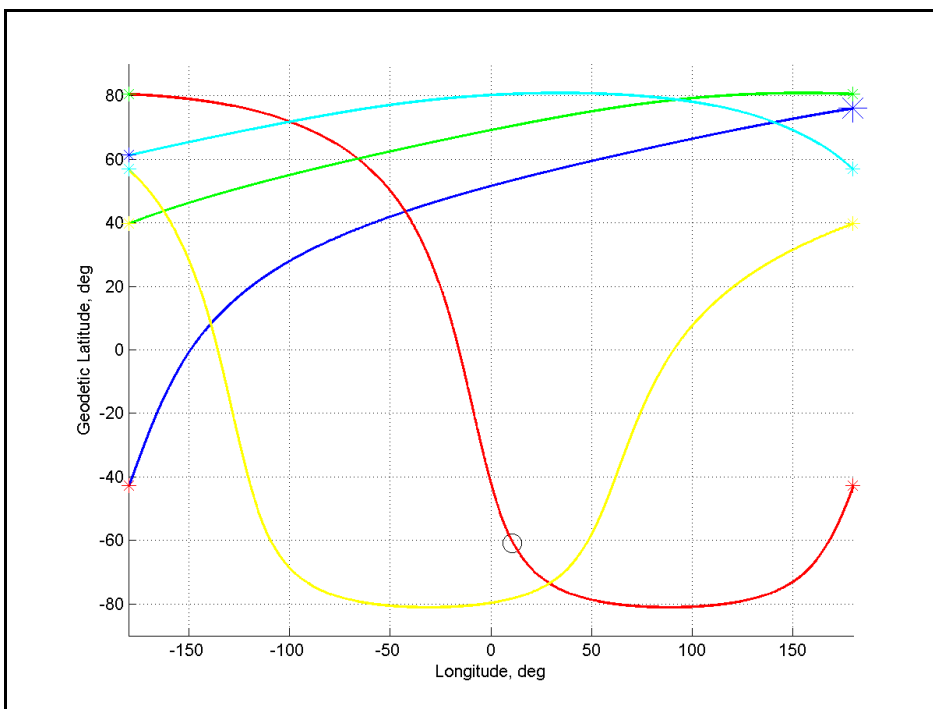
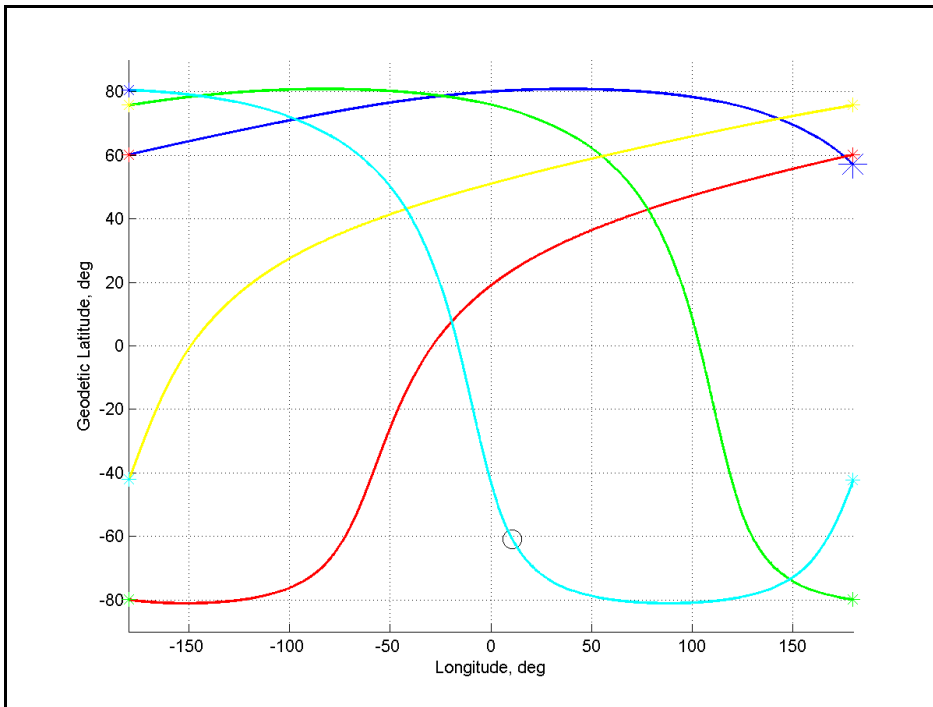
Figures 4-4a and 4-4b: Candidate Science Orbit - Longitude and Latitude.

The spacecraft's tracks are obtained by plotting the Planetodetic Latitude with Longitude. Consecutive plots of five (5) track segments are shown in Figures 4-5a and 4-5b. Each track segment comprises the spacecraft's motion in longitude, continually decreasing from +180 to -180 degrees. 360 degrees is added to the longitude (during computation) in order to begin a new track segment at +180 degrees. Multiple segments are drawn on the same plot in order to discern any patterns in the tracks. The location of arrival - described by the initial orbital elements - is marked with a "*" in Figure 4-5a; and marked with "O" on subsequent figures to maintain reference with Figure 4-5a.

The colors: blue, red, green, yellow, and cyan indicate the 1st, 2nd, 3rd, 4th, and 5th track segment, respectively on each plot. We observe that the 8th section after arrival - in green, Figure 4-5b - passes over a location close to the initial periapse point. It is possible that every seven (7) track sections are nearly repeating. The 15th - Figure 4-5c, cyan - and 22nd track sections - Figure 4-5d, red - confirm the ongoing pattern of nearly repeating tracks. Track segments 16-20 ("Set 3") are omitted from the plot ordering. Figure 4-6 shows every 7th track, which indicates that the spacecraft passes over a location close to the initial periapse longitude and latitude every seven cycles of longitude (+180 to -180 degrees). The numerical integration was extended to 90 days in order to visualize spacecraft tracks, while acknowledging that the risk of numerical error is greater than that of the 30-day numerical integration.



Figures 4-5a and 4-5b: Candidate Science Orbit - Tracks Set 1 and Set 2.



Figures 4-5c and 4-5d: Candidate Science Orbit - Tracks Set 3 and Set 5.

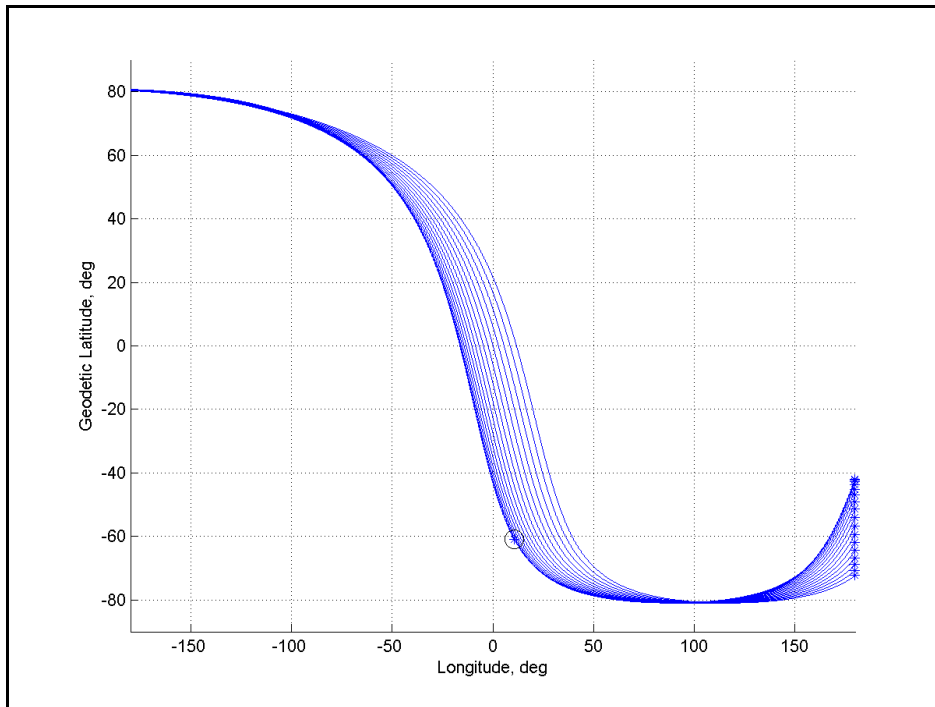


Figure 4-6: Candidate Science Orbit - Nearly Repeating Tracks.

The orbital radius at which the spacecraft crosses the equatorial plane requires cautious planning. The Voyager-2 spacecraft aided in the discovery of tens of Uranus' satellites, and revealed a complex structure of dark, dusty rings about Uranus never before seen. Design of the Science Orbit must minimize risks presented by the array of obstructions. Tables 4-5 and 4-6 show Uranus' known satellites and rings [NSSDC] within the periapse and apoapse distances of the candidate Science Orbit. Miranda is the largest satellite inside the candidate Science Orbit at **235 km** radius; the satellite Ariel (**582 km** radius, not included in Table 4-5) orbits just outside apoapse of the candidate Science Orbit, albeit in the equatorial plane. All other satellites in Table 4-5, orbiting between **49,000 to 98,000 km**, are **less than 100 km** in radius. Uranus' known ring system lies between **41,000 to 52,000 km** orbital radius. The dusty Epsilon ring is the

widest ring in the region, uncertainty in its width estimates prompts greater design consideration than do the other minor Uranian rings. All of the satellites and rings lie in nearly circular, equatorial orbits with the exception of Miranda (**4.22 degrees** inclination). Ring widths are shown in Table 4-6 in lieu of orbital inclination.

Uranian Satellite	Semi-major Axis, km	Inclination, deg	Eccentricity
Miranda	129,390	4.22	0.0027
Cordelia	49,770	0.08	0.0003
Ophelia	53,790	0.10	0.0099
Bianca	59,170	0.19	0.0009
Cressida	61,780	0.01	0.0004
Desdemona	62,680	0.11	0.0001
Juliet	64,350	0.07	0.0007
Portia	66,090	0.06	0.0000
Rosalind	69,940	0.28	0.0001
Cupid	74,800	(unknown)	(unknown)
Belinda	75,260	0.03	0.0001
Perdita	76,400	(unknown)	(unknown)
Puck	86,010	0.32	0.0001
Mab	97,700	(unknown)	(unknown)

Table 4-5: Uranian Satellites Inside the Candidate Science Orbit. ²⁵

²⁵Table 4-5 Reference:

NASA Goddard Space Flight Center, National Space Science Data Center (2010). Uranus Satellite Fact Sheet [*Online Data Sheet*]. Retrieved From: <http://nssdc.gsfc.nasa.gov/planetary/factsheet/uraniansatfact.html>

Uranian Ring	Semi-major Axis, km	Width, km	Eccentricity
Epsilon	51,149	20-96	0.0079
6	41,837	1.5	0.0010
5	42,234	~2	0.0019
4	42,571	~2	0.0011
Alpha	44,718	4 to 10	0.0008
Beta	45,661	5 to 11	0.0004
Eta	47,176	1.6	(unknown)
Gamma	47,627	1 to 4	0.0011
Delta	48,300	3 to 7	~0
Lambda	50,024	~2	(unknown)

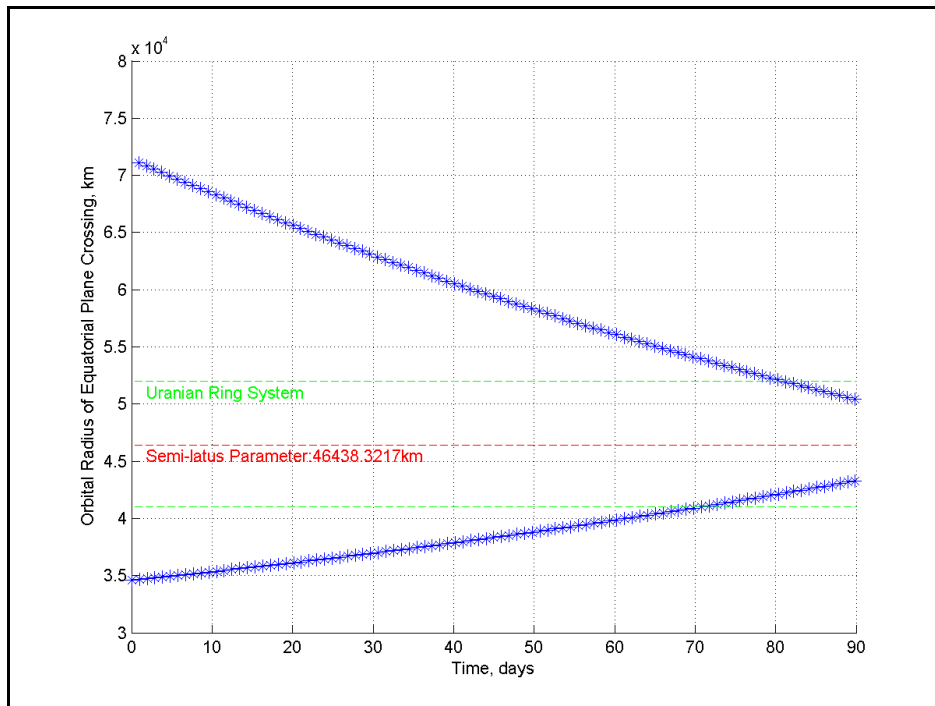
Table 4-6: Uranian Rings Inside the Candidate Science Orbit. ²⁶

Figure 4-7 shows the orbital radius of each equatorial plane crossing in the first 90 days after arrival. Initially in the candidate Science Orbit, Upsilon-1 crosses the equatorial plane at approximately **35,000 km** ascending and **72,000 km** descending. As the orbit precesses, the orbital radius of equatorial crossing, ascending and descending, should converge to the semi-latus parameter of nearly **46,500 km**. It is advisable to adjust the orbit before this occurs, however, as the initial crossing altitudes avoid the Uranian ring system entirely. The initial descending crossing altitude avoids all Uranian satellites listed in Table 4-5; while the ascending crossing altitude lies within a **5,000 km** gap between Rosalind and Cupid. Further work in Science Orbit design could incorporate J_3 effects with respect to "Frozen Orbits" [Tapley, Schutz, and Born; 2004] - in order to minimize orbit precession. However, some compromise must be made, as the spacecraft shall scan slowly over longitude to estimate the location of Uranus' magnetic

²⁶Table 4-6 Reference:

NASA Goddard Space Flight Center, National Space Science Data Center (2010). Uranus Rings Fact Sheet [*Online Data Sheet*]. Retrieved From: <http://nssdc.gsfc.nasa.gov/planetary/factsheet/uranringfact.html>

poles. Upsilon-1's Science Orbit is the heart of the design effort in mission operation stages, and merits extensive further examination.



**Figure 4-7: Candidate Science Orbit -
Orbital Radius of Equatorial Plane Crossings.**

Finally, Figure 4-8 shows full track coverage of the candidate Science Orbit in the 90-day numerical integration. The Science Orbit spans a wide range of longitudes, latitudes, and orbital altitudes; conducive to the planetary magnetic field measurement mission. Uranus' magnetic poles (from its dipole tilt of nearly 60 degrees) may be located near 30 degrees latitude (unknown longitude). The tracks do precess slowly over those latitudes, providing acceptable coverage in the southern hemisphere. Tracks more nearly repeat in the northern hemisphere where the orbit reaches apoapse, mitigating statistical estimation errors at the highest altitudes. In conclusion, initial estimates and

simulations on the candidate Science Orbit satisfy mission objectives and constraints, and mitigates risks associated with Uranus' satellites and ring system, at the current point in the design.

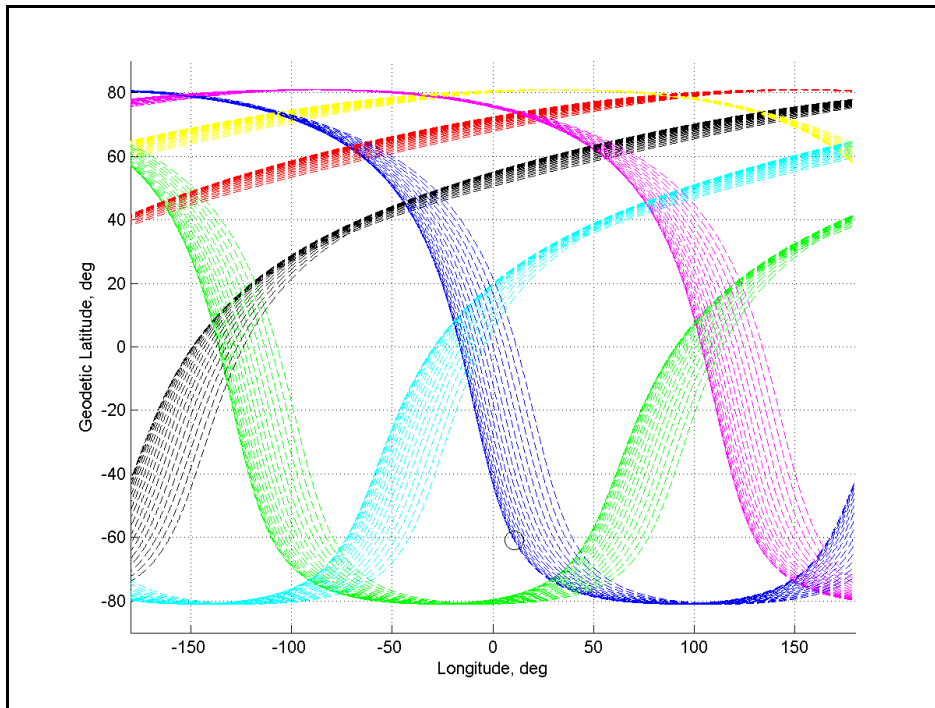


Figure 4-8: Candidate Science Orbit - Full Track Coverage.

4.3 LAUNCH WINDOW AND SCIENCE WINDOW

4.3.1 Concept

The Project Upsilon spacecraft shall launch on a single NASA EELV series, Delta IV-Heavy launch vehicle, utilizing one or more gravity assists to reach Uranus. A 6-year period from 2018 to 2023 was considered as the initial design space [McAdams, Scott, Dankanvich, and Russell; 2011] for the interplanetary problem. Five (5) trajectory configurations were examined: Earth-Jupiter-Uranus (EJU), Earth-Saturn-Uranus (ESU), Earth-Jupiter-Saturn-Uranus (EJSU), Earth-Earth-Jupiter-Uranus (EEJU), and Earth-Earth-Saturn-Uranus (EESU). Earth, Jupiter, and Saturn were considered for gravity assists. Interplanetary trajectory planning assumed a single arrival burn at Uranus made by the Project Upsilon spacecraft, with all other energy requirements satisfied by the launch vehicle and assisting planets. The "one-burn" model was chosen in order to reduce complexity of the spacecraft propulsion system, at this notional stage of design. Flyby ΔV is weighted heavily in order to discern "un-powered gravity assist" opportunities.

The Trajectory Configuration Tool, developed by Marty Brennan (in MATLAB), was extensively leveraged in this part of the design effort. The author sincerely acknowledges Marty Brennan for providing the TRACT code, as well as providing guidance on modifying the code to fit the needs of this work. This report section describes the design space of the interplanetary trajectory to Uranus, and the method used to obtain the candidate Launch Window, Science Window, and Science Orbit.

4.3.2 Trajectory Configuration Tool - TRACT

TRACT combines concepts of patched conics, Lambert's Problem, and MATLAB built-in unconstrained and constrained optimization routines ("fminunc", "fmincon", and "fminsearch") into a flexible initial mission planning tool [Brennan, 2011]. TRACT includes a library of MATLAB sub-functions for various orbital mechanics calculations, catalogues the NASA Jet Propulsion Laboratory planetary ephemeris [NASA JPL Solar System Dynamics, 2014], and manages user-chosen file printouts.

Generally, users choose the following parameters for the interplanetary trajectory problem: 1) optimization method; 2) output contents and media; 3) Julian date of launch; 4) interplanetary nodes; 5) initial estimates of flight times between nodes; 6) launch site latitude; 7) launch vehicle capability and departure parking orbit, 8) initial estimates of flyby periapse at nodes; and 9) orbital elements of the arrival parking orbit. TRACT usually fixes the user's estimate of semi-major axis, eccentricity, and inclination of the arrival parking orbit; and optimizes right ascension of Ascending Node, and argument of periapse. The arrival mean anomaly is fixed at zero, as periapse captures are assumed. The Nelder-Mead "Simplex" optimization routine was chosen for this problem. The simplex method operates independently of implicit derivatives of each parameter, in solving an n-dimensional optimization problem [Press, 2007; Lagarias et al., 1998]. Derivation and discussion of this method is outside of the author's knowledge base, and the scope of this report.

4.3.3 Figures of Merit

The TRACT code was initially used to compare the applicability and performance of EJU, ESU, EJSU, EEJU, and EESU node configurations within the nominal launch period of 2018-2023. The following design Figures of Merit (FOM) were used to quantify the choice of interplanetary node configuration. Delta IV-Heavy launch vehicle performance, and launch parking orbit, were given by the Delta IV Payload Planners Guide [United Launch Alliance, 2007]. The TRACT code was modified to loop for one Earth departure each day at 8:00 A.M. UTC during 2018-2023. Mid-course maneuvers, or deep space maneuvers, were not considered in the trajectory configuration.

Total Interplanetary Trajectory ΔV : Primary optimization result of TRACT. This value, to be minimized, is the sum of all orbital maneuver ΔV required at each node in the interplanetary trajectory.

Planetary Flyby ΔV : Sum of ΔV required during planetary flyby; if this value is nonzero, then the planetary flyby in question is considered a "powered gravity assist". "Un-powered gravity assists" were assigned higher merit in the optimization.

Interplanetary Flight Time: Time required to travel from Earth to Uranus. The flight time is graded with respect to Uranus' northern summer solstice in 2028. The spacecraft shall arrive as close to the solstice event as possible to observe atmospheric insolation effects of the Sun's heating.

Earth Departure C3 Energy: Square of the hyperbolic excess velocity upon leaving Earth's sphere of influence. The C3 energy is graded with respect to the heliocentric Hohmann transfer hyperbolic excess velocity to Jupiter or Saturn. In the case of an Earth-Earth node configuration (EEJU and EESU), the C3 energy is graded with respect to the heliocentric 180-degree phasing maneuver at Earth's orbital radius.

Uranus Arrival ΔV : Magnitude of the orbital maneuver required for capture at Uranus. This value, to be minimized, is directly related to the mass distribution of the Upsilon-0 Propulsion Module, as well as mass allotted to the Upsilon-1 Science Orbiter and Upsilon-2 Atmosphere Probe.

Arrival Orbital Elements: Right ascension of Ascending Node, and argument of periapse, as optimized by TRACT. Greater stability of these orbital elements within a candidate launch window suggests consistency in the interplanetary trajectories generated by TRACT, thusly receiving a higher grade.

The Earth-Jupiter-Uranus node configuration was selected based on the above criteria. As the Synodic Period between Earth and Jupiter (based on their respective orbital periods about the Sun) is approximately 13 months, several candidate Launch Windows were found in 2018-2023. The EJU selection is further detailed in discussion of the TRACT results. One additional FOM - the Observation Angle - was used to distinguish the various launch windows. The candidate Science Window - most simply, the time period during which the Project Upsilon spacecraft remain on the same side of the Sun with Earth, facilitating deep space communications and data transfer - was established with this analysis. The candidate Science Window is defined at the conclusion of this report section.

Observation Angle: Angle at which Earth lags Uranus in counterclockwise orbital motion about the sun; in a heliocentric, non-rotating, inertial reference frame; viewed from a point in the direction normal to the Ecliptic plane. For instance, an Observation Angle of zero (0) indicates that the inertial position vector from the Solar System Barycenter to the Earth is in the same direction as that to Uranus. 150 degrees

was taken as the optimal Observation Angle, as Earth would spend approximately five months trailing Uranus, and another five months leading Uranus, where the communication path is not blocked by the Sun. Such a configuration would yield a 10-month nominal Science Window after the spacecraft arrive at Uranus. The "150-degree lag" configuration is a conservative estimate of a viable Science Window - the author's limited knowledge in the Sun's effects on deep space communications prompted this choice. The first Science Window may begin as soon as the Project Upsilon spacecraft arrive at Uranus, and may not be as long as the full 10 months. All subsequent Science Windows, however, would span the full 10 months.

J2000 was taken as the initial state-time of each planet in our solar system. The mean motion of each planet, about the Solar System Barycenter, was propagated from J2000 to the time of arrival as generated by TRACT. All J2000 data were obtained from the NASA Jet Propulsion Laboratory, Horizons database. The planets' motions were verified with the Horizon system's prediction of future ephemeris. Table 4-7 shows the J2000 positions and mean motions of Earth and Uranus, in the International Celestial Reference Frame (ICRF) [Ma et al., 1998].

Parameter	Value	Unit
Earth X Position	-0.184272	AU
Earth Y Position	0.964446	AU
Earth Z Position	0.000202	AU
Earth Mean Motion	0.985647	deg/day
Uranus X Position	14.4247	AU
Uranus Y Position	-13.7371	AU
Uranus Z Position	-0.237935	AU
Uranus Mean Motion	0.011769	deg/day

**Table 4-7: J2000 State of Earth and Uranus,
Relative to the Solar System Barycenter.**

4.3.4 TRACT Results - Node Configuration Selection

The following weighting was assigned to the Planetary Flyby ΔV , Interplanetary Flight Time, Uranus Arrival ΔV , and Earth Departure C3 Energy FOM. The sum of the weighted FOM comprised a node configuration Performance Index (PI) to be minimized. Note that the data for categories #2, #3, and #4 below is first normalized by the maximum quantity encountered in the simulation, and then multiplied by specified weight. For instance, an Arrival Time Past Solstice (calculated from Interplanetary Flight Time FOM) of 20 years for one particular trajectory, is normalized to 0.5 for a maximum IFT of 40 years encountered, for a particular node configuration.

1) Every **1 km/s** of Planetary Flyby ΔV is multiplied by the weight **1000**, from the rationale discussed in 4.3.1 "Concept".

2) Every **1 year** the quantity (Date of Launch)+(Interplanetary Flight Time), is past the Uranus northern summer solstice (assumed on January 1, 2028); and then is multiplied by the weight **4.0**.

3) Every **1 km/s** of Uranus Arrival ΔV is multiplied by the weight **3.0**.

4) Every $1 \text{ km}^2/\text{s}^2$ of Earth Departure C3 Energy exceeding the nominal value stated in the FOM definition is multiplied by the weight **2.0**.

5) Arrival Orbital Elements were not assigned a weight and did not constitute a part of the node configuration PI; these were plotted with the optimized launch date (found with TRACT) , and examined for stability to further support selection of a particular node configuration.

In reference to data provided by McAdams et al. (2011), the following dates within the nominal launch period of 2018-2023 were selected for each node configuration. The EJU node configuration was simulated for 2018-2020; ESU for 2021-2023; EJSU for 2019-2021; EEJU for 2018-2020; and EESU for 2021-2023. Processing speed of the computer and time required conduct this search were major limitations of this work. Each run of 365 TRACT simulations (one simulation for each day, for one year; 366 for a leap year) with the Nelder-Mead simplex method required between 8-12 hours.

Figures 4-9a to 4-9e show the PI distribution for each trajectory node configuration. The Total PI - not including Earth Departure C3 Energy - is shown in blue, Planetary Flyby ΔV PI is shown in red, and Flight Time PI is shown in green. Total PI of less than 10 is desired for consideration. Next, a Planetary Flyby ΔV PI of nearly zero further narrows available launch dates. Then, we search for a region where the Total PI and Flight Time PI remain nearly constant (without chaotic fluctuations), while satisfying the previous criteria at the same time. We search for a continuous period of at least several days that fits the above description, and the highlighted time span in the EJU PI distribution (Figure 4-9a) best satisfies the imposed constraints. A possible time space in the ESU PI distribution (Figure 4-9b) occurs in late 2021, but the Planetary Flyby ΔV PI fluctuates between zero and nonzero values. The EJSU PI distribution (Figure 4-9c)

also has no time spans where all of each PI remains stable. The EEJU PI distribution (Figure 4-9d) shows brief opportunities in 2018 and 2019, but provides little flexibility in launch date and time. Finally, note that the EESU PI distribution is represented on a scale from 0-1000, instead of 0-10 in the preceding figures. Planetary Flyby ΔV PI dominates the cost function in Figure 4-9e. The EESU node configuration would not be recommended for this particular nominal launch period, 2018-2023.

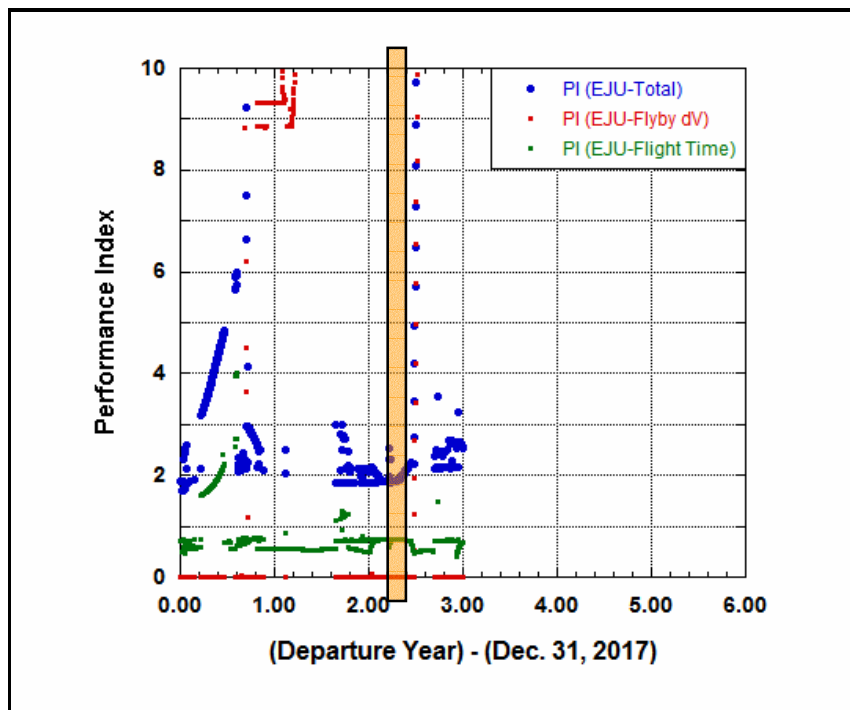
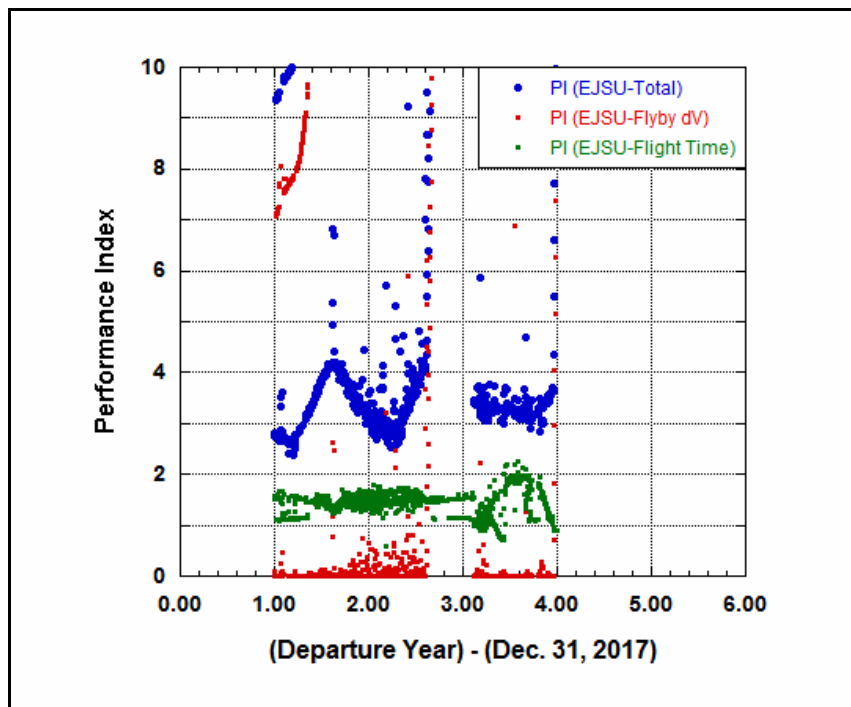
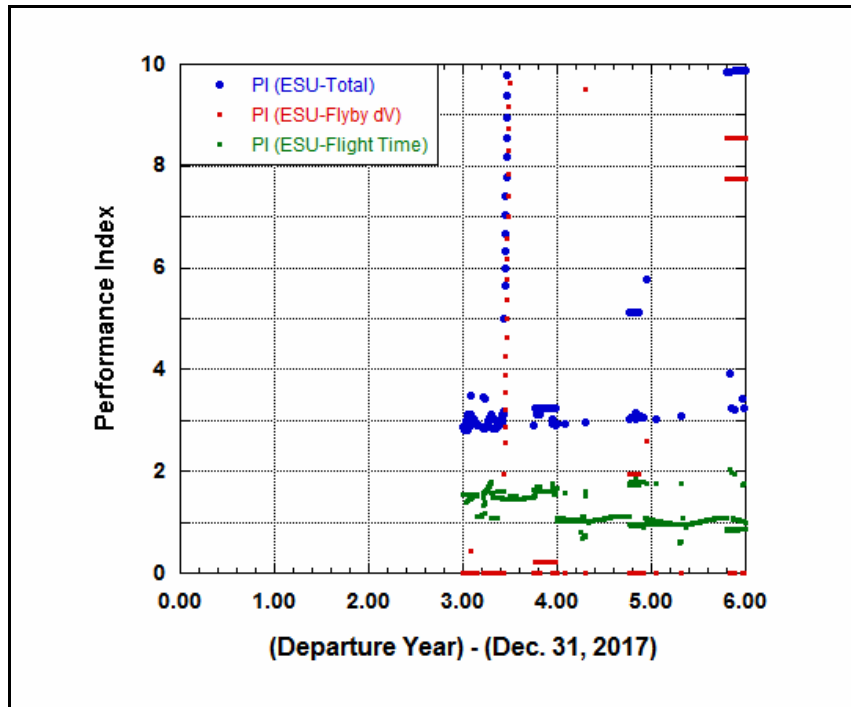
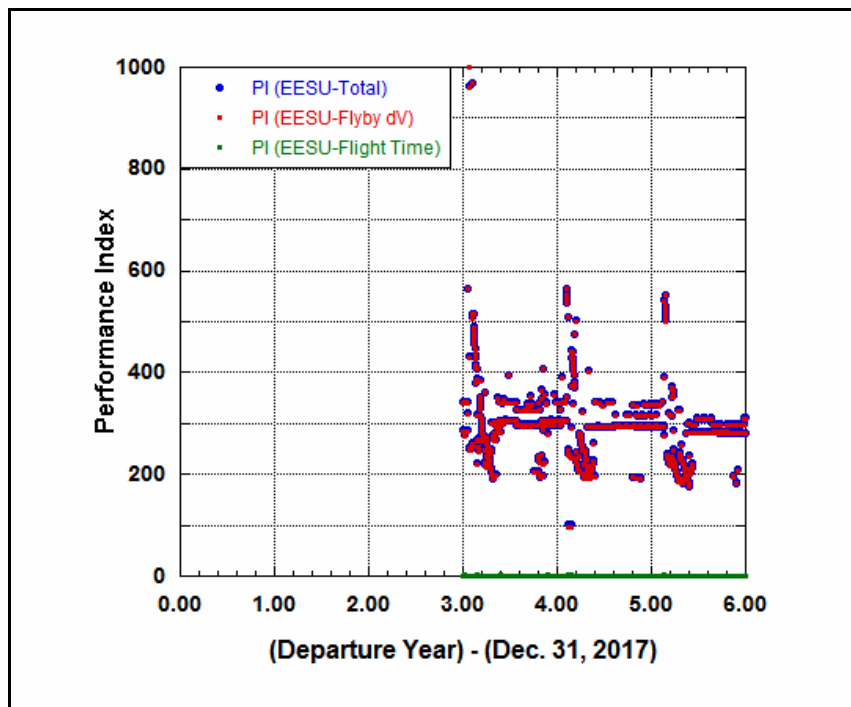
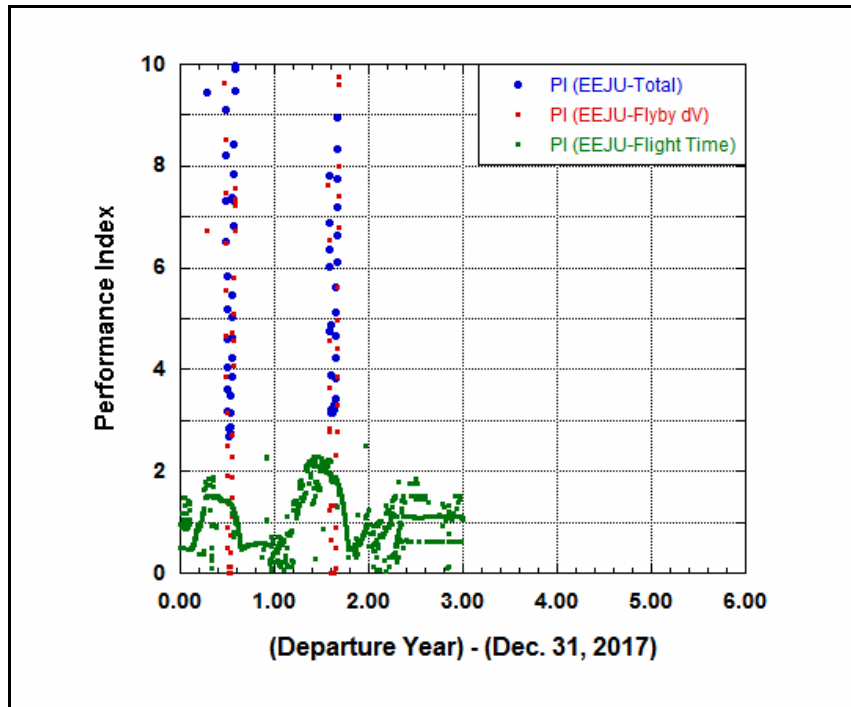


Figure 4-9a: Interplanetary Node Configuration Selection (INCS) - EJU TRACT PI Distribution.

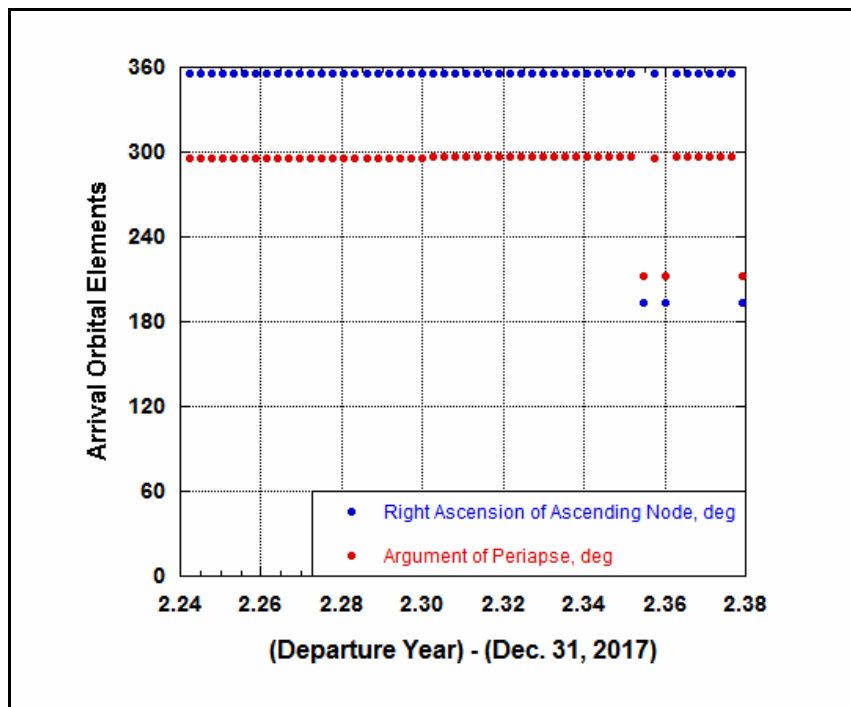
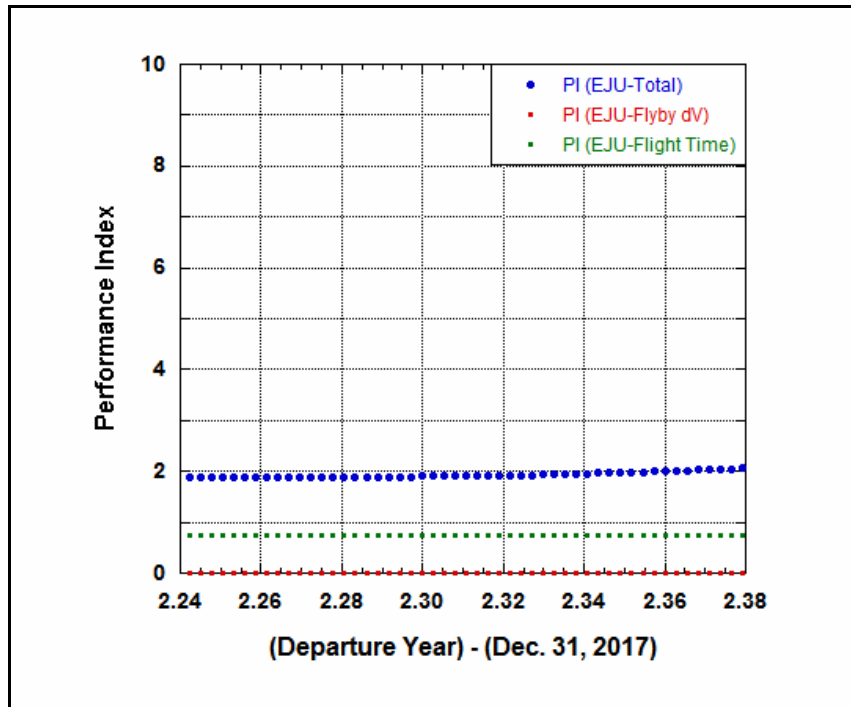


Figures 4-3b and 4-3c: INCS - ESU and EJSU TRACT PI Distribution.



Figures 4-3d and 4-3e: INCS - ESU and EJSU TRACT PI Distribution.

Examination of Figures 4-9a to 4-9e suggests that the EJU node configuration is best recommended for the interplanetary trajectory from Earth to Uranus. A 51-day candidate Launch Window was defined between **March 30 and May 19, 2020** at this point in the design. However, a further analysis with the Observation Angle FOM would show that this period is not recommended, instead a period one Synodic Period (again, 13 months) later. The current candidate Launch Window, though owning advantages in Earth Departure C3 Energy and Uranus Arrival ΔV , was deferred in favor of the candidate Launch Window described in the next section. Nonetheless, the EJU node configuration presented the most feasible interplanetary opportunity for the Project Upsilon mission among the five configurations, at minimized complexity with respect to number of interplanetary nodes and deep space maneuvers. Figures 4-10a and 4-10b show the EJU PI distribution between March 30 and May 19, 2020; along with the optimized arrival orbital elements ("OE" in Figure 4-10b) - Right Ascension of Ascending Node and Argument of Periapse.



Figures 4-10a and 4-10b: INCS - EJU PI Distribution and Arrival OE.

4.3.5 TRACT Results - Launch Window and Science Window Selection

Earth-Jupiter-Uranus, without deep space maneuvers, was selected as the interplanetary node configuration for the Project Upsilon mission. The same TRACT simulation was extended throughout the 2018-2023 period, and modified to include calculation of the Observation Angle FOM. Figure 4-11 shows the Total PI and Observation Angle of the 51-day period between March 30 and May 19, 2020 in a "double-y" plot. Total PI values, shown in blue, are associated with the left-most vertical axis; while Observation Angle values, shown in magenta, are associated with the right-most vertical axis.

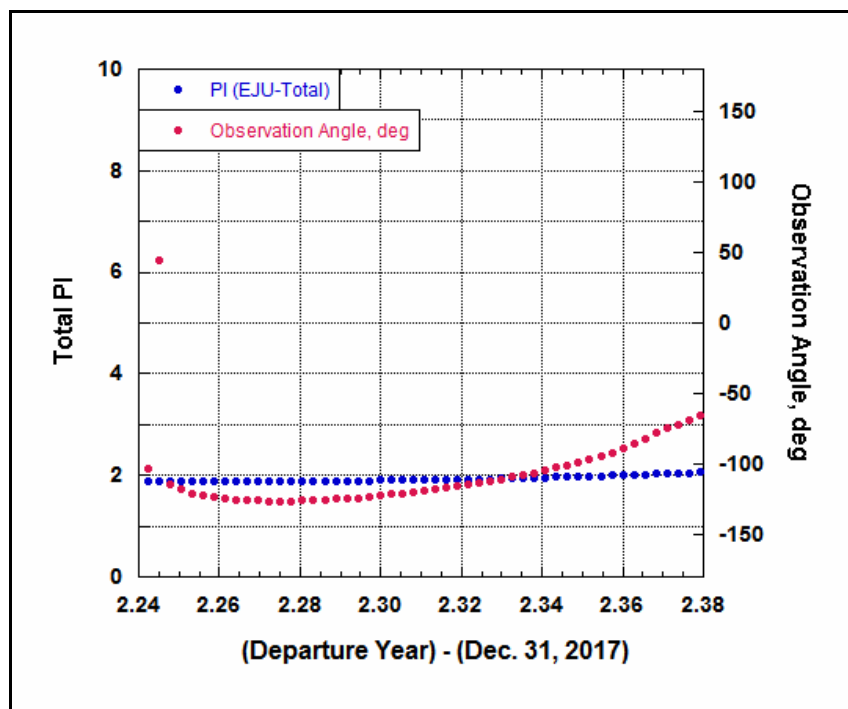


Figure 4-11: Launch Window and Science Window Selection - EJU Total PI and Observation Angle, 2020 Launch Window.

Total PI for optimized interplanetary trajectories launching between March 30 and May 19, 2020 range between **1.87 and 2.06**. Observation Angles range between **-65 and -127 degrees**. Indicating that the Earth leads Uranus in the heliocentric frame by 65 to 127 degrees, upon arrival at Uranus. The first Science Window, at maximum, would span less than three (3) months. Alternative candidate Launch Windows in years 2021, 2022, or 2023 may yield longer initial Science Windows. Years 2018 and 2019 were not considered due to mission scheduling constraints defined in Chapter 1 "Mission Scope" - it would be more advisable to apportion more time (rather than less time) for the research and development mission phases, regardless of the amount of heritage employed.

An alternative candidate Launch Window was found between **April 28 and June 17, 2021** - concurrent with expectation due to the 13-month Synodic Period between Earth and Jupiter. Although inertial orbit constraints differ between the two candidate Launch Windows (as Jupiter's position has changed), a 51-day period was chosen for the most direct comparison possible. The nominal 51-day period may be further truncated to define the true candidate Launch Window. Figure 4-12 shows the Total PI and Observation Angle for the 2021 Launch Window, in the same "double-y" format.

Total PI for optimized interplanetary trajectories launching between April 28 and June 17, 2021 range between **1.88 and 1.93**. Observation Angles range between -135 and 179 degrees. However, the majority (45 of 51) Observation Angles lie between **9 and 60 degrees**. Indicating that the Earth trails Uranus in the heliocentric frame by 9 to 60 degrees, upon arrival at Uranus. Here, the first Science Window may be as long as seven (7) months. The average Observation Angle among the 45 positive values is **46.6 degrees**, which implies Earth would travel slightly more than **196.6 degrees** before it leads Uranus by 150 degrees. The Earth would take approximately **200 days** to travel through the above angle, this amount of time is defined as the candidate Science

Window. The years 2022 and 2023 were examined as a check for choice of the 2021 opportunity, but no viable windows were found.

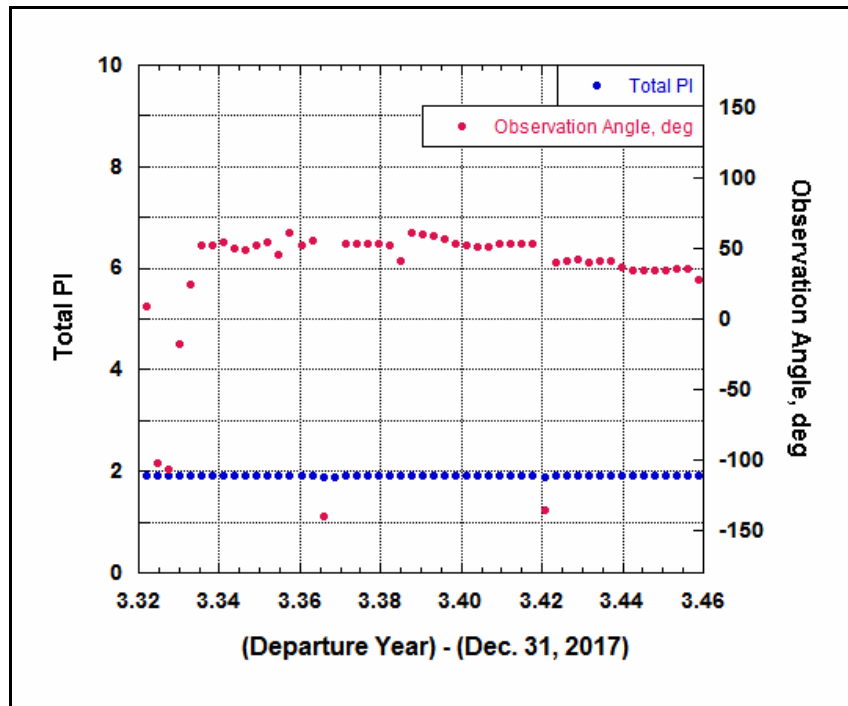


Figure 4-12: Launch Window and Science Window Selection - EJU Total PI and Observation Angle, 2021 Launch Window.

Finally, the Earth Departure C3 Energy was examined for the 2021 opportunity to further constrain our result. Figure 4-13 shows that the period between **May 2-13, 2021** offers C3 Energies most conducive to optimizing launch vehicle payload capability, as well as optimal Observation Angle. The minimum C3 energy required to reach Jupiter (in a back-of-the-envelope calculation), via an interplanetary Hohmann transfer satisfying rendezvous, is approximately **77.5 km²/s²** (which corresponds to hyperbolic excess velocity, or "V_∞", of about 8.80 km/s). The C3 Energies in the optimal period ranges

between **8.74 to km^2/s^2** and **18.8 km^2/s^2** exceeding the best possible Hohmann transfer C3 energy. C3 Energies rapidly increase outside of this period.

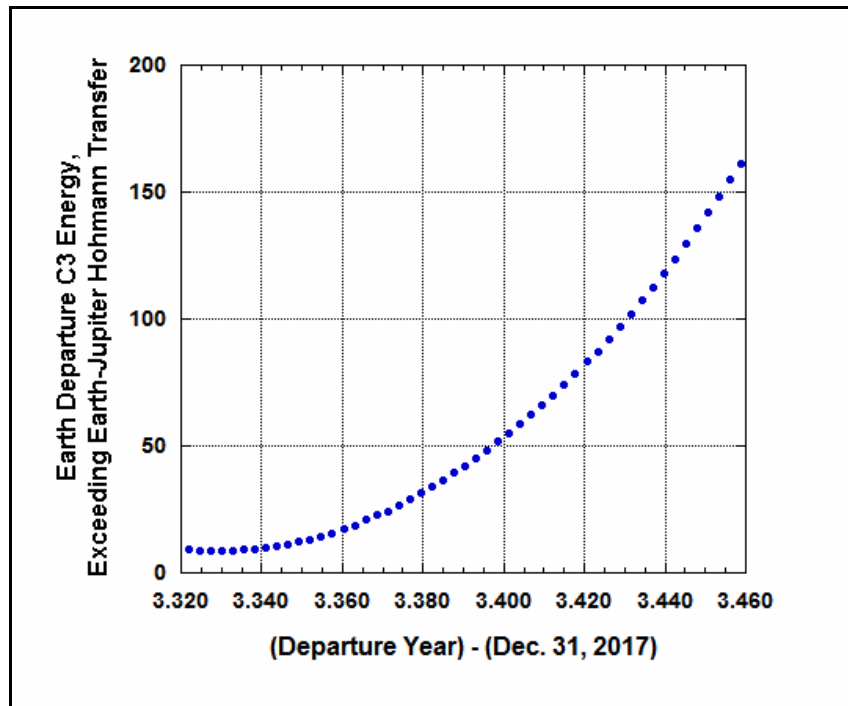


Figure 4-13: Earth Departure C3 Energy Exceeding Jupiter Hohmann Transfer C3 Energy, 2021 Launch Window.

In conclusion, a 12-day period between May 2-13, 2021 is defined as the candidate Launch Window. We assume a successful launch early in the candidate launch window at this point in the design. The Project Upsilon launch on a Delta IV-Heavy vehicle on May 5, 2021. The associated C3 energy is equivalent to V_{∞} of **9.35 km/s**, in turn corresponding to nearly **1520 kg** of payload capability on the Delta-IV Heavy launch vehicle. The upper design limit of 1520 kg is a critical constraint on design of the three Project Upsilon spacecraft.

The spacecraft reach their closest approach of Jupiter on February 19, 2023 (T+655 days); and reach periapse of the candidate Science Orbit on December 13, 2041 (T+6872 days), where orbital capture about Uranus commences. The approximately 200-day first Science Window begins December 13, 2041, and ends July 19, 2042. Taking one "month" as 31 days, the communication path would be blocked for 62 days in every Synodic Period between Uranus' and Earth's orbits about the Sun. The Earth-Uranus Synodic Period is 370 days, thus each subsequent Science Window spans 308 days. The second Science Window begins September 20, 2042, and ends July 25, 2043. The third Science Window, commencing the Project Upsilon extended mission, begins September 26, 2043.

4.4 ESTIMATION METHOD

4.4.1 Concept

This report section describes a statistical estimation method that may be applied to the Upsilon-1 Science Orbiter's planetary magnetic field measurement mission. The goal is to measure, then proceed to model, Uranus' planetary magnetic field, in three quantities: Intensity (F), Inclination (I), and Declination (D); as a function of Planet Centric Latitude (analogous to geographic latitude, for a planet other than Earth - ϕ_G) and orbital radius (r). In addition, a constant scalar Scaling Factor (B_o) comparing Uranus' planetary magnetic field to Earth's may be estimated.

Uranus' planetary magnetic field is peculiar in its tilt and offset, as compared to an ideal dipole field. The magnetic polar axis is tilted approximately 59 degrees, and offset nearly one-third ($1/3$) planetary radius from the planetary rotation axis. While Intensity may be obtained about any three-dimensional reference frame, the Inclination and Declination measurements require careful selection of frame. Location of at least one Magnetic Pole is necessary prior to calculating Inclination and Declination. Therefore, it may be appropriate to devise two Science Phases, and two associated estimation algorithms.

The first estimation shall approximate the location of the Magnetic North Pole based on Intensity, and refine *a priori* estimates of Uranus' gravity field; while the second estimation shall further determine the Inclination and Declination. The spacecraft's orbit shall be determined in the Planetary Inertial reference frame, while Inclination and Declination shall be determined in the Planetary Magnetic reference frame. The spacecraft shall acquire raw magnetic field line measurements in its fixed body frame.

4.4.2 Science Phase I - Locate Magnetic Pole

Science Phase I shall accomplish the following objectives, which are understood as minimum science benchmarks for this phase.

- 1) Determine the spacecraft's orbit.
- 2) Refine *apriori* estimates of Uranus' gravity field.
- 3) Estimate the location of Uranus' Magnetic North Pole.

The state vector for Science Phase I contains the position and velocity vectors of the spacecraft in the PIRF, the Uranus gravitational constant (μ), the Second-degree zonal harmonic (J_2), and the Fourth-degree zonal harmonic (J_4). The subscript "I" is introduced to refer to Science Phase I; the state vector for this phase is 9-by-1.

$$\vec{X}_I(t) = \begin{bmatrix} \vec{r} \\ \vec{v} \\ \mu \\ J_2 \\ J_4 \end{bmatrix} \quad \dot{\vec{X}}_I = \begin{bmatrix} \vec{v} \\ \ddot{\vec{r}} \\ 0 \\ 0 \\ 0 \end{bmatrix} = f(\vec{X}_I, t) \quad [1]$$

The force model is simplified to include only the Second-degree and Fourth-degree zonal harmonic contributions. The science orbit is high enough such that atmospheric drag is negligible, solar (to a lesser extent) and planetary radiation (to a greater extent) are not included, and third-body perturbations are not included. Tidal resonance due to Uranus' rotation is not included; and mean motion resonances with Uranus' satellites are not included. The two-body gravitational potential is truncated to:

$$\Phi(r) = -\frac{\mu}{r} + \frac{\mu}{r} \left(\frac{R}{r}\right)^2 J_2 P_2 \{\sin(\phi_G)\} + \frac{\mu}{r} \left(\frac{R}{r}\right)^4 J_4 P_4 \{\sin(\phi_G)\} + \dots \quad [2]$$

where Uranus' planetary radius of approximately 25559 km is represented by capital (R). Where (ϕ_G) is the Planet Centric Latitude and (r) is the orbital radius; sine of the Planet Centric Latitude is ratio of the z-coordinate to the orbital radius. (P_2) and (P_4) are Legendre Polynomials.

$$P_2 \{ \sin(\phi_G) \} = \frac{3}{2} \sin^2(\phi_G) - \frac{1}{2} \quad [3a]$$

$$P_4 \{ \sin(\phi_G) \} = \frac{35}{8} \sin^4(\phi_G) - \frac{15}{4} \sin^2(\phi_G) + \frac{3}{8} \quad [3b]$$

$$\sin(\phi_G) = \frac{z}{r} \quad [4]$$

Next, the spacecraft's gravitational acceleration is obtained. Let the acceleration in x-direction be represented by capital (L), the acceleration in y-direction be represented by capital (M), the acceleration in x-direction be represented by capital (N).

$$\ddot{\vec{r}} = \vec{\nabla} \cdot \Phi = [L \quad M \quad N]^T \quad [5]$$

$$\begin{aligned} L &= \mu \left\{ \frac{-x}{r^3} - \frac{3J_2R^2}{2} \frac{x}{r^5} + \frac{15J_2R^2}{2} \frac{xz^2}{r^7} + \frac{15J_4R^4}{8} \frac{x}{r^7} - \frac{105J_4R^4}{4} \frac{xz^2}{r^9} + \frac{315J_4R^4}{8} \frac{xz^4}{r^{11}} \right\} \\ M &= \mu \left\{ \frac{-y}{r^3} - \frac{3J_2R^2}{2} \frac{y}{r^5} + \frac{15J_2R^2}{2} \frac{yz^2}{r^7} + \frac{15J_4R^4}{8} \frac{y}{r^7} - \frac{105J_4R^4}{4} \frac{yz^2}{r^9} + \frac{315J_4R^4}{8} \frac{yz^4}{r^{11}} \right\} \\ N &= \mu \left\{ \frac{-z}{r^3} - \frac{9J_2R^2}{2} \frac{z}{r^5} + \frac{15J_2R^2}{2} \frac{z^3}{r^7} + \frac{75J_4R^4}{8} \frac{z}{r^7} - \frac{175J_4R^4}{4} \frac{z^3}{r^9} + \frac{315J_4R^4}{8} \frac{z^5}{r^{11}} \right\} \end{aligned} \quad [6]$$

Equations [5] and [6] are placed inside [1], thus the time rate of change of the state vector has been written as a function of the state vector parameters. The dynamical system in Science Phase I has been linearized. Next, the State Propagation Matrix - the rate of change of the force model with respect to state parameters, is derived. The State

Propagation Matrix for Science Phase I is 9-by-9. The same force model will be used for both Science Phases, hence no subscript.

$$A_I = \frac{\partial f}{\partial X_I} = \left\{ \begin{array}{ccc} \frac{\partial f_1}{\partial X_1} & \cdots & \frac{\partial f_1}{\partial X_n} \\ \cdots & \cdots & \cdots \\ \frac{\partial f_n}{\partial X_1} & \cdots & \frac{\partial f_n}{\partial X_n} \end{array} \right\}_I = \left\{ \begin{array}{ccc} \frac{\partial \dot{x}}{\partial x} & \cdots & \frac{\partial \dot{x}}{\partial (J_4)} \\ \cdots & \cdots & \cdots \\ \frac{\partial (J_4)}{\partial x} & \cdots & \frac{\partial (J_4)}{\partial (J_4)} \end{array} \right\}_I \quad [7]$$

Each element of the State Propagation Matrix is zero unless otherwise stated. The first three elements of (f) comprise the spacecraft's velocity components - (\dot{x}), (\dot{y}), and (\dot{z}) respectively. Therefore, Rows 1-3 are zero vectors except for:

$$A_I(1, 4) = \frac{\partial \dot{x}}{\partial \dot{x}} = 1 \quad [8]$$

$$A_I(2, 5) = \frac{\partial \dot{y}}{\partial \dot{y}} = 1 \quad [9]$$

$$A_I(3, 6) = \frac{\partial \dot{z}}{\partial \dot{z}} = 1 \quad [10]$$

The spacecraft's acceleration (\ddot{r}) depends on all states except the 3 velocity components, so rows 4-6 each contain 6 non-zero elements.

$$A_I(4, 1) = \frac{\partial L}{\partial x} = \frac{L}{x} + \mu x \left\{ \frac{3x}{r^5} + \frac{15J_2R^2}{2} \frac{x}{r^7} - \frac{105J_2R^2}{2} \frac{xz^2}{r^9} \cdots \right. \\ \left. \cdots - \frac{105J_4R^4}{8} \frac{x}{r^9} + \frac{945J_4R^4}{4} \frac{xz^2}{r^{11}} - \frac{3465J_4R^4}{8} \frac{xz^4}{r^{13}} \right\} \quad [11a]$$

$$\begin{aligned}
A_I(4, 2) &= \frac{\partial L}{\partial y} = 0 + \mu x \left\{ \frac{3y}{r^5} + \frac{15J_2R^2}{2} \frac{y}{r^7} - \frac{105J_2R^2}{2} \frac{yz^2}{r^9} \dots \right. \\
&\quad \left. \dots - \frac{105J_4R^4}{8} \frac{y}{r^9} + \frac{945J_4R^4}{4} \frac{yz^2}{r^{11}} - \frac{3465J_4R^4}{8} \frac{yz^4}{r^{13}} \right\} \quad [11b]
\end{aligned}$$

$$\begin{aligned}
A_I(4, 3) &= \frac{\partial L}{\partial z} = 0 + \mu x \left\{ \frac{3z}{r^5} + \frac{45J_2R^2}{2} \frac{z}{r^7} - \frac{105J_2R^2}{2} \frac{z^3}{r^9} \dots \right. \\
&\quad \left. \dots - \frac{525J_4R^4}{8} \frac{z}{r^9} + \frac{1575J_4R^4}{4} \frac{z^3}{r^{11}} - \frac{3465J_4R^4}{8} \frac{z^5}{r^{13}} \right\} \quad [11c]
\end{aligned}$$

$$A_I(4, 7) = \frac{\partial L}{\partial \mu} = \frac{L}{\mu} \quad [12a]$$

$$A_I(4, 8) = \frac{\partial L}{\partial (J_2)} = \mu R^2 x \left\{ \frac{-3}{2r^5} + \frac{15z^2}{2r^7} \right\} \quad [12b]$$

$$A_I(4, 9) = \frac{\partial L}{\partial (J_4)} = \mu R^4 x \left\{ \frac{15}{8r^7} - \frac{105z^2}{4r^9} + \frac{315z^4}{8r^{11}} \right\} \quad [12c]$$

Row 5 is derived in a similar fashion to row 4:

$$\begin{aligned}
A_I(5, 1) &= \frac{\partial M}{\partial x} = 0 + \mu y \left\{ \frac{3x}{r^5} + \frac{15J_2R^2}{2} \frac{x}{r^7} - \frac{105J_2R^2}{2} \frac{xz^2}{r^9} \dots \right. \\
&\quad \left. \dots - \frac{105J_4R^4}{8} \frac{x}{r^9} + \frac{945J_4R^4}{4} \frac{xz^2}{r^{11}} - \frac{3465J_4R^4}{8} \frac{xz^4}{r^{13}} \right\} \quad [13a]
\end{aligned}$$

$$\begin{aligned}
A_I(5, 2) &= \frac{\partial M}{\partial y} = \frac{M}{y} + \mu y \left\{ \frac{3y}{r^5} + \frac{15J_2R^2}{2} \frac{y}{r^7} - \frac{105J_2R^2}{2} \frac{yz^2}{r^9} \dots \right. \\
&\quad \left. \dots - \frac{105J_4R^4}{8} \frac{y}{r^9} + \frac{945J_4R^4}{4} \frac{yz^2}{r^{11}} - \frac{3465J_4R^4}{8} \frac{yz^4}{r^{13}} \right\} \quad [13b]
\end{aligned}$$

$$\begin{aligned}
A_I(5,3) &= \frac{\partial M}{\partial z} = 0 + \mu y \left\{ \frac{3z}{r^5} + \frac{15J_2R^2}{2} \frac{z}{r^7} - \frac{105J_2R^2}{2} \frac{z^3}{r^9} \dots \right. \\
&\quad \left. \dots - \frac{525J_4R^4}{8} \frac{z}{r^9} + \frac{1575J_4R^4}{4} \frac{z^3}{r^{11}} - \frac{3465J_4R^4}{8} \frac{z^5}{r^{13}} \right\}
\end{aligned} \tag{13c}$$

$$A_I(5,7) = \frac{\partial M}{\partial \mu} = \frac{M}{\mu} \tag{14a}$$

$$A_I(5,8) = \frac{\partial M}{\partial (J_2)} = \mu R^2 y \left\{ \frac{-3}{2r^5} + \frac{15z^2}{2r^7} \right\} \tag{14b}$$

$$A_I(5,9) = \frac{\partial M}{\partial (J_4)} = \mu R^4 y \left\{ \frac{15}{8r^7} - \frac{105z^2}{4r^9} + \frac{315z^4}{8r^{11}} \right\} \tag{14c}$$

Row 6 is derived in a similar fashion to rows 4 and 5:

$$\begin{aligned}
A_I(6,1) &= \frac{\partial N}{\partial x} = 0 + \mu z \left\{ \frac{3x}{r^5} + \frac{45J_2R^2}{2} \frac{x}{r^7} - \frac{105J_2R^2}{2} \frac{xz^2}{r^9} \dots \right. \\
&\quad \left. \dots - \frac{525J_4R^4}{8} \frac{x}{r^9} + \frac{1575J_4R^4}{4} \frac{xz^2}{r^{11}} - \frac{3465J_4R^4}{8} \frac{xz^4}{r^{13}} \right\}
\end{aligned} \tag{15a}$$

$$\begin{aligned}
A_I(6,2) &= \frac{\partial N}{\partial y} = 0 + \mu z \left\{ \frac{3y}{r^5} + \frac{45J_2R^2}{2} \frac{y}{r^7} - \frac{105J_2R^2}{2} \frac{yz^2}{r^9} \dots \right. \\
&\quad \left. \dots - \frac{525J_4R^4}{8} \frac{y}{r^9} + \frac{1575J_4R^4}{4} \frac{yz^2}{r^{11}} - \frac{3465J_4R^4}{8} \frac{yz^4}{r^{13}} \right\}
\end{aligned} \tag{15b}$$

$$\begin{aligned}
A_I(6,3) &= \frac{\partial N}{\partial z} = \mu \left\{ \frac{-1}{r^3} + \frac{3z^2}{r^5} - \frac{9J_2R^2}{2r^5} + \frac{90J_2R^2}{2} \frac{z^2}{r^7} - \frac{105J_2R^2}{2} \frac{z^4}{r^9} \dots \right. \\
&\quad \left. \dots + \frac{75J_4R^4}{8r^7} - \frac{1575J_4R^4}{8} \frac{z^2}{r^9} + \frac{4725J_4R^4}{8} \frac{z^4}{r^{11}} - \frac{3465J_4R^4}{8} \frac{z^6}{r^{13}} \right\}
\end{aligned} \tag{15c}$$

$$A(6, 7) = \frac{\partial N}{\partial \mu} = \frac{N}{\mu} \quad [16a]$$

$$A_I(6, 8) = \frac{\partial N}{\partial (J_2)} = \mu R^2 z \left\{ \frac{-9}{2r^5} + \frac{15z^2}{2r^7} \right\} \quad [16b]$$

$$A_I(6, 9) = \frac{\partial N}{\partial (J_4)} = \mu R^4 z \left\{ \frac{75}{8r^7} - \frac{175z^2}{4r^9} + \frac{315z^4}{8r^{11}} \right\} \quad [16c]$$

Finally, since the Uranus gravitational constant, the Second-degree zonal harmonic, and the Fourth-degree zonal harmonic are assumed constant, Rows 7-9 are zero vectors. The State Propagation Matrix for Science Phase I has been derived. The state propagation matrix is used to integrate the State Transition Matrix.

$$\dot{\Phi} = A\Phi \quad [17]$$

Next, an appropriate suite of instruments must be chosen which produces multiple types of observations. Measurements must be acquired such that the dynamical system in Science Phase I is observable. The main challenge in developing an estimation method for this mission is the lack of ground-stations and other satellites. The payload allowance is extremely limited, which bounds the instruments' complexity, as well as data storage and transfer capability of the spacecraft. Using the spacecraft's attitude determination instruments for the added purpose of taking measurements for estimation, is a possible method.

Another challenge arises in the spacecraft's pointing requirements. The spacecraft's attitude may need to be fixed in the PIRF to ensure constant transformation to the PMRF, requiring 3-axis stabilization. If the spacecraft's attitude is fixed in the PIRF, communication hardware must be flexible enough to maintain contact with the

ground segment (on Earth). If possible, the inertial direction of acceleration - the direction from the spacecraft's center of mass to Uranus' center of mass - should be obtained over time.

Suppose the inertial direction of acceleration has been obtained to an acceptable degree of accuracy. Radio frequency emitters and Pseudo-random Number transmitters may determine the Range (ρ) and Range Rate ($\dot{\rho}$) of the spacecraft relative to Uranus' cloud tops - in the direction towards Uranus' center of mass. Star cameras and infrared cameras may determine the Apparent Size (s) and Magnitude (m , with regards to brightness) of Uranus. Finally, magnetometers measure the magnetic flux in the three axis directions of the spacecraft's body reference frame, the magnitude of components is the magnetic field Intensity.

In Science Phase I, the Observation Vector (Y) for estimation consists of range, range rate, apparent size, and apparent magnitude. Raw magnetic Intensity measurements (F) are obtained, but are not considered in the statistical orbit determination model, nor are they used in construction of the Information Matrix (H) during this phase. Hence, (F) is shown separately from the range, range rate, apparent size, and apparent magnitude in equation [18].

$$\vec{Y}_I = \begin{bmatrix} \rho \\ \dot{\rho} \\ s \\ m \\ - \\ F \end{bmatrix} = G(\vec{X}_I, t) + \vec{\epsilon} \quad [18]$$

The Observation Vector is related to the state parameters via the Observation Model equations (G). With our assumptions, Range is the distance between the

spacecraft and Uranus' cloud tops in the direction of Uranus' center of mass, and Range Rate is the time rate of change of that distance. A correction is made to Uranus' planetary radius due to its oblateness in [18], which introduces additional terms to both (ρ) and ($\dot{\rho}$). Let (k) represent the planetary Flattening Factor, approximately **1/43.616** for Uranus, let (C) represent the fraction containing (k).

$$r'(\phi_G) = R \left\{ 1 + \frac{(2k - k^2)}{(1 - k)^2} \sin^2(\phi_G) \right\}^{-\frac{1}{2}} \quad [19]$$

$$\rho = r - R \left\{ 1 + \frac{Cz^2}{r^2} \right\}^{-\frac{1}{2}} ; C = C(k) = \text{const.} \quad [20]$$

$$\dot{\rho} = \frac{(x\dot{x} + y\dot{y} + z\dot{z})}{r} + \frac{CR}{2} \left\{ 1 + \frac{Cz^2}{r^2} \right\}^{-\frac{3}{2}} \left\{ \frac{2z\dot{z}}{r^2} - \frac{2z^2(x\dot{x} + y\dot{y} + z\dot{z})}{r^4} \right\} \quad [21]$$

Apparent Size of Uranus may be used as an orbit determination measurement, provided the planet is viewed fully by the spacecraft's cameras. That is, the Apparent Size must be below some "threshold" size in the camera, which is related to some "threshold" orbital radius. While Uranus is viewed fully by the spacecraft's cameras, the Apparent Size varies with $1/r^2$. If the spacecraft is close enough to Uranus such that the full planetary disk cannot be viewed, that Apparent Size measurement is not included in the Information Matrix - i.e. that row of H is a zero vector. Apparent Magnitude of Uranus may also be used as an orbit determination measurement, provided a similar "threshold" magnitude condition is satisfied. While the Apparent Magnitude is below some "threshold" magnitude, the Apparent magnitude varies with $\ln(\mathbf{r})$ - note here that a larger negative magnitude corresponds to higher brightness. If the Apparent Magnitude is above the "threshold" magnitude, that Apparent Magnitude measurement is not included in the Information Matrix - i.e. that row of H is a zero vector. The "threshold"

size, orbital radius, and magnitude are assumed known - related to instrument specification.

$$\begin{aligned} \text{if} : \left(\frac{r_t}{r}\right) \geq 1; s = 0 \\ \text{else} : s = s_t \left(\frac{r_t}{r}\right)^2 \end{aligned} \quad [22]$$

$$\begin{aligned} \text{if} : (m < m_t); m = 0 \\ \text{else} : m = m_t - \frac{5.024}{\ln(10)} \cdot \ln\left(\frac{r_t}{r}\right) \end{aligned} \quad [23]$$

Equations 20-23 comprise the Observation Model equations. Next, the "H-tilde" Matrix - the rate of change of the Observation Model with respect to state parameters, is derived. The H-tilde Matrix for Science Phase I is 4-by-9.

$$\tilde{H}_I = \frac{\partial G_I}{\partial X_I} = \begin{Bmatrix} \frac{\partial G_1}{\partial X_1} & \cdots & \frac{\partial G_1}{\partial X_n} \\ \cdots & \cdots & \cdots \\ \frac{\partial G_m}{\partial X_1} & \cdots & \frac{\partial G_m}{\partial X_n} \end{Bmatrix} = \begin{Bmatrix} \frac{\partial \rho}{\partial x} & \cdots & \frac{\partial \rho}{\partial(J_4)} \\ \cdots & \cdots & \cdots \\ \frac{\partial m}{\partial x} & \cdots & \frac{\partial m}{\partial(J_4)} \end{Bmatrix} \quad [24]$$

Each element of the H-tilde Matrix is zero unless otherwise stated. Row 1 of (\tilde{H}_I) contains the partial derivatives of Range, which only depends on position.

$$\tilde{H}_I(1, 1) = \frac{\partial \rho}{\partial x} = \frac{x}{r} - CR \left\{ 1 + \frac{Cz^2}{r^2} \right\}^{-\frac{3}{2}} \frac{xz^2}{r^4} \quad [25a]$$

$$\tilde{H}_I(1, 2) = \frac{\partial \rho}{\partial y} = \frac{y}{r} - CR \left\{ 1 + \frac{Cz^2}{r^2} \right\}^{-\frac{3}{2}} \frac{yz^2}{r^4} \quad [25b]$$

$$\tilde{H}_I(1, 3) = \frac{\partial \rho}{\partial z} = \frac{z}{r} - CR \left\{ 1 + \frac{Cz^2}{r^2} \right\}^{-\frac{3}{2}} \left(-\frac{z}{r^2} + \frac{z^3}{r^4} \right) \quad [25c]$$

Row 2 of (\tilde{H}_I) contains the partial derivatives of Range Rate, which depends on both position and velocity.

$$\begin{aligned}\tilde{H}_I(2,1) &= \frac{\partial \dot{\rho}}{\partial x} = \frac{\dot{x}}{r} - \frac{(x\dot{x} + y\dot{y} + z\dot{z})x}{r^2} \frac{x}{r} \dots \\ &+ \frac{3C^2R}{2} \left\{ 1 + \frac{Cz^2}{r^2} \right\}^{-\frac{5}{2}} \frac{xz^2}{r^4} \left\{ \frac{2z\dot{z}}{r^2} - \frac{2z^2(x\dot{x} + y\dot{y} + z\dot{z})}{r^4} \right\} \dots \\ &+ \frac{CR}{2} \left\{ 1 + \frac{Cz^2}{r^2} \right\}^{-\frac{3}{2}} \left\{ -\frac{4xz\dot{z}}{r^4} - \frac{2z^2\dot{x}}{r^4} + \frac{8z^2(x\dot{x} + y\dot{y} + z\dot{z})x}{r^5} \frac{x}{r} \right\}\end{aligned}\quad [26a]$$

$$\begin{aligned}\tilde{H}_I(2,2) &= \frac{\partial \dot{\rho}}{\partial y} = \frac{\dot{y}}{r} - \frac{(x\dot{x} + y\dot{y} + z\dot{z})y}{r^2} \frac{y}{r} \dots \\ &+ \frac{3C^2R}{2} \left\{ 1 + \frac{Cz^2}{r^2} \right\}^{-\frac{5}{2}} \frac{yz^2}{r^4} \left\{ \frac{2z\dot{z}}{r^2} - \frac{2z^2(x\dot{x} + y\dot{y} + z\dot{z})}{r^4} \right\} \dots \\ &+ \frac{CR}{2} \left\{ 1 + \frac{Cz^2}{r^2} \right\}^{-\frac{3}{2}} \left\{ -\frac{4yz\dot{z}}{r^4} - \frac{2z^2\dot{y}}{r^4} + \frac{8z^2(x\dot{x} + y\dot{y} + z\dot{z})y}{r^5} \frac{y}{r} \right\}\end{aligned}\quad [26b]$$

$$\begin{aligned}\tilde{H}_I(2,3) &= \frac{\partial \dot{\rho}}{\partial z} = \frac{\dot{z}}{r} - \frac{(x\dot{x} + y\dot{y} + z\dot{z})z}{r^2} \frac{z}{r} \dots \\ &+ \frac{3C^2R}{2} \left\{ 1 + \frac{Cz^2}{r^2} \right\}^{-\frac{5}{2}} \left(-\frac{z}{r^2} + \frac{z^3}{r^4} \right) \left\{ \frac{2z\dot{z}}{r^2} - \frac{2z^2(x\dot{x} + y\dot{y} + z\dot{z})}{r^4} \right\} \dots \\ &+ \frac{CR}{2} \left\{ 1 + \frac{Cz^2}{r^2} \right\}^{-\frac{3}{2}} \left\{ \frac{2\dot{z}}{r^2} - \frac{4z^2\dot{z}}{r^4} - \frac{2z^2\dot{z}}{r^4} \dots \right. \\ &\left. \dots - \frac{4z(x\dot{x} + y\dot{y} + z\dot{z})}{r^4} + \frac{8z^2(x\dot{x} + y\dot{y} + z\dot{z})z}{r^5} \frac{z}{r} \right\}\end{aligned}\quad [26c]$$

$$\tilde{H}_I(2,4) = \frac{\partial \dot{\rho}}{\partial \dot{x}} = \frac{x}{r} - CR \left\{ 1 + \frac{Cz^2}{r^2} \right\}^{-\frac{3}{2}} \frac{2xz^2}{r^4} \quad [26d]$$

$$\tilde{H}_I(2,5) = \frac{\partial \dot{\rho}}{\partial \dot{y}} = \frac{y}{r} - CR \left\{ 1 + \frac{Cz^2}{r^2} \right\}^{-\frac{3}{2}} \frac{2yz^2}{r^4} \quad [26e]$$

$$\tilde{H}_I(2, 6) = \frac{\partial \dot{\rho}}{\partial \dot{z}} = \frac{z}{r} - CR \left\{ 1 + \frac{Cz^2}{r^2} \right\}^{-\frac{3}{2}} \left(-\frac{z}{r^2} + \frac{z^3}{r^4} \right) \quad [26f]$$

In rows 3 and 4 of (\tilde{H}_I), Both the Apparent Size and Apparent Magnitude measurements depend on position only. Note that in row 4, a positive variation in magnitude corresponds to decreasing brightness.

$$\tilde{H}_I(3, 1) = \frac{\partial s}{\partial x} = \frac{-2s_t r_t^2 x}{r^3} \frac{x}{r} \quad [27a]$$

$$\tilde{H}_I(3, 2) = \frac{\partial s}{\partial y} = \frac{-2s_t r_t^2 y}{r^3} \frac{y}{r} \quad [27b]$$

$$\tilde{H}_I(3, 3) = \frac{\partial s}{\partial z} = \frac{-2s_t r_t^2 z}{r^3} \frac{z}{r} \quad [27c]$$

$$\tilde{H}_I(4, 1) = \frac{\partial m}{\partial x} = \frac{5.024}{\ln(10)} \cdot \frac{x}{r^2} \quad [28a]$$

$$\tilde{H}_I(4, 2) = \frac{\partial m}{\partial y} = \frac{5.024}{\ln(10)} \cdot \frac{y}{r^2} \quad [28b]$$

$$\tilde{H}_I(4, 3) = \frac{\partial m}{\partial z} = \frac{5.024}{\ln(10)} \cdot \frac{z}{r^2} \quad [28c]$$

The H-tilde Matrix for Science Phase I has been derived. The state propagation matrix is used to propagate the Information Matrix.

$$H = \tilde{H}\Phi \quad [29]$$

Equations [1]-[29] are used in the statistical estimation method in Science Phase I. The dynamical system has been linearized in order to determine the spacecraft's orbit, and

refine *a priori* estimates of Uranus' gravity field. The state vector and force model may be extended to include higher-degree zonal harmonics, planetary radiation, third-body perturbations, and tidal and mean motion resonances. The spacecraft's attitude determination instruments are used for the added purpose of taking measurements for estimation.

The estimation method of Science Phase II builds on the current method in order to model Uranus' magnetic field Intensity, Inclination, and Declination.

4.4.3 Science Phase II - Model Magnetic Intensity, Inclination, and Declination

Science Phase II shall yield a model of Uranus' planetary magnetic field over a wide range of Planet Centric Longitudes and Latitudes, as well as orbital altitudes. Expected models for magnetic Intensity, Inclination, and Declination are added to the statistical estimation.

The state vector for Science Phase II contains the state vector for Science Phase I, with four parameters added - Intensity (F), Inclination (I), Declination (D), and Scaling Factor (B_o) - making it 13-by-1. The subscript "II" is used.

$$\vec{X}_{II}(t) = \begin{bmatrix} \vec{r} \\ \vec{v} \\ \mu \\ J_2 \\ J_4 \\ F \\ I \\ D \\ B_o \end{bmatrix} \quad \dot{\vec{X}}_{II} = \begin{bmatrix} \vec{v} \\ \ddot{\vec{r}} \\ 0 \\ 0 \\ 0 \\ \dot{F} \\ \dot{I} \\ \dot{D} \\ 0 \end{bmatrix} = f(\vec{X}_{II}, t) \quad [30]$$

A dipole model for Intensity is introduced. Intensity may be written as a function of the Magnetic Latitude (ϕ_M) of the field point, in place of the Planet Centric Latitude (ϕ_G). For instance, all points on the Earth's surface at a 30-degree spherical angle from the Planetary North Pole, has a Planet Centric Latitude of 60 degrees. Analogously, the Magnetic Latitude of a field point is simply 90 degrees, minus the spherical angle from the Magnetic North Pole. However, if the Magnetic North Pole does not coincide with the Planetary North Pole, the spacecraft's position must be represented in a rotation frame - the PMRF - after which, the spherical angle is taken and the magnetic latitude is obtained.

$$\phi_M[deg] = 90 - \cos^{-1}\left(\frac{\vec{r}_m \cdot \hat{p}}{r}\right) \quad [31a]$$

Where \vec{r}_m is the spacecraft's position in the PMRF, and (\hat{p}) is the unit vector in the PMRF that points to Uranus' Magnetic North Pole. Solving for the sine or cosine of (ϕ_M) may be more convenient for subsequent calculations, so equation [31a] is rearranged to form:

$$\sin(\phi_M) = \frac{\vec{r}_m \cdot \hat{p}}{r} \quad [31b]$$

Next, the position in PMRF is related to the position in PIRF - that is, (\vec{r}_m) is related to (\vec{r}). The PMRF rotates at the same rate (ω) as Uranus' self-rotation, at approximately 17.2 hours per revolution. The position and velocity in PMRF can be written in terms of state parameters (position and velocity), which are estimated in the PIRF. It is assumed the time that the measurement is taken, (t), with respect to some epoch, is known.

$$\begin{aligned}\vec{r}_m &= R_z(\omega t) \cdot \vec{r} = \begin{bmatrix} \cos(\omega t) & \sin(\omega t) & 0 \\ -\sin(\omega t) & \cos(\omega t) & 0 \\ 0 & 0 & 1 \end{bmatrix} \begin{bmatrix} x \\ y \\ z \end{bmatrix} \dots \\ &= \begin{bmatrix} x\cos(\omega t) + y\sin(\omega t) \\ -x\sin(\omega t) + y\cos(\omega t) \\ z \end{bmatrix}\end{aligned}\quad [32]$$

$$\begin{aligned}\dot{\vec{r}}_m &= R_z(\omega t) \cdot \dot{\vec{r}} - (\vec{\omega} \times \vec{r}_m)\dots \\ &= \begin{bmatrix} \cos(\omega t) & \sin(\omega t) & 0 \\ -\sin(\omega t) & \cos(\omega t) & 0 \\ 0 & 0 & 1 \end{bmatrix} \begin{bmatrix} \dot{x} \\ \dot{y} \\ \dot{z} \end{bmatrix} - \begin{bmatrix} 0 \\ 0 \\ \omega \end{bmatrix} \times \vec{r}_m\dots \\ &= \begin{bmatrix} -\omega x\sin(\omega t) + \omega y\cos(\omega t) + \dot{x}\cos(\omega t) + \dot{y}\sin(\omega t) \\ -\omega x\cos(\omega t) - \omega y\sin(\omega t) - \dot{x}\sin(\omega t) + \dot{y}\cos(\omega t) \\ \dot{z} \end{bmatrix}\end{aligned}\quad [33]$$

Then, the Intensity is examined in the spherical reference frame. The field line may be described with components in the radial (\hat{r}), tangential ($\hat{\theta}$), and azimuthal ($\hat{\lambda}$) directions. Let the azimuthal unit direction vector (out of the page) equal the cross product of the radial and tangential unit direction unit vectors (in the plane of the page). At a given distance from the center of a body's magnetic field, the Intensity is twice as large near the poles compared to that at the equator. Equation [34a-c] shows the components of a field line in the three directions described above.

$$B_r = \frac{-2B_o}{r^3}\sin(\phi_M) \quad [34a]$$

$$B_\phi = \frac{B_o}{r^3}\cos(\phi_M) \quad [34b]$$

$$B_\lambda = 0 \quad [34c]$$

The expected Intensity, in any three-dimensional reference frame defined by orthogonal unit directions, is the norm of the three components. The expected Intensity varies with the Scaling Factor, orbital radius, and magnetic latitude. Equation [35] is expressed below, where components of (\hat{P}) in the PMRF are constants p_x , p_y , and p_z , respectively. The time rate of change of Intensity, in equation [36], is expressed in vector form for brevity.

$$\begin{aligned} F &= (B_r^2 + B_\theta^2 + B_\lambda^2)^{\frac{1}{2}} = \left\{ \frac{4B_o^2}{r^6} \sin^2(\phi_M) + \frac{B_o^2}{r^6} \cos^2(\phi_M) \right\}^{\frac{1}{2}} \dots \\ &= \frac{B_o}{r^3} \left\{ 1 + 3\sin^2(\phi_m) \right\}^{\frac{1}{2}} = \frac{B_o}{r^3} \left\{ 1 + \frac{3(\vec{r}_m \cdot \hat{p})^2}{r^2} \right\}^{\frac{1}{2}} \dots \quad [35] \\ &= \frac{B_o}{r^3} \left\{ 1 + \frac{3[xp_x \cos(\omega t) + yp_x \sin(\omega t) - xp_y \cos(\omega t) + yp_y \sin(\omega t) + zp_z]^2}{r^2} \right\}^{\frac{1}{2}} \end{aligned}$$

$$\begin{aligned} \dot{F} &= \frac{-3B_o \dot{r}}{r^4} \left\{ 1 + \frac{3(\vec{r}_m \cdot \hat{p})^2}{r^2} \right\}^{\frac{1}{2}} \dots \\ &+ \frac{3B_o}{r^3} \left\{ 1 + 3\frac{(\vec{r}_m \cdot \hat{p})^2}{r^2} \right\}^{-\frac{1}{2}} \left\{ \frac{-(\vec{r}_m \cdot \hat{p})^2 \dot{r}}{r^3} + \frac{(\vec{r}_m \cdot \hat{p})(\dot{\vec{r}}_m \cdot \hat{p})}{r^2} \right\} \quad [36] \end{aligned}$$

Inclination is the angle between the magnetic field line vector, and the tangent plane to an imaginary spherical surface whose radius is equal to the orbital radius. The magnetic field line only has two components in the dipole model - the radial component is the "opposite leg" of the Inclination angle, and the tangential component is the "adjacent leg". Equation [37] is written below, with substitutions of equation [31a-b].

Note that equation [37] reaches singularity when the spacecraft travels over one of the magnetic poles. Some upper tolerance for the tangent of the magnetic latitude should be set. Again, the time rate of change of Inclination, in equation [38], is expressed in vector form for brevity.

$$\begin{aligned}
 I &= \tan^{-1} \left\{ \frac{-2 \sin(\phi_M)}{\cos(\phi_M)} \right\} \dots \\
 &= \tan^{-1} \left\{ \frac{-2(\vec{r}_m \cdot \hat{p})}{[r^2 - (\vec{r}_m \cdot \hat{p})^2]^{\frac{1}{2}}} \right\} \quad [37]
 \end{aligned}$$

$$\begin{aligned}
 \dot{I} &= \left\{ 1 + \frac{4(\vec{r}_m \cdot \hat{p})^2}{r^2 - (\vec{r}_m \cdot \hat{p})^2} \right\}^{-1} \dots \\
 \dots &\left\{ \frac{-2(\dot{\vec{r}}_m \cdot \hat{p})}{[r^2 - (\vec{r}_m \cdot \hat{p})^2]^{\frac{1}{2}}} + \frac{2(\vec{r}_m \cdot \hat{p})[r\dot{r} - 2(\vec{r}_m \cdot \hat{p})(\dot{\vec{r}}_m \cdot \hat{p})]}{[r^2 - (\vec{r}_m \cdot \hat{p})^2]^{\frac{3}{2}}} \right\} \quad [38]
 \end{aligned}$$

Declination is the angle between the Magnetic Meridian, and the unit vector pointing to the Planetary North Pole on the tangent plane - called the Local North unit vector. The magnetic field line always points in the Local North direction in the dipole model, so the expected Declination is zero. The time rate of change of Declination is also zero.

$$D = 0 \quad [39]$$

$$\dot{D} = 0 \quad [40]$$

The additional state parameters have been described. The State Propagation Matrix for Science Phase II is 13-by-13, derived in the same fashion as in equation [7]. The top-right 9-by-9 sub-matrix is equal to the State Propagation Matrix for Science

Phase I, and elements in the first 9 rows in columns 10 to 13 are zero. Thus, new partial derivatives need only to be calculated for rows 10 to 13. The dot products $(\vec{r}_m \cdot \hat{p})$ and $(\dot{\vec{r}}_m \cdot \hat{p})$ appear several times in equations [36] and [38], they are replaced by V and W for brevity. The partial derivatives of these dot products are calculated (with the operating state parameter serving as the subscript) and placed into the State Propagation Matrix elements that follow.

$$\begin{aligned} V &= (\vec{r}_m \cdot \hat{p}) \dots \\ &= xp_x \cos(\omega t) + yp_x \sin(\omega t) - xp_y \sin(\omega t) + yp_y \cos(\omega t) \end{aligned} \quad [41]$$

$$V_x = \frac{\partial(\vec{r}_m \cdot \hat{p})}{\partial x} = p_x \cos(\omega t) - p_y \sin(\omega t) \quad [42a]$$

$$V_y = \frac{\partial(\vec{r}_m \cdot \hat{p})}{\partial y} = p_x \sin(\omega t) + p_y \cos(\omega t) \quad [42b]$$

$$V_z = \frac{\partial(\vec{r}_m \cdot \hat{p})}{\partial z} = p_z \quad [42c]$$

$$\begin{aligned} W &= (\dot{\vec{r}}_m \cdot \hat{p}) \dots \\ &= p_x \{-\omega x \sin(\omega t) + \omega y \cos(\omega t) - \dot{x} \cos(\omega t) + \dot{y} \sin(\omega t)\} \dots \\ &+ p_y \{-\omega x \cos(\omega t) + \omega y \sin(\omega t) - \dot{x} \sin(\omega t) + \dot{y} \cos(\omega t)\} \dots \\ &\quad + \dot{z} p_z \end{aligned} \quad [43]$$

$$W_x = \frac{\partial(\dot{\vec{r}}_m \cdot \hat{p})}{\partial x} = -p_x \omega \sin(\omega t) - p_y \omega \cos(\omega t) \quad [44a]$$

$$W_y = \frac{\partial(\dot{\vec{r}}_m \cdot \hat{p})}{\partial y} = p_x \omega \cos(\omega t) - p_y \omega \sin(\omega t) \quad [44b]$$

$$W_z = \frac{\partial(\dot{\vec{r}}_m \cdot \hat{p})}{\partial z} = 0 \quad [44c]$$

$$W_{\dot{x}} = \frac{\partial(\dot{\vec{r}}_m \cdot \hat{p})}{\partial \dot{x}} = p_x \cos(\omega t) - p_y \sin(\omega t) \quad [44d]$$

$$W_{\dot{y}} = \frac{\partial(\dot{\vec{r}}_m \cdot \hat{p})}{\partial \dot{y}} = p_x \sin(\omega t) + p_y \cos(\omega t) \quad [44e]$$

$$W_{\dot{z}} = \frac{\partial(\dot{\vec{r}}_m \cdot \hat{p})}{\partial \dot{z}} = p_z \quad [44f]$$

Equation [45] describes the first 9 rows (in pseudo-MATLAB code convention) of the State Propagation Matrix for Science Phase II.

$$A_{II}(1 : 9, :) = [A_I \quad \text{zeros}(9, 4)] \quad [45]$$

Row 10 contains the partial derivatives of (\dot{F}). Equation [46] gives the partial derivative of (\dot{F}) with respect to (x); the same operations with respect to (y) and (z) are similar with several paralleling adjustments. To obtain the other two partial derivatives, all instances of (x) should be changed to (y) or (z), respectively; all instances of (V_x) should be changed to (V_y) or (V_z), respectively; and all instances of (W_x) should be changed to (W_y) or (W_z), respectively. $A_{II}(10,1)$, $A_{II}(10,2)$, and $A_{II}(10,3)$ have been derived.

$$\begin{aligned} A_{II}(10, 1) &= \frac{\partial \dot{F}}{\partial x} = \frac{-12B_o x \dot{r}}{r^6} \left\{ 1 + \frac{3V^2}{r^2} \right\}^{\frac{1}{2}} \dots \\ &\quad - \frac{9B_o \dot{r}}{r^4} \left\{ 1 + \frac{3V^2}{r^2} \right\}^{-\frac{1}{2}} \left(\frac{-xV^2}{r^4} + \frac{VV_x}{r^2} \right) \dots \\ &\quad - \frac{9B_o x}{r^5} \left\{ 1 + \frac{3V^2}{r^2} \right\}^{-\frac{1}{2}} \left(\frac{-V^2 \dot{r}}{r^3} + \frac{VW}{r^2} \right) \dots \\ &\quad - \frac{9B_o}{r^3} \left\{ 1 + \frac{3V^2}{r^2} \right\}^{-\frac{3}{2}} \left(\frac{-xV^2}{r^4} + \frac{VV_x}{r^2} \right) \left(\frac{-V^2 \dot{r}}{r^3} + \frac{VW}{r^2} \right) \dots \end{aligned} \quad [46]$$

$$\begin{aligned}
& + \frac{3B_o}{r^3} \left\{ 1 + \frac{3V^2}{r^2} \right\}^{-\frac{1}{2}} \left(\frac{3xV^2\dot{r}}{r^5} - \frac{2VV_x\dot{r}}{r^3} \dots \right. \\
& \left. \dots - \frac{2xVW}{r^4} + \frac{V_xW}{r^2} + \frac{VW_x}{r^2} \right)
\end{aligned}$$

Equation [47] gives the partial derivative of (\dot{F}) with respect to (\dot{x}) ; the same operations with respect to (\dot{y}) and (\dot{z}) are similar with several paralleling adjustments. To obtain the other two partial derivatives, all instances of (x) should be changed to (y) or (z) , respectively; and all instances of (W_x) should be changed to (W_y) or (W_z) , respectively. $A_{II}(10,4)$, $A_{II}(10,5)$, and $A_{II}(10,6)$ have been derived.

$$\begin{aligned}
A_{II}(10,4) &= \frac{\partial \dot{F}}{\partial \dot{x}} = \frac{-3B_o x}{r^5} \left\{ 1 + \frac{3V^2}{r^2} \right\}^{\frac{1}{2}} \dots \\
& + \frac{3B_o}{r^3} \left\{ 1 + \frac{3V^2}{r^2} \right\}^{-\frac{1}{2}} \left(\frac{-xV^2}{r^4} + \frac{VW_x}{r^2} \right) \quad [47]
\end{aligned}$$

$A_{II}(10,7)$, $A_{II}(10,8)$, $A_{II}(10,9)$, $A_{II}(10,10)$, $A_{II}(10,11)$, and $A_{II}(10,12)$ are zero. $A_{II}(10,13)$ is nonzero, as (\dot{F}) linearly scales with (B_o) . Recall that (\dot{F}) is defined in equation [36].

$$A_{II}(10,13) = \frac{\partial \dot{F}}{\partial (B_o)} = \frac{\dot{F}}{B_o} \quad [48]$$

Row 11 contains the partial derivatives of (\dot{J}) . Equation [49] gives the partial derivative of (\dot{J}) with respect to (x) ; the same operations with respect to (y) and (z) are similar with several paralleling adjustments. To obtain the other two partial derivatives,

all instances of (x) should be changed to (y) or (z), respectively; instances of (\dot{x}) should be changed to (\dot{y}) or (\dot{z}), respectively; all instances of (V_x) should be changed to (V_y) or (V_z), respectively; and all instances of (W_x) should be changed to (W_y) or (W_z), respectively. $A_{II}(11,1)$, $A_{II}(11,2)$, and $A_{II}(11,3)$ have been derived.

$$\begin{aligned}
A_{II}(11,1) &= \frac{\partial \dot{I}}{\partial x} = \dots \\
-16 \left\{ 1 + \frac{4V^2}{r^2 - V^2} \right\}^{-2} &\left[\frac{VV_x}{r^2 - V^2} - \frac{4V^2(2x - 2VV_x)}{(r^2 - V^2)^2} \right] \left[\frac{-2W}{(r^2 - V^2)^{\frac{1}{2}}} - \frac{2V(r\dot{r} - 2VW)}{(r^2 - V^2)^{\frac{3}{2}}} \right] \dots \\
+2 \left\{ 1 + \frac{4V^2}{r^2 - V^2} \right\}^{-1} &\left[\frac{-W_x}{(r^2 - V^2)^{\frac{1}{2}}} + \frac{W(x - VV_x)}{(r^2 - V^2)^{\frac{3}{2}}} + \frac{V_x(r\dot{r} - 2VW)}{(r^2 - V^2)^{\frac{3}{2}}} \dots \right. \\
\dots &\left. - \frac{3V(r\dot{r} - 2VW)(x - VV_x)}{(r^2 - V^2)^{\frac{5}{2}}} + \frac{V(\frac{x\dot{r}}{r} + \dot{x} - 2V_xW - 2VW_x)}{(r^2 - V^2)^{\frac{3}{2}}} \right] \quad [49]
\end{aligned}$$

Equation [50] gives the partial derivative of (\dot{I}) with respect to (\dot{x}); the same operations with respect to (\dot{y}) and (\dot{z}) are similar with several paralleling adjustments. To obtain the other two partial derivatives, all instances of (x) should be changed to (y) or (z), respectively; and all instances of (W_x) should be changed to (W_y) or (W_z), respectively. $A_{II}(11,4)$, $A_{II}(11,5)$, and $A_{II}(11,6)$ have been derived.

$$\begin{aligned}
A_{II}(11,4) &= \frac{\partial \dot{I}}{\partial \dot{x}} = \dots \\
2 \left\{ 1 + \frac{4V^2}{r^2 - V^2} \right\}^{-1} &\left[\frac{-W_{\dot{x}}}{(r^2 - V^2)^{\frac{1}{2}}} + \frac{V(x - 2VW_{\dot{x}})}{(r^2 - V^2)^{\frac{3}{2}}} \right] \quad [50]
\end{aligned}$$

Additionally, $A_{II}(11,7)$, $A_{II}(11,8)$, $A_{II}(11,9)$, $A_{II}(11,10)$, $A_{II}(11,11)$, $A_{II}(11,12)$, and $A_{II}(11,13)$ are zero. The final two state parameters, Declination and Scaling Factor,

are assumed constant, thus Rows 12 and 13 are zero vectors. The State Propagation Matrix for Science Phase II has been derived. The state propagation matrix is used to integrate the State Transition Matrix.

In Science Phase II, the Observation Vector (Y) for estimation has been modified to include the Intensity, Inclination, and Declination; all of these are used to construct the Information Matrix (H) during this phase. During the spacecraft's operation, raw magnetic field line measurements made in the spacecraft's body-fixed frame are transformed to Intensity, Inclination, and Declination. The necessary transformations are discussed, before proceeding to derive the H-tilde Matrix for Science Phase II.

$$\vec{Y}_{II} = \begin{bmatrix} \rho \\ \dot{\rho} \\ s \\ m \\ F \\ I \\ D \end{bmatrix} = G(\vec{X}_{II}, t) + \vec{\epsilon} \quad [51]$$

The spacecraft shall take raw magnetic field line measurements in its fixed body frame - the SBRF. If the spacecraft employs a three-axis stabilization algorithm, then the body angles with respect to the PIRF remain approximately constant over time. Any set of Euler Angle transformations ("3-1-3" , "3-2-1", etc.) may be used to spacecraft's measurements in PIRF. Let the raw measurement taken by the spacecraft (\vec{b}) consist of $\{b_1, b_2, b_3\}$ components in the $\{S_1, S_2, S_3\}$ directions, respectively. Let (α) , (β) , and (γ) represent a set of "3-1-3" Euler Angles (sometimes referred to as the Classical Euler Angle Sequence), the raw measurement in SBRF is transformed to that in PIRF - $\{b_x, b_y,$

b_z } by the following direction cosine matrix, the trigonometric functions cosine() and sine() have been written in shorthand "c()" and "s()".

$$\begin{aligned} \begin{bmatrix} b_x \\ b_y \\ b_z \end{bmatrix} &= R_3(-\gamma)R_1(-\beta)R_3(-\alpha) \begin{bmatrix} b_1 \\ b_2 \\ b_3 \end{bmatrix} = \dots \\ &= \begin{bmatrix} -s(\alpha)c(\beta)s(\gamma) + c(\alpha)c(\gamma) & c(\alpha)c(\beta)s(\gamma) + s(\alpha)c(\gamma) & s(\beta)s(\gamma) \\ -s(\alpha)c(\beta)c(\gamma) - c(\alpha)s(\gamma) & c(\alpha)c(\beta)c(\gamma) - s(\alpha)s(\gamma) & s(\beta)c(\gamma) \\ s(\alpha)s(\beta) & -c(\alpha)s(\beta) & c(\beta) \end{bmatrix} \begin{bmatrix} b_1 \\ b_2 \\ b_3 \end{bmatrix} \end{aligned} \quad [52]$$

The measured Intensity may be obtained from raw measurements in any reference frame, while the measured Inclination and Declination may be obtained only after another transformation to the PMRF.

$$F = \|\vec{b}\| \quad [53]$$

The measurement in PIRF may be transformed to the PMRF in a similar manner to equation [32]. The measured Inclination and Declination depend on the spacecraft's PMRF position unit direction vector and the magnetic field line unit direction vector. For instance, if the magnetic field line is parallel to the PMRF position, and in the same direction, then the Inclination is 90 degrees. If the magnetic field line is perpendicular to the PMRF position, then the Inclination is 0 degrees. Inclination, in degrees, is found with the dot product.

$$I = \sin^{-1} \left(\frac{\vec{b}_m \cdot \vec{r}_m}{F \cdot r} \right) \quad [54]$$

With the Inclination found, the magnetic field line may be decomposed into an *out-of-plane* and an *in-plane* component. The out-of-plane component is in the direction *normal* to - and in the direction of (\vec{r}) a spherical Gaussian surface whose radius is equal to the orbital radius, while the in-plane component is that of the magnetic field line *projected* onto the spherical Gaussian surface. Equation [55] describes the in-plane component, which is the magnetic field line in PMRF minus the out-of-plane component. Direction of the in-plane component is referred to as the Magnetic Meridian.

$$\vec{b}_{proj} = \vec{b}_m - \frac{F \sin(I)}{r} \vec{r}_m \quad [55]$$

Declination is the angle between the Magnetic Meridian and the Local North unit direction vector, which depends on the Planet Centric Longitude and Latitude over which the spacecraft is traveling. The Planet Centric Longitude and Latitude are found with the spacecraft's position in the PMRF. The Planet Centric Latitude, used for calculating the spacecraft's gravitational potential, is given in equation [4]; however, it is advisable to correct the Planet Centric Latitude to Planetodetic Latitude when determining groundtrack position. On a planet as oblate as Uranus, this latitude correction may reach the order of one degree. Equation [56] shows the latitude correction. Then, let (λ_G) represent the Planet Centric Longitude. In equation [57], the pseudo-MATLAB code function "atan2()" - referring to four-quadrant arc-tangent - is used. The first argument is the y-coordinate in PMRF, and the second argument is the x-coordinate in PMRF. Equation [58] gives the Local North unit direction vector. Declination, in degrees, is measured counterclockwise from the Local North.

$$\lambda_G = \text{atan2} \{ -x \sin(\omega t) + y \cos(\omega t), x \cos(\omega t) + y \sin(\omega t) \} \quad [56]$$

$$\tan(\phi'_G) = (1 - k^2) \tan(\phi_G) \quad [57]$$

$$\hat{n} = \begin{bmatrix} -\sin(\phi'_G) \cos(\lambda_G) \\ -\sin(\phi'_G) \sin(\lambda_G) \\ \cos(\phi'_G) \end{bmatrix} \quad [58]$$

$$\begin{aligned} \text{if : } (\hat{n} \times \vec{b}_{proj}) \geq 0; D = \cos^{-1} \left(\frac{\vec{b}_{proj} \cdot \hat{n}}{\|\vec{b}_{proj}\|} \right) \\ \text{else : } D = \cos^{-1} \left(\frac{\vec{b}_{proj} \cdot \hat{n}}{\|\vec{b}_{proj}\|} \right) - 360 \end{aligned} \quad [59]$$

The raw magnetic field line measurements made in the spacecraft's body-fixed frame have been transformed to Intensity, Inclination, and Declination. The H-tilde Matrix for Science Phase II is 7-by-13, and contains the 4 rows of the H-tilde Matrix for Science Phase I. Since Intensity, Inclination, and Declination are measured directly, i.e. without Observation Model equations, the additional rows of H-tilde are elementary. Equation [60] describes the first 4 rows (in pseudo-MATLAB code convention) of the H-tilde Matrix for Science Phase II.

$$\tilde{H}_{II}(1 : 4, :) = [\tilde{H}_I \quad \text{zeros}(3, 4)] \quad [60]$$

$$\tilde{H}_{II}(5, 10) = \frac{\partial F}{\partial F} = 1 \quad [61]$$

$$\tilde{H}_{II}(6, 11) = \frac{\partial I}{\partial I} = 1 \quad [62]$$

$$\tilde{H}_{II}(7, 12) = \frac{\partial I}{\partial I} = 1 \quad [63]$$

Equations [30]-[63] are added to the statistical estimation method in Science Phase II. Uranus' magnetic field shall be modeled based on a dipole field and the three characteristic quantities - Intensity, Inclination, and Declination. This report chapter concludes with discussion of the Nominal Trajectory and *a priori* estimates at the start of Science Phase I.

4.4.4 Nominal Trajectory and *A priori* Estimate

The spacecraft's trajectory upon arriving at Uranus has been determined, and is discussed in the previous report chapter. The arrival trajectory is integrated forward in time for 15 orbits, which corresponds to approximately 14.1 days, in order to obtain the Nominal Trajectory at the start of Science Phase I. This 14-day period is an assumed time during which communication is established between the ground segment and spacecraft, and the spacecraft's on-board instruments are activated. Table 4-8 shows slight changes in the orbit over the spacecraft's first 20 orbits.

Orbital Elements	Arrival Trajectory	Nominal Trajectory
Semi-major Axis, km	98770.0	98575.1
Eccentricity	0.727897	0.727382
Inclination, deg	99.2500	99.2518
Right Ascension of A.N., deg	-5.92806	-4.717623
Argument of Periapse, deg	298.186	294.873

**Table 4-8: Keplerian Orbital Elements of the Arrival Trajectory
and the Nominal Trajectory.**

The Nominal Trajectory shows position in km, velocity in km/s, and the Uranus gravitational constant in km^3/s^2 ; and includes *a priori* estimates of the Uranus gravitational constant (μ), the Second-degree zonal harmonic (J_2), and the Fourth-degree zonal harmonic (J_4). The Uranus gravitational constant and Second-degree zonal harmonic are taken from the NASA National Space Science Data Center database, and higher-degree zonal harmonics are taken from Hubbard and Marley (1989). To compare, the arrival trajectory orbital radius and velocity are 26876 km and 19.301 km/s, respectively; while the nominal trajectory orbital radius and velocity are 26874 km and 19.299 km/s, respectively.

$$\vec{X}_I^*(t_0) = \begin{bmatrix} \vec{r}_0^* \\ \vec{v}_0^* \\ \mu^* \\ J_2^* \\ J_4^* \end{bmatrix} = \begin{bmatrix} 11586.7 \\ 2976.93 \\ -24063.7 \\ 17.3427 \\ -2.74067 \\ 5.79455 \cdot 10^6 \\ 3.34343 \cdot 10^{-3} \\ -3.19000 \cdot 10^{-5} \end{bmatrix}$$

Chapter 5: Preliminary Spacecraft Design

Chapter 5 "Preliminary Spacecraft Design" describes design methods and processes for the Upsilon-0 Propulsion Module, Upsilon-1 Science Orbiter, and Upsilon-2 Atmosphere Probe in Phase A of the project life cycle. A subsystem-to-subsystem, flowing approach is implemented to achieve preliminary mass and power allocations for the spacecraft system and within each spacecraft. Quantitative mass allocations are presented for Upsilon-0 and Upsilon-1, while Upsilon-2 is qualitatively sized.

The three spacecraft are implemented to achieve the minimum mission goals: 1) further the accomplishments of the Voyager-2 mission in exploring the outer solar system; 2) achieve the first orbital capture at an Ice Giant planet; 3) refine Uranus gravity models; 4) measure Uranus' planetary magnetic field strength and direction; 5) characterize deviations from the ideal dipole model; and 6) observe the effects of seasonal forcing on Uranus' atmosphere. The minimum measurement objectives shall be achieved: 1) provide observations of Uranus' planetary magnetic field and atmosphere, for at least 20 months during the first two years following orbital capture; 2) approximate the location of at least one of Uranus' Magnetic Poles; and 3) create a model of Uranus' planetary magnetic field - by qualitatively estimating the magnetic Intensity, Inclination, and Declination - spanning at minimum -60 to +60 degrees latitude.

The Upsilon-0 Propulsion Module shall facilitate the Uranus arrival burn, and de-orbit into Uranus thereafter; the Upsilon-1 Science Orbiter shall measure and characterize Uranus' magnetic field, and carry one or more Upsilon-2 Atmospheric Probes, which shall descend into unique weather formations as they are observed. The following pages show hand-drawn vehicle concepts with initial approximated measurements and

dimensions; the methods, assumptions, and estimates used to arrive at the proposed design is discussed thereafter.

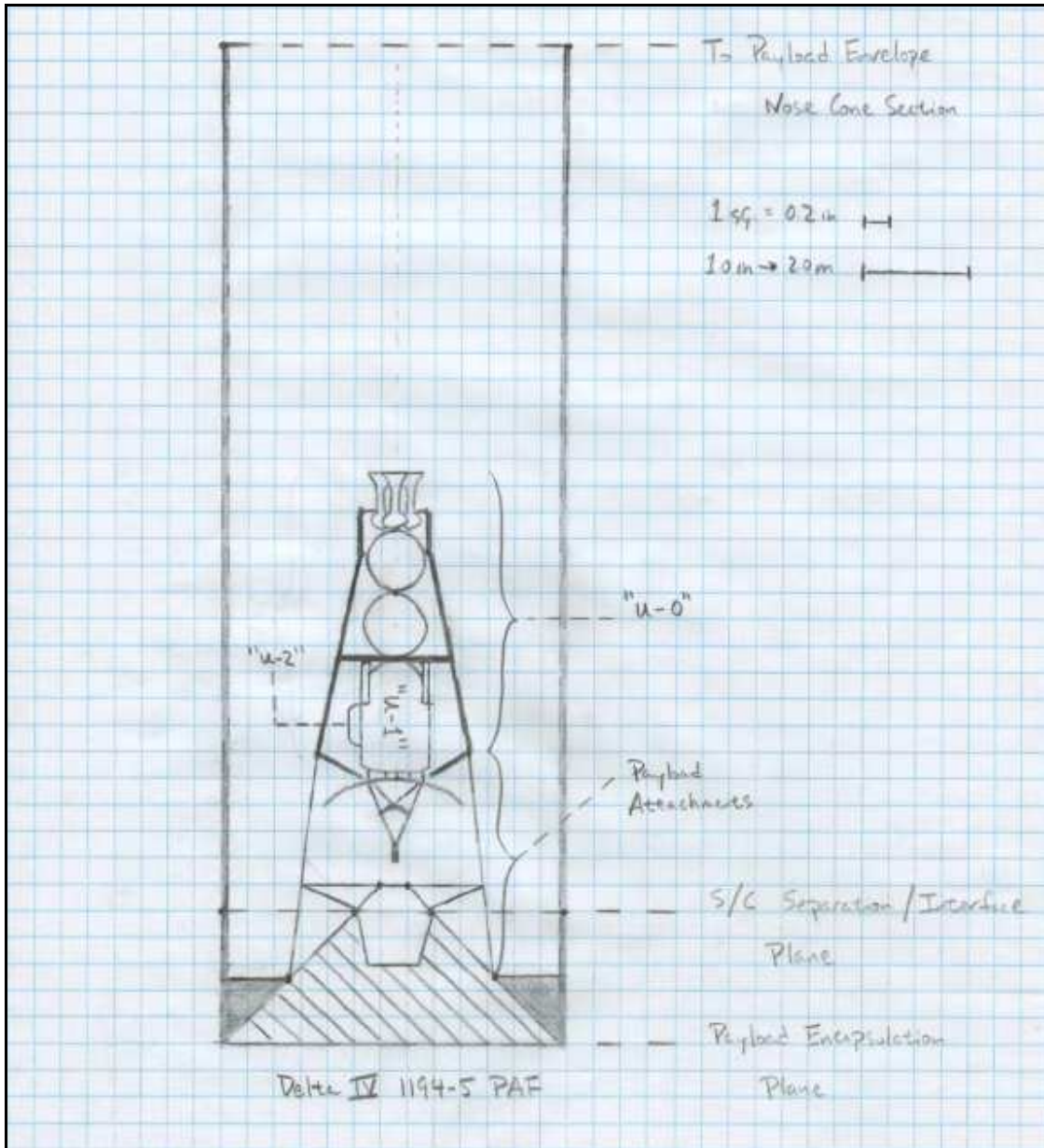


**Figure 5-1: Project Upsilon Spacecraft Schematic -
Launch Configuration.**

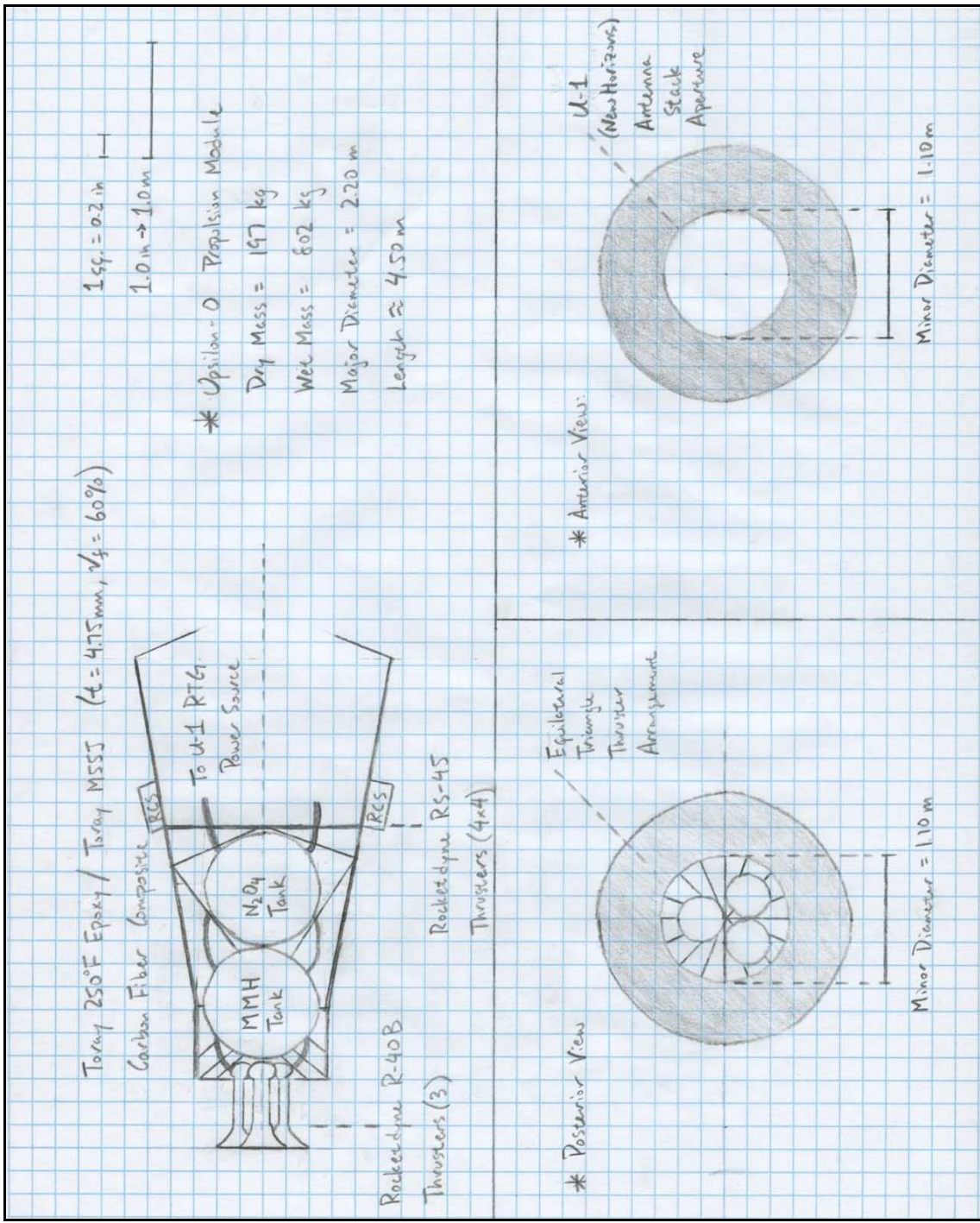


Figure 5-2: Project Upsilon Spacecraft Schematic - Upsilon-0 Propulsion Module.

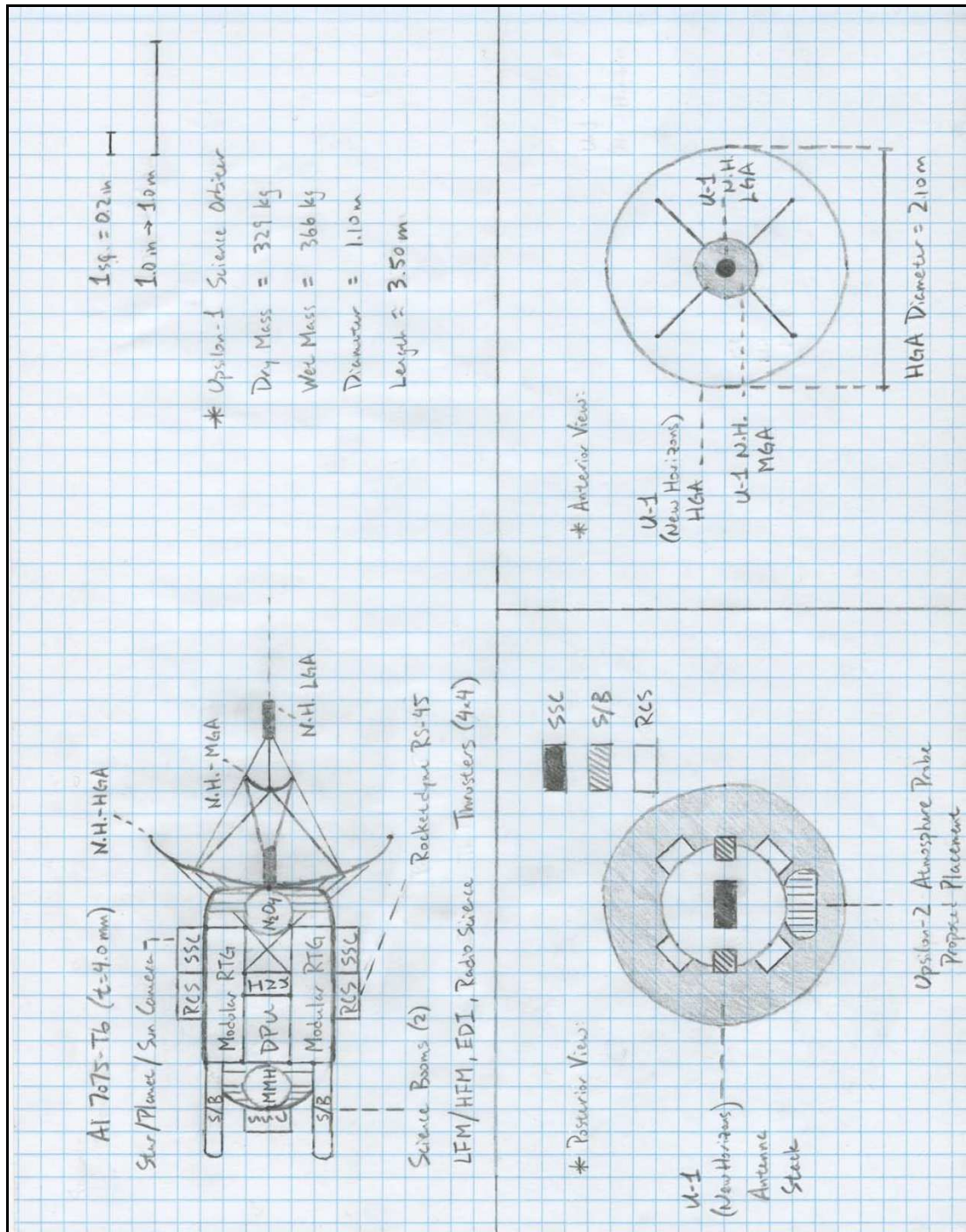


Figure 5-3: Project Upsilon Spacecraft Schematic - Upsilon-1 Science Orbiter.

5.1 UPSILON-0 PROPULSION MODULE

The Upsilon-0 Propulsion Module carries the Upsilon-1 and Upsilon-2 spacecraft to Uranus, facilitate the Uranus arrival burn, and de-orbits into Uranus thereafter. The launch configuration into the interplanetary trajectory to Uranus ,constrains the total mass of the spacecraft system; while the Delta IV-Heavy launch vehicle constrains the packaged size and volume. Mass allocation of Upsilon-0 is first examined in a top-down design scheme.

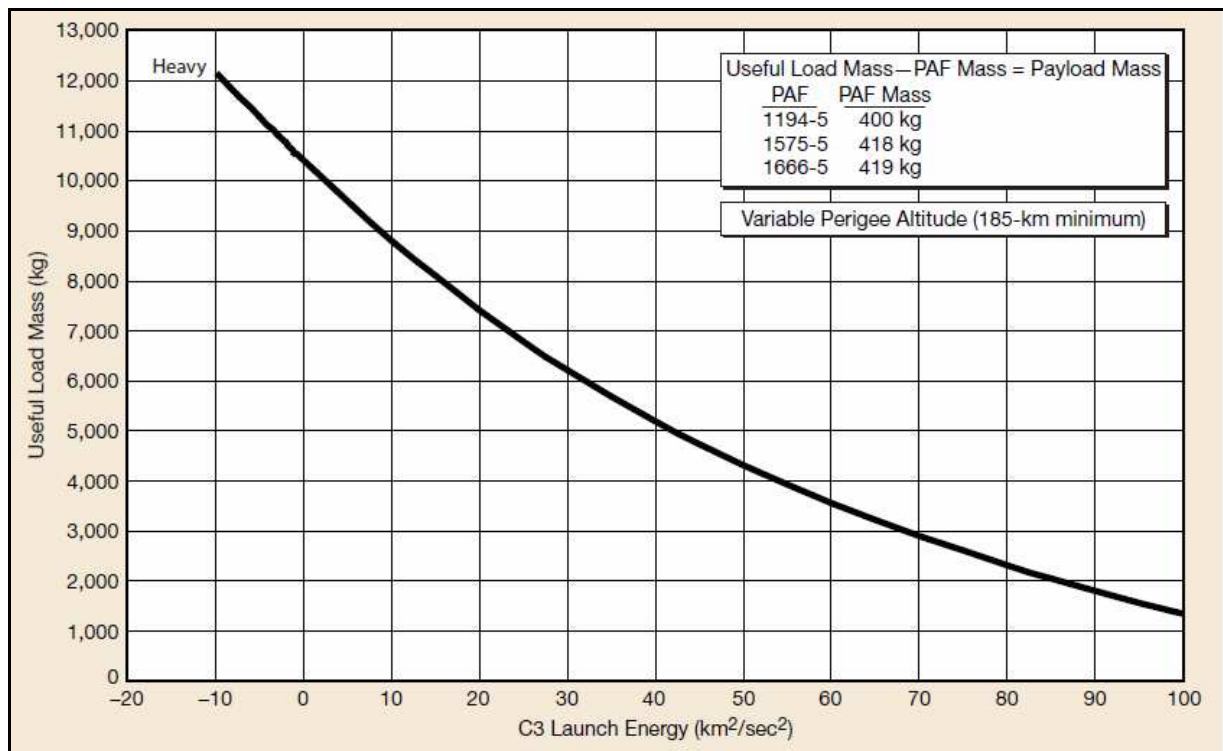


Figure 5-4: "Delta IV-H, C3 Launch Energy Capability (Eastern Range)." ²⁷

Courtesy of the United Launch Alliance.

²⁷Figure 5-4 Image Source:

United Launch Alliance (2007).
Delta IV, Payload Planners Guide.
Littleton, CO. pp. 76 of 267.

Hyperbolic excess velocity of 9.35 km/s (C3 energy of 87.5 km²/s²), was estimated via TRACT for the proposed May 5, 2021 launch. From Figure 5-4, this C3 Energy limits the Useful Load Mass to 1920 kg; the Payload Attachment Fairing mass must then be subtracted. Equation [1] is used to arrive at the Allocated Payload Mass [Bettadpur, 2013], where (M_{UP}) is the Useful Load Mass, (M_{PAF}) is the Payload Attachment Fitting Mass (assuming the "1194-5" model, 400 kg mass), and (m) is the mass margin. 15% mass margin is the best achieved at this point in the design. The Current Best Estimate is obtained by applying contingency; and a 5% contingency is assumed initially. Using equation [2], the **Current Best Estimate Payload Mass is 1250 kg**. Table 5-1 summarizes these calculations, and bounds the total mass of the spacecraft system with respect to margin and contingency constraints.

$$M_{AP} = \frac{M_{UP} - M_{PAF}}{1 + m} \quad [1]$$

$$M_{CBE} = \frac{M_{AP}}{1 + c} \quad [2]$$

Parameter	Mass, kg	Percentage, %
Design Limit	1520	--
Margin	200	15.1
Allocated	1320	--
Contingency	70	5.6
Current Best Estimate	1250	--

Table 5-1: System-Level Mass Allocations.

The largest fairing, 5.0 meters in diameter and 19.1 meters in length, is used on the Delta IV-Heavy (direct quote) [United Launch Alliance, pp. 85 of 267]. Figure 5-5 shows the Delta IV-Heavy fairing, including the Fairing Envelope, Usable Payload

Envelope, Negotiable Envelope (which is not recommended to be occupied by the payload), Payload Attachment Fairing, and Acoustic Blankets. Table 5-2 summarizes dimensions of the Usable Payload Envelope derived from dimensions in Figure 5-5, and bounds the size of the spacecraft system.

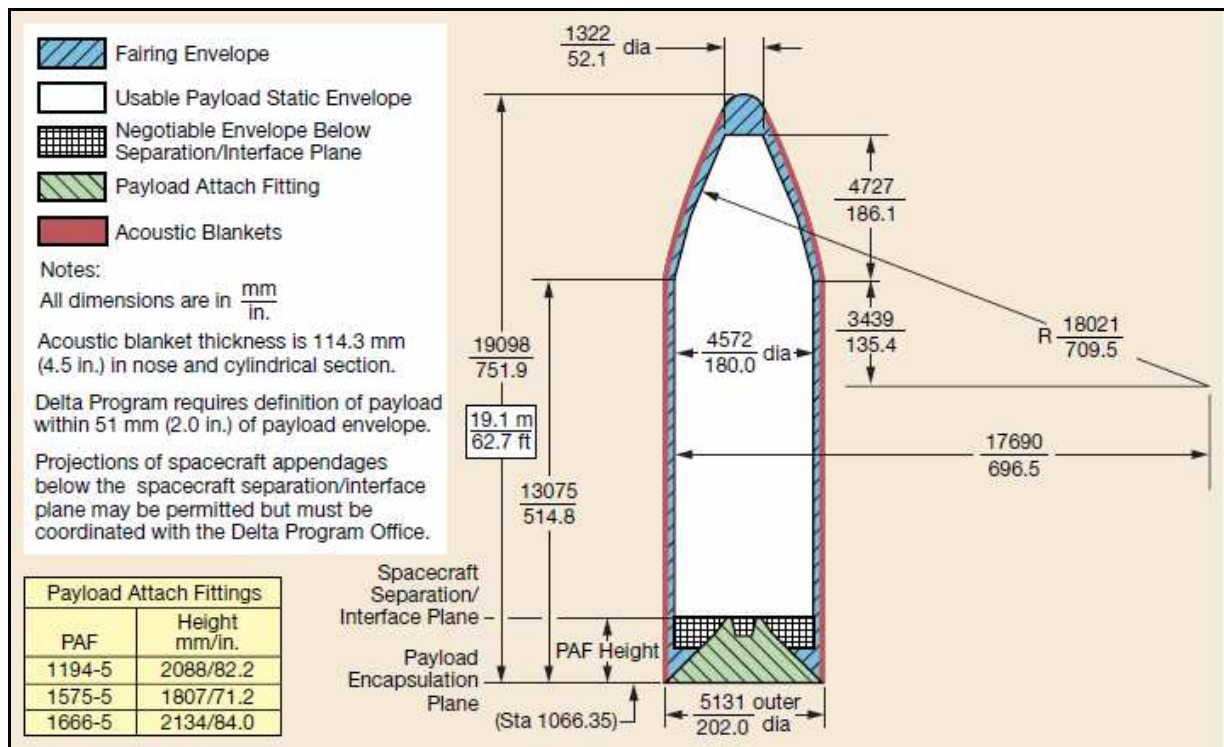


Figure 5-5: "Payload Static Envelope, 5-m-dia by 19.1-m Composite Fairing." ²⁸

Courtesy of the United Launch Alliance.

The Usable Payload Envelope is modeled as a cylinder and frustum. The "frustum incline angle" is used to approximate the curvature of the payload envelope near

²⁸Figure 5-4 Image Source:

United Launch Alliance (2007).
Delta IV, Payload Planners Guide.
Littleton, CO. pp. 85 of 267.

the nose section. Size and volume constraints are important to catalogue, though the nature of our interplanetary mission suggests that mass constraints will be much more limiting.

Parameter	Value	Unit
Cylinder Diameter	4.90	m
Cylinder Height	10.9	m
Frustum Incline Angle	69.2	deg
Frustum Height	4.72	m
Usable Envelope Volume	244	m³

Table 5-2: System-Level Size and Volume Constraints.

The Current Best Estimate mass of 1250 kg is distributed among the Project Upsilon spacecraft. According to the Launch Window, Science Window, and Science Orbit analyses in Chapter 4, the interplanetary flight time to Uranus is nearly 21 years, with a 1.70 km/s maneuver required for orbital capture. A space-storable propellant combination of Nitrogen Tetroxide (N₂O₄) and Monomethylhydrazine (MMH) was chosen to accommodate the interplanetary journey, and additional propellant is allocated such that a 1.79 km/s maneuver may be performed - yielding a 5% ΔV margin. An important limiting factor is that Uranus' surface acceleration of 8.92 m/s² is more than 10% lower than Earth's - increasing the required allotment of propellant mass, and lowering the remaining allotment of inert mass.

The Upsilon-0 Propulsion Module shall implement one or more commercially produced, space-qualified N₂O₄/MMH rocket engines. Engine selection was made with respect to the following design parameters and rationale. The rocket equation is used to allocate propellant mass for Upsilon-0.

$$(m_p)_{U0} = M_{CBE} \left\{ 1 - \exp \left(\frac{-\Delta V_{arrival}}{I_{sp} g_0} \right) \right\} \quad [3]$$

The Specific Impulse and Steady-state Vacuum Thrust are considered in the initial engine selection. Higher (I_{sp}) corresponds to lower required propellant mass. The TRACT patched conic interplanetary trajectory analysis assumes impulsive orbital maneuvers at all nodes. The impulsive orbital maneuver yields the minimum possible required propellant mass. Required propellant mass would increase as thrust decreases, as the orbital maneuver is deviating from the impulse model to the low-thrust model. In addition, the nominal rated Mass Flow Rate and Burn Time for each candidate engine may not be exceeded. The Rocketdyne-Astrium Aestus-II, Rocketdyne ATE, and Aerojet-Rocketdyne R40B, engines and thrusters were examined, comprising a wide range of engine sizes and thrust levels. Table 5-3 shows vital design data on the four candidate engines. The Encyclopedia Astronautica, Delft University of Technology, and EADS Astrium contributed this data, available online. Table 5-4 shows the distribution of propellant mass and inert mass for the spacecraft system, an additional 5% mass contingency was applied for the remaining inert mass.

Parameter	Aestus-II	ATE	R-40B	Unit
Engine Mass	138	58.0	13.6	kg
Engine Length	2.29	1.72	0.72	m
Nozzle Diameter	1.30	0.76	0.41	m
Specific Impulse	340	347	303	s
Vacuum Thrust	55.4	20.0	4.0	kN
Rated Mass Flow	16.5	(unknown)	140	kg/s
Rated Burn Time	600	(unknown)	25000	s
Oxidizer-Fuel Mass Ratio	1.90	1.86	1.65	--

Table 5-3: Selected Design Parameters of Candidate Engines and Thrusters. ²⁹

Parameter	Aestus-II	ATE	R-40B	Unit
Engine Mass	138	58.0	13.6	kg
Propellant Mass	558	548	605	kg
Contingency Mass	26.4	30.6	30.0	kg
Remaining Inert Mass	527	612	600	kg

Table 5-4: Required Mass Distribution to Complete Uranus Arrival Burn.

The R-40B thruster is selected as the main propulsion of Upsilon-0. Although the ATE engine offers more remaining inert mass, little reliable information was obtained about its mass flow and burn time - thus the R-40B, providing similar capability, was

²⁹Table 5-3 References:

Encyclopedia Astronautica (2014).

N2O4/MMH: Associated Spacecraft, Associated Engines, Associated Stages [*Education and Outreach*].

Retrieved From: <http://www.astronautix.com/props/n2o4mmh.htm>

Delft University of Technology (2014).

Performance and Operating Data of Typical Rocket Engines [*Education and Outreach*].

Retrieved From: <http://www.lr.tudelft.nl/en/organisation/departments/space-engineering/space-systems-engineering/expertise-areas/space-propulsion/design-data/performance-and-operating-data/>

EADS Astrium, Airbus Defense & Space (2014).

Space Propulsion. For the Access, Utilisation and Exploration of Space. Aestus II / RS 72 Rocket Engine. [*Online Data Sheet*]. Retrieved From: <http://cs.astrium.eads.net/sp/launcher-propulsion/rocket-engines/>

preferred. The Aestus-II engine is not recommended due to its size and mass detracting from the remaining inert mass. Since the R-40B thruster provides the lowest Specific Impulse and Steady-state Vacuum Thrust, part or all of the contingency mass (30 kg) may be assigned to propellant mass if necessary. If all of the contingency mass is consumed, then the orbital maneuver capability of Upsilon-0 rises to 1.92 km/s, which corresponds to a 8.8% ΔV margin. Multiple thrusters shall be implemented in order to increase reliability, part of the remaining inert mass shall be consumed by way of redundant R-40B thrusters. For instance with **three redundant R-40B thrusters, 572 kg** remain to accommodate the inert mass of Upsilon-0 and wet masses of Upsilon-1 and Upsilon-2. Choice of the R-40B thruster is further supported when adding redundancy to the system, as duplicating the other candidate thrusters consumes far more inert mass.

Spherical propellant tanks, capable of holding Upsilon-0's maximum possible propellant mass (635 kg, design propellant mass plus contingency mass in Table 5-4), are assumed. The density of N₂O₄ and MMH are 1440 kg/m³ and 870 kg/m³ respectively, the propellant mass is split between N₂O₄ and MMH at 1.65 oxidizer-to-fuel ratio (OFR). Table 5-5 shows preliminary sizing of Upsilon-0 propellant tanks. A parametric Mass Estimating Relation (MER) is used to obtain the mass of a tank with propellant management devices (PMD). This, and all subsequent MER are provided in "Mass Estimating Relations" [Akin, 2011]. Propulsion MER's are implemented to estimate thrust structure mass and gimbal mass. Chamber pressure (P_o) for the R-40B thruster is approximately 10.34 bar [Encyclopedia Astronautica].

$$M_{oxi} = m_p \cdot \frac{OFR}{1 + OFR} \quad [4a]$$

$$M_{fuel} = m_p \cdot \frac{1}{1 + OFR} \quad [4b]$$

$$M_{PMD-Tank}[kg] = 34.69V[m^3] + 2 \quad [5]$$

$$M_{TS}[kg] = 2.55 * 10^{-4} \cdot T[N] \quad [6]$$

$$M_{Gim}[kg] = 237.8 \cdot \left\{ \frac{T[N]}{P_o[Pa]} \right\}^{0.9375} \quad [7]$$

Parameter	Value	Unit
N2O4 Mass	396	kg
N2O4 Volume	0.275	m ³
N2O4 Diameter	0.98	m
MMH Mass	239	kg
MMH Volume	0.276	m ³
MMH Diameter	0.98	m
U-0 N2O4 Tank Mass	12	kg
U-0 MMH Tank Mass	12	kg
Thrust Structure	4	kg
Gimbals	4	kg

Table 5-5: Upsilon-0 Propulsion Structure - Mass Allocation.

A fairing and shroud shall provide radiation shielding and thermal insulation, and/or dissipation, over the 21-year journey to Uranus. The Upsilon-1 and Upsilon-2 science spacecraft require protection after disengaging from the Delta IV-Heavy upper stage. The fairing and shroud shall withstand launch stresses, as well as acoustic and vibrational loads associated with the launch environment. In addition, the fairing and shroud shall safely encompass the volume of all mission components above, and its mass shall be minimized to allow for optimal allotment of mass for the science spacecraft. The fairing and shroud, considered a subsystem of Upsilon-0, shall interface with the U-1 power subsystem during the interplanetary journey. The fairing and shroud shall expose

the antenna stack after launch, and detach from the science spacecraft after completing the Uranus arrival burn.

The New Horizons spacecraft, described in Chapter 3 "Heritage", provides a reasonable starting point for size estimation of the science spacecraft, and therefore the Upsilon-0 fairing and shroud. Dimensions for the New Horizons spacecraft are approximately no more than 3.5m-by-2.5m-by-2.5m from photographs and computer models in Fountain et al. (2009). However, initial visions for the Upsilon-1 Science Orbiter picture a more rounded, axisymmetric spacecraft, with the RTG units mounted symmetrically onto the main structure. At this point in the design, the Upsilon-1 Science Orbiter is estimated at 2.2 meters in the longitudinal direction, with the New Horizons heritage telecommunications antenna stack (2.1 meters diameter, ~1.0 meter height) mounted on the spacecraft's rear. Two Upsilon-2 Atmosphere Probes are attached on the sides. All components shall be stacked axially to accommodate launch loads. Estimated height of the fairing and shroud is 3.0 meters, shielding the science spacecraft and antenna stack. Table 5-6 shows the dimensions and surface area distribution of the Upsilon-0 fairing and shroud ("U-0 F/S" in Table 5-6). The frustum slant angle is the bisected vertex angle if the frustum closed to form a cone.

Parameter	Value	Unit
Frustum Height	3.0	m
Frustum Minor Diameter	1.0	m
Frustum Major Diameter	2.2	m
Frustum Slant Angle	78	deg
Total F/S Surface Area	15	m²

Table 5-6: Upsilon-0 Fairing and Shroud - Size Estimation.

The surface area of 15 m² is multiplied by the thickness and density of material to obtain the structural mass. The same area is to be covered by thermal casings (one or more among - multi-layer insulation, radiator panels, and heat pipes). The fairing and shroud shall accommodate the Delta IV-Heavy launch environment and satisfy the following NASA standard structural design Factors of Safety (FOS), shown in Table 5-7. The fairing and shroud is identified as "Primary Structure" and shall provide positive Margin of Safety (MOS) along with 2.0 FOS. FOS and MOS are applied in equation [6], where (σ_{allow}) represents the allowable load of the spacecraft component (of any particular type - compression, buckling, bending etc.), typically given by the material strength; and (σ_{ref}) represents the reference required load incurred during a particular mission critical event. Figure 5-6 shows the Delta IV-Heavy launch acceleration and vibrational loads.

Structure Type	FOS
Primary Structure	2.0
Secondary Structure	1.4
Pressurized Window	4.0
Pressurized Tanks and Lines	3.0

Table 5-7: NASA Minimum Design and Test Factors of Safety. ³⁰

$$MOS = \frac{\sigma_{allow}}{FOS \cdot \sigma_{ref}} - 1 \quad [8]$$

³⁰Table 5-7 Reference:

NASA (2008).
Structural Design and Test Factors of Safety for Spaceflight Hardware.
NASA Technical Standard NASA-STD-5001A, National Aeronautics and Space Administration.

pre-launch state, which corresponds to 75000 N inertial load. A lightweight space-qualified material shall be chosen for the fairing and shroud. Initially, a composite matrix-fiber configuration of Toray 250°F (curing temperature) Epoxy Resin and Toray M55J High Modulus Fiber (60% volume fraction, uni-directional) is examined. Tables 5-8a and 8b show mechanical properties of this carbon fiber composite material. Note that the fiber density is given, though the composite density is not. The composite density is initially assumed at 1700 kg/m³.

Parameter	Value	Unit
Tensile Strength	4,020	MPa
Tensile Modulus	540,000	MPa
Density	1910	kg/m ³
Filament Diameter	5.0	μm

Table 5-8a: Toray M55J High Modulus Carbon Fiber - Mechanical Properties. ³²

Parameter	Value	Unit
Tensile Strength	2,010	MPa
Compressive Strength	880	MPa
Flexural Strength	1,230	MPa
Tensile Modulus	340,000	MPa
Flexural Modulus	280,000	MPa

Table 5-8b: Toray 250°F Epoxy/M55J Composite - Mechanical Properties.

The fairing and shroud may undergo thin tube buckling and compressive yielding in axial loading. Buckling, or bending, is assumed as the primary failure mode in this

³²Tables 5-8a and 5-8b Reference:

Toray Carbon Fibers America, Inc. (undated).
Torayca® M55J Data Sheet [*Online Data Sheet*].
Retrieved from: <http://www.toraycfa.com/pdfs/M55JDataSheet.pdf>

configuration, and the critical buckling stress associated is shown in equation [9], from "Roark's Formulas". The critical buckling stress represents the allowable load in equation [6]; increasing with thickness-to-radius ratio (t/R) - the major radius, 1.1 meters, is initially taken as (R). Flexural Modulus of 280,000 MPa is used for (E), Poisson's Ratio (not provided the Toray Data Sheet) is assumed to be 0.35. Axial load applied over the cross-sectional area (about the cylinder's longitudinal axis) results in compressive stress, shown in equation [10]. Compressive stress represents the reference load in equation [6]. Figure 5-7 shows the allowable load and reference load (FOS applied), along with MOS, for various thicknesses of the carbon fiber composite. All positive MOS are plotted (all negative MOS are masked), indicating the cylinder thickness that satisfies 2.0 FOS.

$$\sigma_{crit} \approx \frac{0.4E}{\sqrt{3(1-\nu^2)}} \frac{t}{R} \quad [9]$$

$$\sigma_{axial} = \frac{P}{2\pi Rt} \quad [10]$$

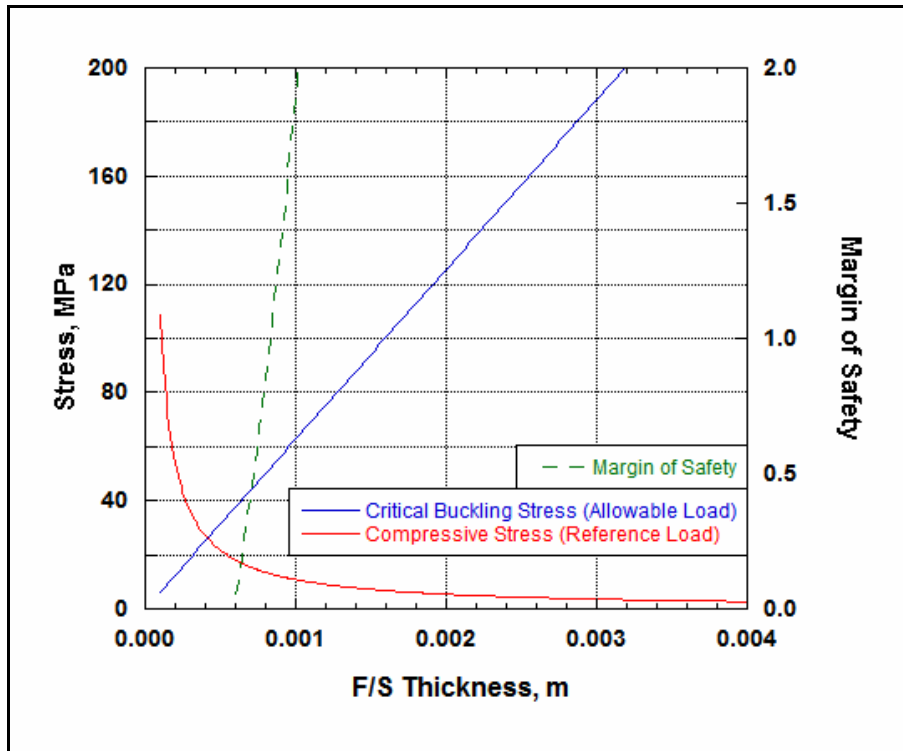


Figure 5-7: Upsilon-0 Fairing and Shroud - Stress and Margin of Safety.

Thickness of 4.0 mm, yielding large positive MOS, is chosen for the cylindrical section. Although MOS reaches positive values at less than 1.0 mm, this would not be a practical measurement with respect to manufacturing and production. Also, it must be presumed that mechanical properties drastically change at extremely small thicknesses - thus 4.0 mm is a more reliable starting point. Next, a more complex conical bending model is considered. The frustum's slant angle of 78 degrees gives rise to a bending moment coupled with the axial load. Both the axial load and bending moment is assumed to be applied at the joining of the cylinder and frustum, where unfavorable stress concentrations are most likely to arise. The bending moment is estimated from a distributed load applied in the frustum's longitudinal direction over the effective length of 0.75 meters - the difference between major and minor radii. Assuming symmetrical

loads, 37,500 N (one-half of the inertial load) is applied on each sloped face of the frustum. The applied bending moment from integrating the 37,500 N load over 0.75 meters is 18,750 N-m. The applied bending moment per length is 25,000 N.

Figure 5-8 shows the coupled load concept, courtesy of "Roark's Formulas". Equations [11a-c] give the Cone Parameters, describing the cone and used to estimate maximum stresses on full cones and truncated cones (i.e. the frustum section); where (α) is the slant angle. (k_A) and (k_B) represent the Cone Parameter (k) calculated at the major radius, and minor radius, respectively. Equations [12-14] are used to calculate the effective bending moment per length (Q_1), as a ratio of the applied bending moment per length (Q_A) at the joining of the cylinder and frustum sections. Finally, equation [15] shows the effective bending stress. Table 5-9 shows values obtained for each of these calculations for the proposed frustum design.

$$k(r) = \frac{2}{\sin(\alpha)} \left[\frac{12(1 - \nu^2)r^2}{t^2 \sec^2(\alpha)} \right]^{\frac{1}{4}} \quad [11a]$$

$$\mu = \left| \frac{k_A - k_B}{\sqrt{2}} \right| \quad [11b]$$

$$\beta = 12\sqrt{1 - \nu^2} \quad [11c]$$

$$Q_1 = Q_A \left(\frac{k_A}{k_B} \right)^{\frac{3}{2}} \left[\left(F_8 + \frac{\sqrt{8}}{k} \nu F_2 \right)_B \cos(\mu) + \left(F_7 + \frac{\sqrt{8}}{k} \nu F_1 \right)_B \sin(\mu) \right] \quad [12]$$

$$C_1 = (F_5)_A + \frac{\sqrt{8}}{k_A} \nu (F_2)_A \quad [13]$$

$$F_1 = 0 \quad [14a]$$

$$F_2 = 1 - \frac{2.652}{k} + \frac{3.516}{k^2} - \frac{2.610}{k^3} + \frac{0.038}{k^4} \quad [14b]$$

$$F_5 = 1 - \frac{3.359}{k} + \frac{7.266}{k^2} - \frac{10.068}{k^3} + \frac{5.787}{k^4} \quad [14c]$$

$$F_7 = 1 - \frac{2.652}{k} + \frac{1.641}{k^2} - \frac{0.290}{k^3} + \frac{2.211}{k^4} \quad [14d]$$

$$F_8 = F_5 \quad [14e]$$

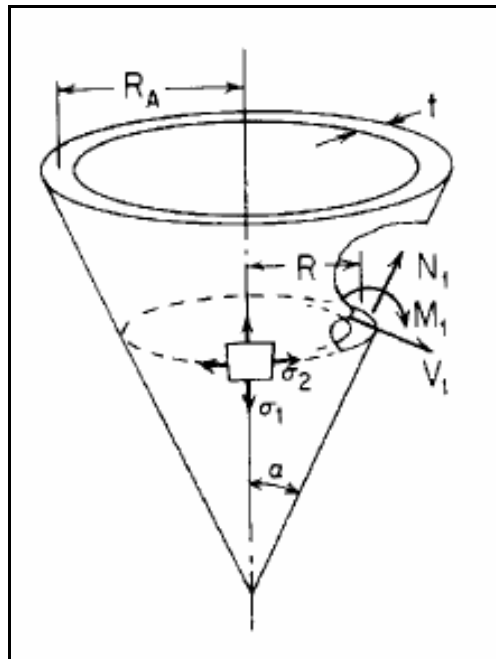


Figure 5-8: "Long Conical Shells with Edge Loads." ³³

Courtesy of W. C. Young [University of Wisconsin, Madison],

and R. G. Budynas [Rochester Institute of Technology].

³³Figure 5-8 Image Source:

Young, W. C., & Budynas, R. G. (2002).
 Roark's formulas for stress and strain (Vol. 7).
 New York: McGraw-Hill.

$$\sigma_{bending} = \frac{-6Q_1}{t^2} \quad [15]$$

Parameter	Value
k_A	27.9
k_B	18.8
μ	6.42
β	11.2
$(F_2)_A$	0.909
$(F_2)_B$	0.868
$(F_5)_A$	0.888
$(F_5)_B$	0.840
$(F_7)_A$	0.907
$(F_7)_B$	0.863
C_1	0.921
Q_1, N	44800
$\sigma_{Bending}, MPa$	1680

Table 5-9: Cone Bending Parameters.

The composite's Flexural Strength is 1230 MPa is lower than the effective bending stress at 4.0 mm - the FOS is not satisfied. The thickness is increased to 4.75 mm, which corresponds to effective bending stress of 579 MPa, satisfies FOS, and yields MOS of 0.06. Initially satisfying column buckling and thin shell bending, mass of the proposed fairing and shroud is estimated. Table 5-10 shows the mass allocation for the Upsilon-0 Propulsion Module at this point in the design. Remaining inert mass is allocated to the Upsilon-1 Science Orbiter, and Upsilon-2 Atmosphere Probe(s) in the following sections.

In all, current design of the Upsilon-0 Propulsion Module satisfies constraints presented by the Uranus Arrival Burn, providing up to 8.8% ΔV margin. The spacecraft system as a whole shall launch with 15% mass margin with 5% mass contingency, with

respect to the Delta IV-Heavy payload capability. The Upsilon-0 fairing and shroud protects the Upsilon-1 and Upsilon-2 science spacecraft up to arrival at Uranus - which may extend the science spacecraft's operational lifetime.

Item	Allocated Mass, kg
U-0 Fairing and Shroud	123
U-0 N2O4 Tank	12
U-0 MMH Tank	12
U-0 R-40B Thrusters (3)	42
U-0 Propulsion Structure	4
U-0 Gimbals	4
U-0 Dry Mass	197
U-0 N2O4 Propellant	396
U-0 MMH Propellant	239
U-0 Propellant Mass	605
U-0 Wet Mass	802
Current Best Estimate	1250
U-0 Contingency	30
Remaining Inert Mass (U-1 and U-2)	418

Table 5-10: Upsilon-0 Propulsion Module - Mass Allocation.

5.2 UPSILON-1 SCIENCE ORBITER

The Upsilon-1 Science Orbiter shall provide observations of Uranus' planetary magnetic field and atmosphere, for at least 20 months during the first two years following orbital capture. The communications subsystem, and power subsystem, are paramount to the design. The communication subsystem imposes requirements on the power subsystem via the Link Budget. Adopting heritage from the New Horizons spacecraft, the Upsilon-1 Science Orbiter shall implement the aligned triple antenna stack comprising one High-gain Antenna, one MGA, and one LGA. For simplicity of design, all communication links between the Project Upsilon spacecraft, and downlink communication shall operate on the same frequency. Choice of Deep Space Network operating frequency band dictates uplink communications. Constraints to the Project Upsilon operating frequency selection include DSN band availability, the Earth's atmospheric absorption, and Uranus' atmospheric absorption.

Table 5-11a shows Deep Space Network band availability provided by the NASA Jet Propulsion Laboratory DSN website. Note that band availability differs between uplink and downlink. Absorption of each frequency band by the Earth's atmosphere, and (current knowledge of) Uranus' atmosphere is compared to support frequency selection. The GATS Inc. Spectral Calculator is used to compute absorption spectra, the HITRAN2008 database [Rothman et al., 2009] is assumed. Operating bands in frequency units are converted to wavenumber units used by the Spectral Calculator, in Table 5-11b. Rounding error is introduced such that the wavenumber window includes frequencies just outside the given bands. Tables 5-12a and 5-12b show atmospheric compositions of Earth and Uranus. Up to six gases may be superimposed in the Spectral Calculator simulation, thus the five most abundant gases - whose data are listed in HITRAN2008 - are listed for Earth's atmosphere [NSSDC]. Ozone (O₃) concentration of five (5) parts

per million is added, with reference to the U.S. Standard Atmosphere Model [NOAA, USAF]. Note that only a statistically estimated water vapor (H₂O) concentration is given due to its variability near Earth's surface. The most likely absorbers of electromagnetic radiation have been catalogued in the Earth atmosphere input.

For simplicity of simulation, the Earth's atmosphere is assumed constant composition throughout the first 5 km; while 100 km is used for the nominal furthest distance below Uranus' cloud tops that Upsilon-2 may communicate with Upsilon-1, upon termination of atmospheric experiments. 100 km is speculated based on Uranus internal model data in Podolak and Cameron (1974) and heritage discussion of the Galileo probe. Nominal pressure of 1 atm (1013 mbar) and temperature of 295 K serve as inputs to generating Earth absorption spectra; 1 atm and 84 K (from Podolak and Cameron) serve as inputs to generating Uranus absorption spectra. For the Earth model - the S-Band, X-Band, and Ka-Band transmittances are approximately 0.98, 0.96, and 0.87 respectively. Uranus' upper atmosphere only negligibly absorbs radiation in the candidate frequency bands. Spectral constraints to the communication subsystem have been examined, and S-Band frequencies - **2.120 GHz for uplink, 2.300 GHz for downlink**, are selected.

DSN Operating Band	Uplink, MHz	Downlink, MHz
S-Band	2110-2120	2290-2300
X-Band	7145-7490	8400-8450
Ka-Band	34200-34700	31800-32300

Table 5-11a: Deep Space Network Operating Frequency Bands (Frequency). ³⁴

³⁴Table 5-11a Reference:
 NASA Jet Propulsion Laboratory (2005). Deep Space Network - Frequently Asked Questions [*Education and Outreach*]
 Retrieved From: <http://deepspace.jpl.nasa.gov>

DSN Operating Band	Uplink, cm ⁻¹	Downlink, cm ⁻¹
S-Band	0.0703-0.0708	0.0763-0.0768
X-Band	0.238-0.250	0.280-0.282
Ka-Band	1.14-1.16	1.06-1.08

Table 5-11b: Deep Space Network Operating Frequency Bands (Wavenumber). ³⁵

Earth's Atmosphere		Uranus' Atmosphere	
Gas Specie	Composition, %	Gas Specie	Composition, %
N ₂	78.08	H ₂	82.5
O ₂	20.95	He	15.2
H ₂ O	~1.0	CH ₄	2.30
CO ₂	0.0400	² H	0.0148
O ₃	0.0005		
CH ₄	0.0002		

Tables 5-12a and 5-12b: Spectral Simulation of Planetary Atmospheres - Earth and Uranus Constituents. ³⁶

Link budgets for the Upsilon-1-to-DSN downlink, and DSN-to-Upsilon-1 uplink are calculated. In the method presented by J.A. Christian (2010), uplink and downlink signals propagate through several conceptual nodes, experiencing amplification or attenuation at each node. For instance, the Upsilon-1-to-DSN downlink consists of: 1) Power input to Upsilon-1 HGA (amplification); 2) Power received by HGA at a given

³⁵Table 5-11a Reference:

Spectral Calculator - Hi-resolution Gas Spectra (2005).
GATS Inc., Boulder, CO [*Online Guided User Interface*].
Retrieved From: <http://www.spectralcalc.com/calc/spectralcalc.php>

³⁶Tables 5-12a and 5-12b Reference:

NASA Goddard Space Flight Center, National Space Science Data Center (2013).
Earth Data Sheet. Uranus Data Sheet [*Online Data Sheets*].
Retrieved From: <http://nssdc.gsfc.nasa.gov/planetary/factsheet/earthfact.html>
<http://nssdc.gsfc.nasa.gov/planetary/factsheet/uranusfact.html>

electronic efficiency (attenuation); 3) Power radiated by HGA parabolic dish (amplification); 4) Power entering Earth's atmosphere after space loss (attenuation); 5) Power through Earth's atmosphere at some zenith angle (attenuation); 6) Power received by DSN, affected by pointing error loss (attenuation); and 7) Power magnified by DSN 70-meter dish (amplification). The DSN-to-Upsilon-1 uplink lists the same nodes in reverse. The Carrier-to-Noise Ratio is calculated with the Noise Temperature and desired Bandwidth, for one unit of power input to the first node. Finally, the Carrier-to-Noise Ratio is used to find the required power input to the first node, through satisfying a certain Link Margin.

The following assumptions are employed in the Link Budget calculation. The Upsilon-1 HGA has 50% electronic efficiency and 50% antenna efficiency. The HGA diameter is equal to that of the New Horizons HGA - 2.1 meters. Space loss is calculated at a nominal distance of 20 AU, which is not exceeded during the Science Window defined in Chapter 4 "Mission Planning Considerations". Atmospheric transmittance is 0.9. The downlink signal reaches Earth near the Equator; and of the three DSN stations, the Madrid 70-meter dish is located at the highest latitude of 40 degrees, which is taken as the zenith angle. Typical spacecraft pointing error (S/C P.E.) of 20 milli-degree (md); and typical DSN receiver pointing error (DSN P.E.) of 6 milli-degree [Slobin and Pham, 2010], are assumed. 600 Hz Bandwidth (equivalent to "data rate") from New Horizons heritage, and 20 K deep space Noise Temperature [Stelzried et al., 2003], are assumed. The nominal objective downlink Link Margin is 5 dB.

Comm. Link	Input, decimal	Output, decimal	Output, dB	Notes
A: Unit Power Input, Space Segment	1.000e+00	1.000e+00	0.00	1 unit of power (W) into the U-1 HGA.
B: Power to U-1 HGA	5.000e-01	5.000e-01	-3.01	0.50 efficiency assumed; f=2.300 GHz.
C: Power Radiated from HGA	1.281e+03	6.405e+02	28.06	New Horizons HGA: d=2.1m.
D: Power after Space Loss	1.207e-29	7.730e-27	-261.12	Nominal distance = 20.0 AU.
E: Power after Atmospheric Loss	2.745e-01	2.122e-27	-266.73	Maximum zenith angle = 40 deg; A. Trans. = 0.9.
F: Power after Pointing Loss	9.964e-01	2.114e-27	-266.75	S/C P.E. = 20 md DSN P.E. = 6 md
G: Power Amplified by DSN Antenna	1.423e+06	3.009e-21	-205.22	Madrid 70-m Antenna Receiving.
H: Carrier-to-Noise Ratio	6.036e+18	1.816e-02	-17.41	Noise Temp. = 20K; Bandwidth = 600 Hz.
I: Comm. System Power Requirement	1.741e+02	3.163e+00	5.00	Power Input meets Link Requirement

Table 5-13a: Link Budget -

Upsilon-1 (New Horizons) HGA, On-orbit Downlink to DSN 70-m Antenna.

Comm. Link	Input, decimal	Output, decimal	Output, dB	Notes
A: Unit Power Input, Ground Segment	1.000e+00	1.000e+00	0.00	1 unit of power (W) into the DSN Antenna.
B: Power Amplified by DSN Antenna	1.209e+06	1.209e+06	60.82	Madrid 70-m Antenna; f=2.120 GHz.
C: Power after Pointing Loss	9.964e-01	1.205e+06	60.81	S/C P.E. = 20 md DSN P.E. = 6 md
D: Power after Atmospheric Loss	2.745e-01	3.307e+05	55.19	Maximum zenith angle = 40 deg; A. Trans. = 0.9.
E: Power after Space Loss	1.421e-29	4.698e-24	-233.28	Nominal distance = 20.0 AU.
F: Power Amplified by U-1 HGA	1.088e+03	5.112e-21	-202.91	New Horizons HGA: d=2.1m.
G: Power Received by U-1	5.000e-01	2.556e-21	-205.92	0.50 efficiency assumed.
H: Carrier-to-Noise Ratio	6.036e+18	1.543e-02	-18.12	Noise Temp. = 20K; Bandwidth = 600 Hz.
I: Comm. System Power From Downlink	1.741e+02	2.687e+00	4.29	Power Input to Uplink L.M.

Table 5-13b: Link Budget -

DSN 70-m Antenna, Uplink to On-orbit Upsilon-1 (New Horizons) HGA.

The Upsilon-1 HGA requires 175 W power input in order to secure a 5 dB downlink Link Margin. A 4.29 dB uplink Link Margin is achieved while operating at this power level. The nominal downlink objective has been achieved, and the uplink Link Margin is satisfactory in initial spacecraft design. Several limiting assumptions may be relaxed as the design matures - spacecraft electronic and antenna efficiency may be increased, atmospheric transmittance may be increased to 0.98 as found in simulation, and the required Bandwidth may be relaxed depending on data type. Nonetheless, 175 W input to the communications subsystem serves as the starting point for power subsystem design and power budgeting.

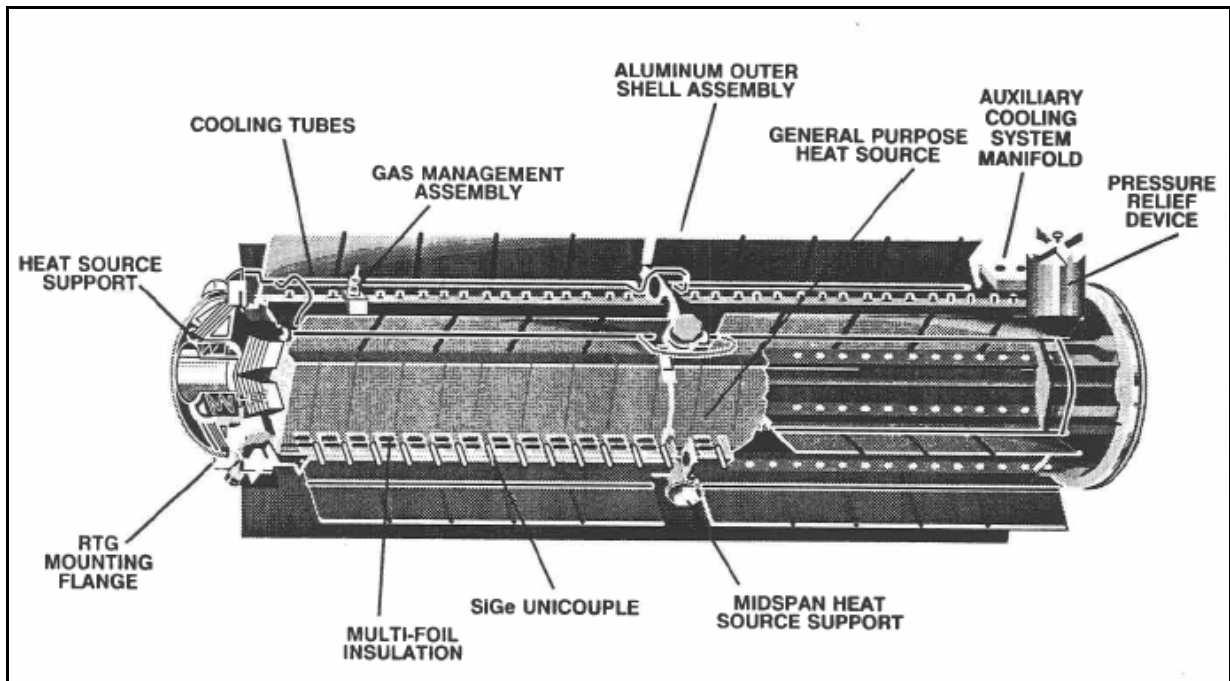


Figure 5-9: "General Purpose Heat Source - Radioisotope Thermoelectric Generator." ³⁷ *Courtesy of E. F. Mastal [U.S. Department of Energy].*

³⁷Figures 5-9 and 5-10 Image Source; Table 5-14 Reference:
Mastal, E. F. (1991). Radioisotope Power Systems for the Common Lunar Lander Program.
Lecture taught by Edward F. Mastal, July 1-2, 1991. U.S. Department of Energy, Washington, D.C.
Lecture conducted during the Common Lunar Lander Workshop, NASA Johnson Space Center.

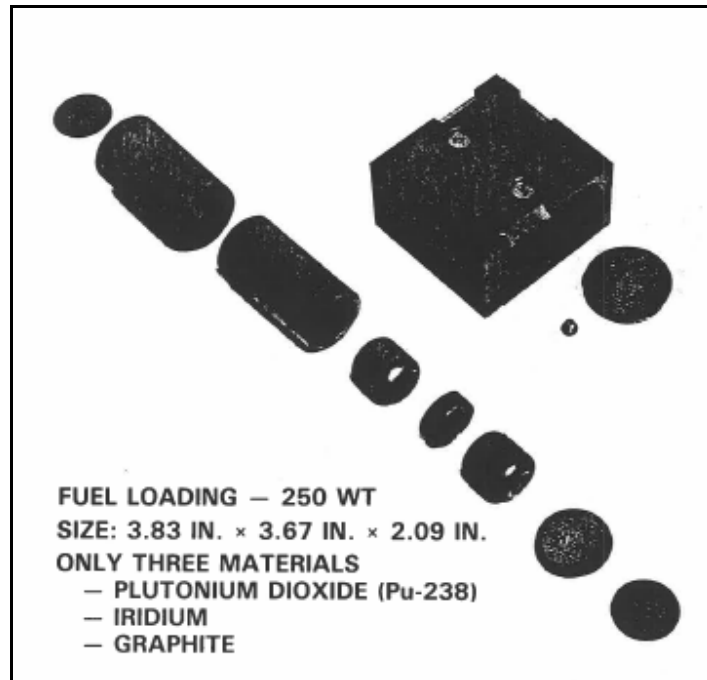


Figure 5-10: Single "General Purpose Heat Source" Module.

Courtesy of E. F. Mastal [U.S. Department of Energy].

One or more Radioisotope Thermoelectric Generators shall provide power to all of the Project Upsilon spacecraft. Figure 5-9 shows the RTG schematic diagram. The radioactive isotope implemented is Plutonium-238, with 87.7 year half-life [Mastal, 1991]. Modular RTG models, individually shown in Figure 5-10, presented by Mastal are rated "from 19 to 340 W" power output (direct quote). One or more "18-module" 340-W rated RTG are required for the Project Upsilon mission. In a back-of-the-envelope calculation, power output of a nominally 340-W RTG decays to 270 W (approximately 80% output) over the 7-year research and development period, and 21-year interplanetary journey. 175 W shall be allocated to the communications subsystem early in the design. In order to accommodate the communication subsystem, and all other subsystems' power consumption, two (2) "18-module" RTG units shall be installed on the

Upsilon-1 Science Orbiter. Upsilon-0 and Upsilon-2 shall interface with these RTG to draw necessary power. Table 5-14 shows vital design parameters for a single "18-module", 340-W rated RTG, the mass is estimated by dividing the nominal power output, by the specific power per mass. Implementation of the dual RTG provides redundancy and necessary power margin over the lifetime of all Project Upsilon spacecraft.

Parameter	Value	Unit
Voltage	30.8	V
Power Output	340	W
Specific Power	7.7	W/kg
Converter Efficiency	7.6	%
Mass (Estimated from above)	45	kg
Length	1.08	m
Diameter	0.33	m

**Table 5-14: Selected Design Parameters of the "18-module",
340-W Modular RTG.**

After meeting power requirements with the Modular RTG, Upsilon-1's thermal footprint is examined. Combination of solar and planetary radiation, spacecraft coating and insulation, and internal power, determine the internal temperature at which electronics and instrumentation operate. Temperature ratings for electronics and instrumentation shall be obeyed in every thermal configuration. Equations [16a-b] show the thermal balance between the spacecraft's interior and the deep space environment, assuming a circular cross-section is exposed to the Sun. Heat is incident upon the spacecraft via solar radiation; while heat radiates out of the spacecraft due to the temperature gradient at the spacecraft-space boundary. The symbol (Q) refers to heat, instead of the bending moment per length used in an earlier section. (I_s) represents the

incident solar flux: 1394 W/m^2 at 1 AU distance (near Earth), and 4 W/m^2 at 20 AU distance from the Sun (near Uranus) [Akin, 2011]. Here, (α) and (ϵ) refer to the thermal absorptivity and emissivity of the spacecraft surface finish, respectively. Figure 5-11 shows acceptable values of (α) and (ϵ) for various surface finishes.

$$Q_{in} = \alpha I_s A_{cs} \quad [16a]$$

$$Q_{out} = \epsilon \sigma_s A_{rad} (T_{eq})^4 \quad [16b]$$

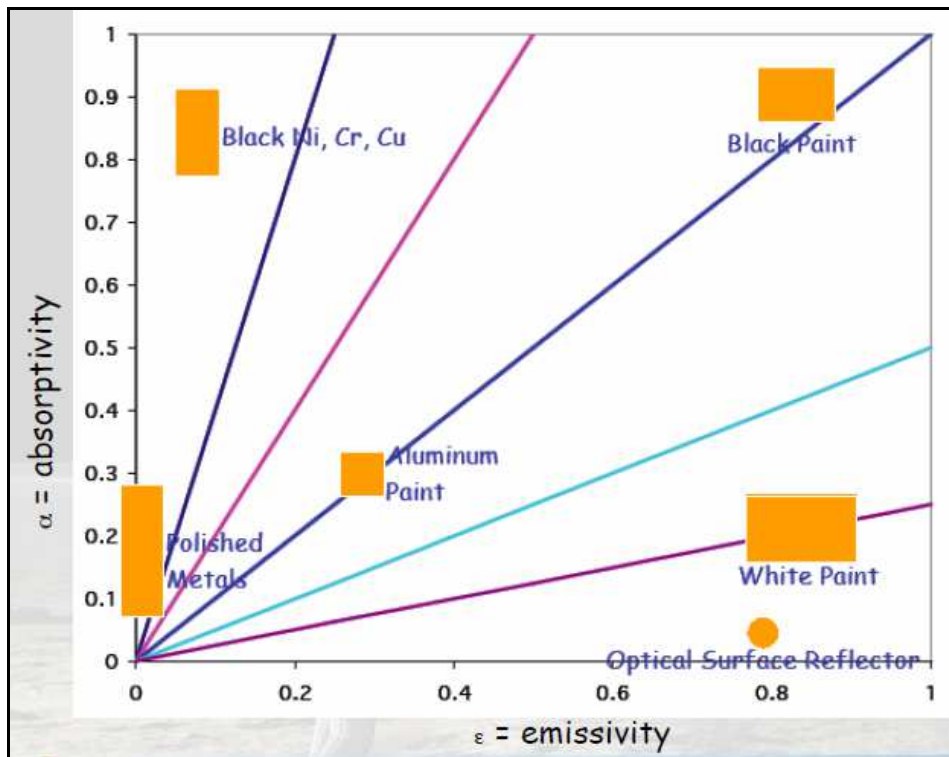


Figure 5-11: "Effect of Surface Coating on Temperature." ³⁸

Courtesy of D. L. Akin [University of Maryland, College Park].

³⁸Figure 5-11 Image Source:

Akin, D. L. (undated). Thermal Analysis and Design. Lecture taught by Dr. David L. Akin, October 23, 2013, Department of Aerospace Engineering, University of Maryland, College Park.

In equation [16b], (A_{rad}) represents the spacecraft's total surface area radiating heat, (σ_s) the Stefan-Boltzmann constant ($5.67 \cdot 10^{-8} \text{ Wm}^{-2}\text{K}^{-4}$), and (T_{eq}) the Equilibrium Temperature. The Equilibrium Temperature is obtained by balancing the incoming and outgoing heat. For instance, consider a bare Aluminum hull for the Upsilon-1 Science Orbiter, with a surface finish ratio (α/ϵ) of 1.1, on-orbit about Uranus ($I_s = 4 \text{ W/m}^2$). In order to house the dual Modular RTG, consider the shape of the hull as an extruded octagonal shell with height nearly equal to that of the RTG ($\sim 1.10 \text{ m}$), bookended by hemispherical endcaps. The Upsilon-0 fairing and shroud accommodates approximately 2.2 meters height (of Upsilon-1, not including antenna stack), thus the hemispherical endcaps are about 1.1 meters in diameter. An octagonal cross-section is incident to the solar flux, but is approximated by a circle (A_{cs}). Equation [16c] gives the Equilibrium Temperature; here, the total surface area is 7.6 m^2 , while the cross-sectional area is 0.95 m^2 . The Equivalent Temperature of Upsilon-1 in this case is 56 K, which is a far too low temperature for electronics and instrumentation to operate. However, the dual RTG constitute a large thermal mass acting on the spacecraft. Some surface finish with (α/ϵ) much less than 1.0, nearly 1.0 (Aluminum), and much greater than 1.0; in combination with the RTG thermal mass, shall achieve the appropriate thermal environment for the spacecraft's instruments.

$$T_{eq} = \left(\frac{\alpha I_s A_{cs}}{\epsilon \sigma_s A_{rad}} \right)^{\frac{1}{4}} \quad [16c]$$

Five other on-orbit thermal configurations are considered: 2) "Black Ni, Cr, Cu" surface finish, with surface finish ratio (α/ϵ) approximately 8.5; 3) "Optical Surface Reflector" surface finish (gold foil, for instance), with surface finish ratio (α/ϵ)

approximately 0.04; 4) Aluminum surface finish with internal power, the thermal balance is adjusted by accounting for the internal power supplied by the dual Modular RTG; 5) "Black Ni, Cr, Cu" surface finish, with internal power (P_{int}); and 6) "Optical Surface Reflector" surface finish, with internal power (P_{int}). Equations [17a-b] show the modified thermal balance and "powered" Equilibrium Temperature, respectively. The dual modular RTG supplying a nominal 4400 W thermal power beginning-of-mission, and 3700 W upon arrival at Uranus, estimated from data given in the Uranus REBEL design report [Rebernak et al., 2012]. Since the RTG are installed outside Upsilon-1, heat pipes may be designed to a certain conduction efficiency directing heat into the spacecraft - assuming a conduction efficiency of 0.5, thermal power from the RTG to the spacecraft are halved. Table 5-15 shows Upsilon-1's Equilibrium Temperature for each thermal configuration. (T_{eq}^*) represents the "powered" Equilibrium Temperature in cases #3 and #4.

$$\alpha I_s A_{cs} + P_{int} = \varepsilon \sigma_s A_{rad} (T_{eq}^*)^4 \quad [17a]$$

$$T_{eq}^* = \left(\frac{\alpha I_s A_{cs} + P_{int}}{\varepsilon \sigma_s A_{rad}} \right)^{\frac{1}{4}} \quad [17b]$$

Surface Finish	Thermal Power, W	Eq. Temp., K
Aluminum	0	55.8
Black Ni, Cr, Cu	0	93.1
Optical Reflector	0	24.4
Aluminum	1850	345
Black Ni, Cr, Cu	1850	455
Optical Reflector	1850	271

Table 5-15: Upsilon-1 Thermal Analysis - Equilibrium Temperature for Various On-orbit Thermal Configurations.

The Aluminum surface finish, combined with dual RTG power supply, yields a 271 K Equilibrium Temperature for Upsilon-1. This thermal configuration is chosen for on-orbit operations, and is applied in the same calculation simulating Earth departure. For Earth departure, $I_s = 1394 \text{ W/m}^2$ and $P_{int} = 2200 \text{ W}$. A new term Environment Temperature (T_{env}) is introduced, representing the low-Earth orbit planetary environment temperature, estimated 280 K [Akin, 2011]. Equations [18a-b] show the re-modified thermal balance, accounting for Environment Temperature, and "powered" Equilibrium Temperature, respectively. The solar irradiation term is set to zero for when the Earth blocks the Sun. The Earth-shaded Equilibrium Temperature is 334 K, while the Sun-exposed Equilibrium Temperature is 335 K. However, the Sun-exposed Equilibrium Temperature assumes solar flux directly incident on Upsilon-1, when the Upsilon-0 fairing and shroud (shielding Upsilon-1) is actually exposed. At the conclusion of thermal analysis and design, a electronics and instrumentation required operating temperature rating is set at approximately 270-340 K. The "Optical Surface Reflector" surface finish with dual Modular RTG, provides acceptable Equilibrium Temperatures for on-orbit operations, the size and volume of Upsilon-1 accommodates the dual Modular RTG and utilizes a satisfactory combination of radiating area and cross-sectional area. Further heat control and regulation is required to achieve the optimal instrument operation thermal environment of approximately 275-325 K [Keese, 2003], however, minimal constraints on the spacecraft's thermal environment have been met.

$$\alpha I_s A_{cs} + P_{int} = \varepsilon \sigma_s A_{rad} \left\{ (T_{eq}^*)^4 - (T_{env})^4 \right\} \quad [18a]$$

$$T_{eq}^* = \left\{ \frac{\alpha I_s A_{cs} + P_{int}}{\varepsilon \sigma_s A_{rad}} + (T_{env})^4 \right\}^{\frac{1}{4}} \quad [18b]$$

Upsilon-1's size and shape are known, which leads well into its structural mass allocations and propulsion capability. Al 7075-T6 is chosen as the hull material; mechanical properties are shown in Table 5-16. The same cylinder buckling analysis used to estimate the Upsilon-0 fairing and shroud mass, is performed on the extruded octagonal shell section of the Upsilon-1 hull. Figure 5-12 shows the allowable load and reference load (FOS applied), along with MOS, for various thicknesses of Al 7075-T6. The cylinder approximates the octagonal shell in shape, but considerations must be made on the octagonal shell's corners - where stress concentrations are most likely to arise. A commonly used factor of 3.0 is applied onto the axial stress incurred by launch loads to model stress concentrations.

Parameter	Value	Unit
Tensile Strength	503	MPa
Fatigue Strength	159	MPa
Shear Strength	332	MPa
Tensile Modulus	71,700	MPa
Density	2810	kg/m ³
Poisson's Ratio	0.33	μm
Coeff. of Thermal Expansion	25.2	10 ⁻⁶ /K

Table 5-16: Al 7075-T6 - Mechanical Properties. ³⁹

³⁹Table 5-16 References:

ASM Material Data Sheet - Al 7075-T6; 7075-T651 (undated).
Aerospace Specification Metals Inc. 2501 N.W. 34th Place #B28, Pompano Beach, FL 33069.
Retrieved From: <http://asm.matweb.com/search/GetReference.asp?bassnum=MA7075T6>

Internal References:

Aluminum Association (1979). Aluminum standards and data. *Aluminum Association*.

Aluminum Association (2006). International alloy designations and chemical composition limits for wrought aluminum and wrought aluminum alloys. *The Aluminum Association, Arlington, Virginia*.

ASM International Handbook Committee (1990).
Metals handbook, vol. 2. - Properties and Selection: Nonferrous Alloys and Special-Purpose Materials.
ASM International 10th Ed. OH: Metals Park.

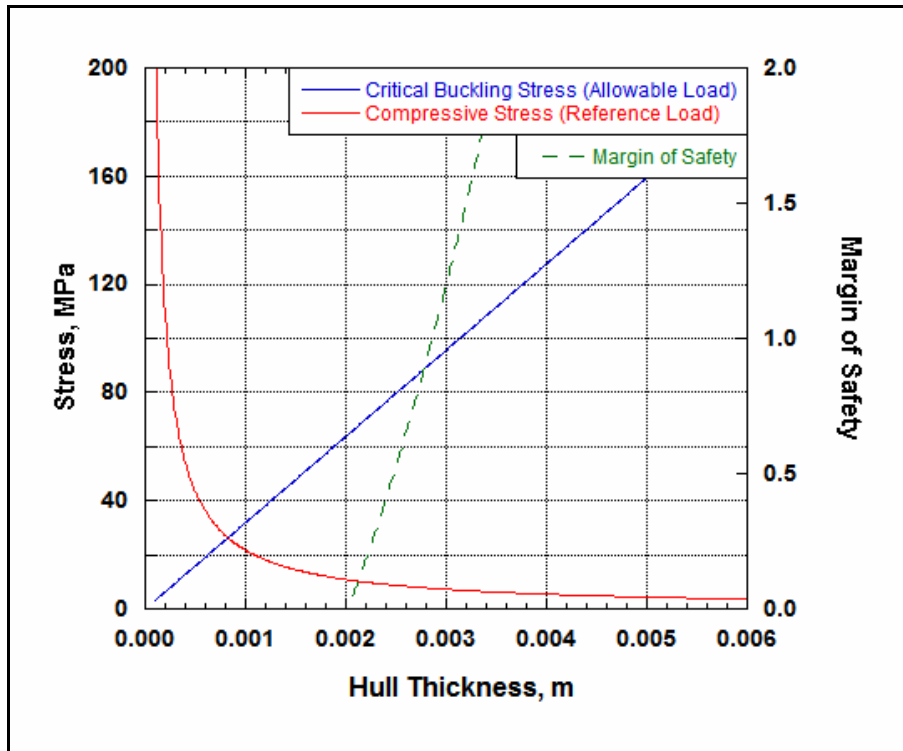


Figure 5-12: Upsilon-1 Structure - Stress and Margin of Safety.

Thickness of 4.0 mm, yielding large positive MOS, is chosen for the hull. Unlike the Upsilon-0 fairing and shroud, the Upsilon-1 hull is pressurized at 1 atm throughout the mission - introducing pressurization stresses. The temperature gradient between spacecraft and environment may reach 350 K, thermal expansion stresses are considered. At the 4.0 mm thickness, the axial stress is 6 MPa, the pressurization stress is 14 MPa, while the thermal expansion stress is 70 MPa. The Al 7075-T6, with yield strength of 503 MPa, at the current thickness, is satisfactory in accommodating launch loads.

Next, propulsion subsystem masses for Upsilon-1 is allocated. Upsilon-1 shall have 0.25 km/s ΔV capability over mission operations, with respect to the current remaining inert mass of 418 kg. The propellant shall be distributed among 16 Rocketdyne RS-45 reaction control thrusters (assemblies of four, on four of eight sides of

the extruded octagonal hull), consuming N2O4-MMH at 1.60 OFR, providing specific impulse of 300 seconds [TU Delft]. N2O4 and MMH propellant tanks are required.

Then, masses of the communications antenna stack (discussed in Chapter 3 "Heritage) and Modular RTG are allocated. 25 kg is given to the Upsilon-1 Planetary Science Package, shown in Table 5-17 consisting of eight (8) distinct instruments. MERs, shown in equations [19] and [20] are used to estimate avionics and wiring masses [Akin, 2011]. The quantity (m_o) is assumed the total mass of all Upsilon-1 components, including propellant. Approximate length of the science orbiter is 2.2 m. Finally, another 5% mass contingency is accumulated for Upsilon-1. Table 5-18 shows mass allocation for the Upsilon-1 Science Orbiter at this point in the design. Remaining inert mass is allocated to the Upsilon-2 Atmosphere Probe(s) in the following section.

In all, current design of the Upsilon-1 Science Orbiter satisfies communication subsystem, power subsystem, thermal subsystem, and structural constraints. The spacecraft's Planetary Science Package shall accomplish the mission's science goals and measurement objectives.

Instrument	Science Goal(s)	Heritage
Star, Planetary, and Sun Cameras	All	Many
Data Processing Unit	All	New Horizons
Low-field Magnetometer	Magnetic Field	Voyager-2
High-field Magnetometer	Magnetic Field	Voyager-2
Electron Drift Instrument	Magnetic Field	Voyager-2
Science Booms	Magnetic Field	--
Radio Science	Gravity Field	Many
Inertial Navigation Unit	Gravity Field	Many

Table 5-17: Upsilon-1 Science Orbiter - Planetary Science Package.

$$M_{avi}[kg] = 10 \{m_o[kg]\}^{0.361} \quad [19]$$

$$M_{wir}[kg] = 1.058 \cdot l[m]^{0.25} \sqrt{m_o[kg]} \quad [20]$$

Item	Allocated Mass, kg
U-1 Main Hull	86
U-1 N2O4 Tank	1
U-1 MMH Tank	1
U-1 RS-45 Thrusters (16)	12
U-1 Comm. Antenna Stack	16
U-1 Modular RTG (2)	90
U-1 Planetary Science Package	25
U-1 Avionics / Flight H.W.	76
U-1 Wiring	22
U-0 Dry Mass	329
U-0 N2O4 Propellant	23
U-0 MMH Propellant	14
U-1 Propellant Mass	37
U-1 Wet Mass	366
Current Best Estimate	418
U-1 Contingency	21
Remaining Inert Mass (U-2)	31

Table 5-18: Upsilon-1 Science Orbiter - Mass Allocation.

5.3 UPSILON-2 ATMOSPHERE PROBE

The Upsilon-2 Atmosphere Probe shall deploy in the extended mission phase, obtaining in-situ physical and chemical measurements below Uranus' cloud tops. The current design flowdown has limited the size and scope of Upsilon-2 to approximately that of a single "micro-satellite" or "microsat" less than 100 kg in mass [Hastrup et al., 1999]. For the complex science objectives and short time scale of the probing mission, the microsat template shall be modified with an emphasis on scientific instruments, while propulsion capability shall be minimized to satisfy Uranus entry maneuvers only. The notion of Upsilon-2 is feasible, given recent advances in "small satellite" research both at the national institutional level and the university level [Heidt et al., 2000].

Upsilon-2 shall detach from Upsilon-1 at or near the Science Orbit apoapse, and perform an orbital transfer to lower its orbital periapse to a distance below that of Uranus' planetary radius. The Science Orbit periapse and apoapse are 26880 km and 170670 km, respectively; the apoapse orbital velocity is 3.04 km/s. Table 5-19 shows the inert mass-propellant mass distribution for the Upsilon-2 atmospheric entry burn, for various depths below Uranus' cloud tops.

Maximum possible mass of the Upsilon-2 Atmosphere Probe is the Current Best Estimate Mass (of the spacecraft system) of 1250 kg, minus the Wet Masses of Upsilon-0 and Upsilon-1, which yields 82 kg. Any projected mass for Upsilon-2 (in kg) may be multiplied to the following percentages in order to obtain the actual inert mass and propellant mass (in kg). A storable mono-propellant is recommended for the propulsion system, eliminating the need for dual tanks. EADS Astrium offers 1 N, 20 N, and 400 N Hydrazine thrusters, all less than 3 kg mass, with operation heritage since 1997. Table 5-19 assumes the Uranus entry maneuver may be completed with a single 20 N Hydrazine thruster burn, consuming all available propellant. The 20 N thruster provides 225 s

specific impulse [EADS Astrium]. A 15% mass contingency is applied in calculating the inert mass fraction. To ensure the desired depth within Uranus' atmosphere is achieved, all of the contingency mass may be assigned as propellant.

Periapse Radius, km	Depth, km	ΔV , km/s	Inert Mass, %	Propellant Mass, %
25560	0	0.0654	84.1	15.9
25360	200	0.0756	83.7	16.3
25160	400	0.0858	83.2	16.8
24960	600	0.0960	82.8	17.2
24760	800	0.107	82.4	17.6
24560	1000	0.117	81.9	18.1

Table 5-19: Upsilon-2 Atmosphere Probe - Mass Distribution.

An optimal entry depth of periapse between 0-1000 km shall be chosen. The various depths stated in Table 5-19 yield increasing Flight Path Angles⁴⁰ in atmospheric entry. The Flight Path Angle is the angle between the local horizontal and the velocity vector at any point in the orbit. For an initial calculation, the orbit equation [21] is used to find the true anomaly on entry, setting the orbital radius to the planetary radius. The Flight Path Angle is found with [22] with true anomaly as input. Ballistic entry properties of the U-2 probe must be found to determine the optimal entry depth.

$$r(\theta) = \frac{a(1 - e^2)}{1 + e \cos(\theta)} \quad [21]$$

$$\tan(\gamma) = \frac{e \sin(\theta)}{1 + e \cos(\theta)} \quad [22]$$

⁴⁰Federal Aviation Administration (undated).

Section III.4.1.7 - Returning From Space: Re-entry [*Education and Outreach*].

Retrieved From:

https://www.faa.gov/other_visit/aviation_industry/designees_delegations/designee_types/ame/media/Section%20III.4.1.7%20Returning%20from%20Space.pdf

Periapse Radius, km	Depth, km	γ, deg
25560	0	0
25360	200	4.68
25160	400	6.63
24960	600	8.13
24760	800	9.41
24560	1000	10.5

Table 5-20: Upsilon-2 Atmosphere Probe - Entry Flight Path Angles.

Upsilon-2 shall implement a single New Horizons heritage MGA, in order to compromise between signal coverage and amplification. The probe shall remain in low-power, standby state during the interplanetary journey, drawing power from Upsilon-1. Upsilon-2 loses its primary heat source after disengaging from Upsilon-1, thus RTG units shall again be implemented. The SNAP-19 (Systems for Nuclear Power-19), 14 kg in mass, providing 25 W electrical power (beginning-of-life; up to 20 W beginning-of-mission) [Bennett, 2006] may be re-commissioned, fitting the size and scope of Upsilon-2. Several smaller SNAP-3 units (3 kg mass, 3 W beginning-of-life power) may serve as an alternative implementation, albeit yielding lower power output-to-mass.

Upsilon-2 shall employ the Galileo heritage Neutral Mass Spectrometer as its primary atmospheric science instrument; along with some combination of the Voyager-2 heritage Ultraviolet Spectrometer, Infrared Spectrometer and Radiometer, and Photo-polarimeter. Data Processing Units draw from New Horizons heritage, and Inertial Navigation Units are included.

Component / Instrument	Component Mission(s)	Heritage
Medium-gain Antenna	All	New Horizons
Data Processing Unit	All	New Horizons
Inertial Navigation Unit	All	Many
Neutral Mass Spectrometer	Atmosphere	Galileo
Ultraviolet Spectrometer	Atmosphere	Voyager-2
Infrared Spect./Radiometer	Atmosphere	Voyager-2
Photo-polarimeter	Atmosphere	Voyager-2
SNAP-19 RTG	Power	Many
Astrium 20 N Thruster	Entry	Many

**Table 5-21: Upsilon-2 Atmosphere Probe -
Spacecraft Components and Atmospheric Science Package.**

In all, design of the Upsilon-2 Atmosphere Probe is constrained by mass, power, and volume available, much more so than Upsilon-0 and Upsilon-1. The current design impasse is encountered via the top-down flow of resource allocation. In a future effort, a small-to-large design process may result in greater science capability for Upsilon-2; though effects of that added capability (thereby inducing added complexity) on the two larger Project Upsilon vehicles is yet to be explored. Table 5-21 lists spacecraft components and scientific instruments that may be installed on Upsilon-2, in order to successfully complete its probing mission.

5.4 COST ESTIMATION

Parametric Cost Estimating Relations (CER) are used to approximate research and development costs of each Project Upsilon spacecraft. Table 5-21 shows parameters for various space vehicle classifications [Akin, 2011]. The output cost varies as a function of the spacecraft's Dry Mass, raised to a certain power (b), and multiplied by a constant (a). Note that both (a) and (b) may differ between the Non-recurring Cost and 1st Unit Production Cost. This model estimates cost in millions USD FY-2008.

Spacecraft Type	a (N.R.C.)	b (N.R.C.)	a (R.C.)	b (R.C.)
Launch Vehicle Stage	8.662	0.55	0.2057	0.662
Manned Spacecraft	21.95	0.55	0.6906	0.662
Unmanned Planetary	13.89	0.55	1.071	0.662
Unmanned Earth Orbital	4.179	0.55	0.4747	0.662
Liquid Rocket Engine	34.97	0.55	0.1924	0.662
Scientific Instrument	2.235	0.50	0.3163	0.700

Table 5-22: "Spacecraft / Vehicle Level Costing Model." ⁴¹

Dry Masses of the Upsilon-0 Propulsion Module and Upsilon-1 Science Orbiter are 197 kg, 329 kg, and 82 kg respectively. Upsilon-0, Upsilon-1, and Upsilon-2 are modeled as: "Launch Vehicle (Upper) Stage", "Unmanned Planetary", and "Scientific Instrument", respectively. 85% Learning Curve - factor applied to cost estimation of subsequent vehicles after successful production of the first vehicle - is applied. Table 5-23 shows Non-recurring and Recurring cost estimates for the Project Upsilon spacecraft.

⁴¹Table 5-22 Reference:

Akin, D. L. (undated). Cost Estimation and Engineering Economics.
Lecture taught by Dr. David L. Akin, September 20, 2013, Department of Aerospace Engineering, University of Maryland, College Park.

Spacecraft	N.R.C, M 08-USD	1st Unit, M-08 USD	2nd Unit, M-08 USD	Subtotal, M-15 USD
U-0 Propulsion Module	159	7	6	226
U-1 Science Orbiter	337	50	43	566
U-2 Atmosphere Probe	21	7	6	45
Total (R&D+Prod.) Cost	837			

Table 5-23: Project Upsilon Spacecraft Total R&D and Production Cost.

The Uranus Orbiter and Probe mission, as proposed in the Planetary Science Decadal Survey is estimated to cost 2.7 billion USD (FY-2015). 4% Inflation Rate is applied to the 2008-USD estimate to extrapolate to 2015-USD. 840 million USD (FY-2015) is estimated for the Project Upsilon spacecraft. It may be advisable to allocate at least twice this value in order to account for testing, launch, and system infrastructure costs. A nominal cost estimate for the Project Upsilon mission, through all project life cycle phases, is **1.7 billion USD**. This final value is lower than cost estimates stated by the Planetary Science Decadal Survey, partly due to size limitations on the spacecraft. Hubbard et al. (2012) led NASA studies on a Uranus Orbiter and Probe mission employing solar-electric propulsion, and devised a 4500-kg spacecraft system with 1100-kg payload on arrival. Arridge et al. (2010) led similar ESA studies, and devised a 2800-kg spacecraft system with 900-kg payload (orbiter only) on arrival. The current design of Project Upsilon fits within the NASA Planetary Science Flagship Class Mission notion, and may be further down-ranked to a "sub-Flagship" class mission.

Chapter 6: Conclusions

Project Upsilon is a proposed NASA Flagship Class, Uranus Orbiter and Probe mission concept to investigate Uranus' planetary magnetic field. Three spacecraft - the Upsilon-0 Propulsion Module, the Upsilon-1 Science Orbiter, and the Upsilon-2 Atmosphere Probe - shall be implemented to meet needs, goals, and objectives as stated by the NASA Solar System Planetary Science Decadal Survey 2013-2022.

Project Upsilon aims to extend our knowledge of Giant Planet magnetic fields, and Ice Giant Planet dynamics. The planetary magnetic field measurement mission seeks to deliver real-time observations for at least 20 months during the first two years. Meanwhile, one or more atmosphere probes descend into unique weather formations on Uranus. An extended mission commences at the end of the initial two-year period, for as long as possible allowable by the science orbiter. The Project Upsilon mission plan draws heritage from the Voyager-2, ESA CHAMP, Galileo, and New Horizons missions. The mission unites NASA, national research institutions and universities, and amateur observers in the human infrastructure.

The Science Orbit about Uranus utilizes nearly repeating spacecraft tracks, slowly scanning over longitude in order to approximate the location at least one Magnetic Pole. The orbit spans a wide range of latitudes; and spans from 1,500 km above Uranus' cloud tops, to more than 170,000 km orbital radius, just below the region where Uranus's magnetosphere interacts with solar, cosmic, and galactic streams. The orbit avoids Uranus' ring system, and crosses the equatorial plane with little hazard from Uranus' moons.

The Launch Window arrives after a 7-year research and development, testing and verification, and integration period of the project life cycle. Launch is scheduled, via a

NASA EELV Delta IV-Heavy vehicle, on May 5, 2021 during a 7-day optimal window within a 21-day best candidate window. The first 140-day Science Window begins immediately after the spacecraft arrive at Uranus, in December 2041. Subsequent 180-day Science Windows are available in each subsequent year.

The Estimation Method for mission science phases is derived with respect to three characteristic quantities of the planetary magnetic field - Intensity, Inclination, and Declination. Two Science Phases are devised. During the first Science Phase, location of at least one of Uranus' Magnetic Poles shall be approximated. During the second Science Phase, the planetary magnetic field shall be modeled as a function of latitude and orbital altitude. Introductory numerical models and *a priori* estimates are presented.

The Upsilon-0 Propulsion Module shall facilitate the Uranus arrival burn, and de-orbit into Uranus thereafter. The propulsion spacecraft has a wet mass of approximately 800 kg, with 600 kg propellant. Upsilon-0 provides Upsilon-1 and Upsilon-2 with radiation and space debris shielding, extending the science spacecraft's operational lifetime at Uranus. An epoxy-carbon fiber composite is implemented in order to provide structural reliability at reduced mass. Space-storable N₂O₄-MMH bi-propellant combination is chosen.

The Upsilon-1 Science Orbiter shall measure and characterize Uranus' magnetic field. The science orbiter has a wet mass of approximately 370 kg, with 40 kg propellant. Operating on dual Modular Radioisotope Thermoelectric Generators, 540 W beginning-of-mission power is allocated among spacecraft subsystems. Upsilon-1 employs the New Horizons heritage triple antenna stack - the 2.1-meter High-gain Antenna facilitates communication with the Deep Space Network.

The Upsilon-2 Atmospheric Probe shall descend into unique weather formations as they are observed, as part of an extension to the planetary magnetic field mission plan.

The probe has a upper bound wet mass of approximately 80 kg, within the "micro-satellite" or "microsat" regime. Approximate inert mass-propellant mass distributions have been calculated for Uranus entry maneuvers. The probe utilizes Galileo and Voyager-2 heritage instrumentation to obtain in-situ physical and chemical data below Uranus' cloud tops. In all, Project Upsilon is estimated to incur 2.1 billion USD (FY-2015) in costs through the entire project life cycle.

This report presents a notional mission plan and spacecraft design for the Uranus Orbiter and Probe Mission. The nature of space mission planning and analysis, along with space systems design, suggests much future work is required before consideration for NASA Announcements of Opportunity. The design in this report contains mission planning and systems engineering concepts in the Pre-phase A and Phase A of the project life cycle. A full concept design, for consideration to NASA Announcements of Opportunity, would require a comprehensive and exhaustive examination of the entire mission architecture and all spacecraft systems.

Nonetheless, the author gained essential knowledge and skills, combining and integrating engineering concepts learned at both the undergraduate and graduate level. The author hopes this report may offer some contribution to the efforts of future Space Systems Engineering Design, and Spacecraft and Mission Design teams. Through performing the analysis shown, and compiling this report, the author has gained an appreciation for the space mission planning process, and sincerely wishes that a Uranus Orbiter and Probe Mission is successfully completed during his career. The author has gained an interest and enthusiasm for the planetary sciences, and research of our solar system.

Bibliography

- [1] National Research Council, Space Studies Board (2012).
Vision and Voyages for Planetary Science in the Decade 2013-2022.
National Academies Press.
- [2] Hofstadter, M.
The Case for a Uranus Orbiter.
White Papers for the Planetary Science Decadal Survey.
- [3] Hofstadter, M.
The Atmospheres of the Ice Giant Planets, Uranus and Neptune.
White Papers for the Planetary Science Decadal Survey.
- [4] Maharik, M., & Fischhoff, B. (1993).
Contrasting perceptions of the risks of using nuclear energy sources in space.
Journal of Environmental Psychology, 13 (3), 243-250.
- [5] Dawson, S. A. (2006).
New Horizons risk communication strategy, planning, implementation, and lessons learned.
Pasadena, CA: Jet Propulsion Laboratory, National Aeronautics and Space Administration.

- [6] Bettadpur, S. V. (2013).
Project Life Cycle Module.
Lecture taught by Dr. Srinivas V. Bettadpur, September 3, 2013; ASE 374K: Space Systems Engineering Design, Cockrell School of Engineering, The University of Texas at Austin.
- [7] Bettadpur, S. V. (2013).
Mission Scope: Design Reference Mission (DRM) and Concept of Operations (ConOps) Module.
Lecture taught by Dr. Srinivas V. Bettadpur, September 5, 2013; ASE 374K: Space Systems Engineering Design, Cockrell School of Engineering, The University of Texas at Austin.
- [8] NASA Jet Propulsion Laboratory, Mars Exploration Program (undated)
Theme: Mars Exploration [*Online Technical Report*].
Retrieved From: http://www.nasa.gov/pdf/55390main_07%20MEP.pdf
- [9] NASA Jet Propulsion Laboratory, Deep Space Network (undated).
The Evolution of Technology in the Deep Space Network - A History of the Advanced Systems Program, "Advanced Systems Program and the Galileo Mission to Jupiter" [*Historical Article*].
Retrieved From:
http://deepspace.jpl.nasa.gov/technology/95_20/gll_case_study.html
- [10] NASA Goddard Space Flight Center, National Space Science Data Center (2010).
Uranus Data Sheet [*Online Data Sheet*].
Retrieved From: <http://nssdc.gsfc.nasa.gov/planetary/factsheet/uranusfact.html>

- [11] Podolak, M., & Cameron, A. G. W. (1974).
Models of the Giant Planets.
Icarus, 22 (2), 123-148.
- [12] Ness, N. F., Acuna, M. H., Behannon, K. W., Burlaga, L. F., Connerney, J. E., Lepping, R. P., & Neubauer, F. M. (1986).
Magnetic Fields at Uranus.
Science, 233 (4759), 85-89.
- [13] Connerney, J. E. P., Acuña, M. H., & Ness, N. F. (1987).
The Magnetic Field of Uranus.
Journal of Geophysical Research: Space Physics (1978–2012), 92 (A13), 15329-15336.
- [14] Newburn Jr., R. L., & Gulikis, S. (1973).
A survey of the outer planets Jupiter, Saturn, Uranus, Neptune, Pluto, and their satellites.
Space Science Reviews, 14(2), 179-271.
- [15] Hofstadter, M. D., & Butler, B. J. (2003).
Seasonal change in the deep atmosphere of Uranus.
Icarus, 165(1), 168-180.
- [16] Hammel, H. B., De Pater, I., Gibbard, S., Lockwood, G. W., & Rages, K. (2005).
Uranus in 2003: Zonal winds, banded structure, and discrete features.
Icarus, 175(2), 534-545.

- [17] Klein, W. D., Mandt, G. A., & Gagliardo, J. (1992).
Defense Meteorological Satellite Program..
In 6th Conference on Satellite Meteorology and Oceanography (Vol. 1, pp. 450-452).
- [18] Lühr, H., Schwintzer, P., & Wickert, J. (2005).
Earth observation with CHAMP.
C. Reigber (Ed.). Springer.
- [19] Friis-Christensen, E., Luhr, H., & Hulot, G. (2006).
Swarm: A constellation to study the Earth's magnetic field.
Earth, Planets, and Space, 58(4), 351-358.
- [20] Maus, S., Macmillan, S., McLean, S., Hamilton, B., Thomson, A., Nair, M., & Rollins, C. (2010).
The US/UK world magnetic model for 2010-2015.
NOAA National Geophysical Data Center.
- [21] Grand, S. P. (2013).
Magnetism, Earth's Magnetic Field.
Lecture taught by Dr. Stephen P. Grand, January 30, 2013; GEO384D - Global Geophysics / Physics of Earth, Jackson School of Geosciences, The University of Texas at Austin.

- [22] NASA Goddard Space Flight Center (2009).
 Rules for the Design, Development, Verification, and Operation of Flight Systems.
Goddard Technical Standards, GSFC-STD-1000E.
- [23] Kohlhase, C. E., & Penzo, P. A. (1977).
 Voyager mission description.
Space science reviews, 21 (2), 77-101.
- [24] Cesarone, R. J., Sergeevsky, A. B., & Kerridge, S. J. (1984).
 Prospects for the Voyager extra-planetary and interstellar mission.
British Interplanetary Society, Journal (Interstellar Studies) (ISSN 0007-084 X), 37, 99-116.
- [25] Ludwig, R., & Taylor, J. (2002).
 Voyager telecommunications.
DESCANSO Design and Performance Summary Series.
- [26] NASA Jet Propulsion Laboratory (1979-86).
 Voyager Bulletins. Mission Status Report No. 45. July 5, 1979.
 Voyager Bulletins. Mission Status Report No. 68. April 10, 1985.
 Voyager Bulletins. Mission Status Report No. 69. June 20, 1985.
 Voyager Bulletins. Mission Status Report No. 70. August 20, 1985.
 Voyager Bulletins. Mission Status Report No. 73. December 4, 1985.
 Voyager Bulletins. Mission Status Report No. 77. February 5, 1986.
 Voyager Bulletins. Mission Status Report No. 79. February 12, 1986.
 [News Bulletins]
 Retrieved From: <http://www.planetary.org/explore/resource-library/voyager-mission-status.html>

- [27] de Pater, I., & Dames, H. A. (1979).
Jupiter's radiation belts and atmosphere.
Astronomy and Astrophysics, 72, 148-160.
- [28] Matousek, S. (2007).
The Juno new frontiers mission.
Acta Astronautica, 61(10), 932-939.
- [29] Behannon, K. W., Acuna, M. H., Burlaga, L. F., Lepping, R. P., Ness, N. F., & Neubauer, F. M. (1977).
Magnetic field experiment for Voyagers 1 and 2.
Space Science Reviews, 21 (3), 235-257.
- [30] Sabaka, T. J., Olsen, N., & Purucker, M. E. (2004).
Extending comprehensive models of the Earth's magnetic field with Ørsted and CHAMP data.
Geophysical Journal International, 159 (2), 521-547.
- [31] Olsen, N., Lühr, H., Sabaka, T. J., Manda, M., Rother, M., Tøffner-Clausen, L., & Choi, S. (2006).
CHAOS - a model of the Earth's magnetic field derived from CHAMP, Ørsted, and SAC-C magnetic satellite data.
Geophysical Journal International, 166 (1), 67-75.

- [32] Lesur, V., Wardinski, I., Rother, M., & Manda, M. (2008).
GRIMM: the GFZ Reference Internal Magnetic Model based on vector satellite and observatory data.
Geophysical Journal International, 173 (2), 382-394.
- [33] Niemann, H. B., Atreya, S. K., Carignan, G. R., Donahue, T. M., Haberman, J. A., Harpold, D. N., ... & Way, S. H. (1996).
The Galileo probe mass spectrometer: Composition of Jupiter's atmosphere.
Science, 272 (5263), 846-849.
- [34] Niemann, H. B., Atreya, S. K., Carignan, G. R., Donahue, T. M., Haberman, J. A., Harpold, D. N., ... & Way, S. H. (1998).
The composition of the Jovian atmosphere as determined by the Galileo probe mass spectrometer.
Journal of Geophysical Research: Planets (1991–2012), 103(E10), 22831-22845.
- [35] Young, R. E. (1998).
The Galileo probe mission to Jupiter: Science overview.
Journal of Geophysical Research: Planets (1991–2012), 103(E10), 22775-22790.
- [36] Hammel, H. B., Sromovsky, L. A., Fry, P. M., Rages, K., Showalter, M., de Pater, I., ... & Deng, X. (2009).
The Dark Spot in the atmosphere of Uranus in 2006: Discovery, description, and dynamical simulations.
Icarus, 201(1), 257-271.

- [37] Showman, A. P., & Dowling, T. E. (2000).
Nonlinear simulations of Jupiter's 5-micron hot spots.
Science, 289 (5485), 1737-1740.
- [38] Hammel, H. B., Rages, K., Lockwood, G. W., Karkoschka, E., & de Pater, I. (2001).
New measurements of the winds of Uranus.
Icarus, 153(2), 229-235.
- [39] Stern, S. A. (2009).
The New Horizons Pluto Kuiper belt mission: an overview with historical context.
In New Horizons (pp. 3-21). Springer New York.
- [40] DeBoy, C. C., Haskins, C. B., Brown, T. A., Schulze, R. C., Bernacik, M. A., Jensen, J. R., ... & Hill, S. (2004, March).
The RF telecommunications system for the New Horizons mission to Pluto.
In Aerospace Conference, 2004. Proceedings. 2004 IEEE (Vol. 3). IEEE.
- [41] Christian, J. A. (2010). Communications Subsystem.
Lecture taught by Dr. Wallace T. Fowler, undated 2013; ASE 387P2 - Mission Analysis and Design, Department of Aerospace Engineering and Engineering Mechanics, The University of Texas at Austin.
- [42] Fowler, W. T. (undated). Repeating Groundtracks.
Lecture taught by Dr. Wallace T. Fowler, February 8, 2013; ASE 387P2 - Mission Analysis and Design, Department of Aerospace Engineering and Engineering Mechanics, The University of Texas at Austin.

- [43] Hahn, J. (2013).
The Dynamics of Planetary Systems and Astrophysical Disks.
Wiley-Interscience.
- [44] Kaula, W. M. (2000).
Theory of satellite geodesy: applications of satellites to geodesy.
Courier Dover Publications.
- [45] NASA Goddard Space Flight Center, National Space Science Data Center (2010).
Uranus Satellite Fact Sheet [*Online Data Sheet*].
Retrieved From:
<http://nssdc.gsfc.nasa.gov/planetary/factsheet/uraniansatfact.html>
- [46] NASA Goddard Space Flight Center, National Space Science Data Center (2010).
Uranus Rings Fact Sheet [*Online Data Sheet*].
Retrieved From: <http://nssdc.gsfc.nasa.gov/planetary/factsheet/uranringfact.html>
- [47] Tapley, B. D., Schutz, B. E., & Born, G. H. (2004).
Statistical orbit determination.
Burlington: Elsevier Academic Press.
- [48] McAdams, J., Scott, C., Guo, Y., Dankanich, J., & Russell, R. (2011).
Conceptual Mission Design of a Polar Uranus Orbiter and Satellite Tour.
Spaceflight Mechanics, 140.

- [49] Brennan, M. J. (2011).
Patched Conic Interplanetary Trajectory Design Tool [*M.S. Thesis*].
The University of Texas at Austin, Austin, TX.
- [50] NASA Jet Propulsion Laboratory - Solar System Dynamics (2014).
JPL Planetary AND Lunar Ephemerides [*Online Data Sheet*].
Retrieved From: http://ssd.jpl.nasa.gov/?planet_eph_export
- [51] Press, W. H. (2007).
Numerical recipes 3rd edition: The art of scientific computing.
Cambridge university press.
- [52] Lagarias, J. C., Reeds, J. A., Wright, M. H., & Wright, P. E. (1998).
Convergence properties of the Nelder--Mead simplex method in low dimensions.
SIAM Journal on Optimization, 9 (1), 112-147.
- [53] United Launch Alliance (2007).
Delta IV Payload Planners Guide.
Littleton, CO.
- [54] Ma, C., Arias, E. F., Eubanks, T., Fey, A. L., Gontier, A. M., Jacobs, C. S., ... & Charlot, P. (1998).
The international celestial reference frame as realized by very long baseline interferometry.
The Astronomical Journal, 116(1), 516.

- [55] Curtis, H. (2013).
Orbital mechanics for engineering students.
Butterworth-Heinemann.
- [56] Seidelmann, P. K., Archinal, B. A., A’hearn, M. F., Conrad, A., Consolmagno, G. J., Hestroffer, D., ... & Williams, I. P. (2007).
Report of the IAU/IAG Working Group on cartographic coordinates and rotational elements: 2006.
Celestial Mechanics and Dynamical Astronomy, 98 (3), 155-180.
- [57] Rim, H. J., & Schutz, B. E. (2002).
Precision orbit determination (POD).
Geoscience Laser Altimeter System (GLAS), Algorithm Theoretical Basis Document, Center for Space Research, The University of Texas at Austin, Austin, Texas, USA.
- [58] Bae, S. & Schutz, B. E. (2002).
Precision attitude determination (PAD).
Geoscience Laser Altimeter System (GLAS), Algorithm Theoretical Basis Document Version, 2., Center for Space Research, The University of Texas at Austin, Austin, Texas, USA.
- [59] Hubbard, W. B., & Marley, M. S. (1989).
Optimized Jupiter, Saturn, and Uranus interior models.
Icarus, 78(1), 102-118.

- [60] Bettadpur, S. V. (2013).
Margins and Contingency Module.
Lecture taught by Dr. Srinivas V. Bettadpur, October 29, 2013; ASE 374K: Space Systems Engineering Design, Cockrell School of Engineering, The University of Texas at Austin.
- [61] Akin, D. L. (Undated).
Mass Estimating Relations.
Lecture taught by Dr. David L. Akin, September 25, 2011; ENAE483 - Principles of Space Systems Design, A. James Clark School of Engineering, University of Maryland-College Park.
- [62] Fountain, G. H., Kusnierkiewicz, D. Y., Hersman, C. B., Herder, T. S., Coughlin, T. B., Gibson, W. C., ... & Williams, S. P. (2009).
The new horizons spacecraft.
In New Horizons (pp. 23-47). Springer New York.
- [63] NASA (2008).
Structural Design and Test Factors of Safety for Spaceflight Hardware.
NASA Technical Standard NASA-STD-5001A.
- [64] Young, W. C., & Budynas, R. G. (2002).
Roark's formulas for stress and strain (Vol. 7).
New York: McGraw-Hill.

- [65] Baker, E. H., Cappelli, A. P., Kovalevsky, L., Rish, F. L., & Verette, R. M. (1968).
Shell analysis manual.
North American Aviation Inc., Downey, CA.
- [66] Toray Carbon Fibers America, Inc. (undated).
Torayca® M55J Data Sheet [*Online Data Sheet*].
Retrieved from: <http://www.toraycfa.com/pdfs/M55JDataSheet.pdf>
- [67] Rothman, L. S., & Gordon, I. (42). Colleagues, (2009).
The HITRAN 2008 molecular spectroscopic database.
J. Quant. Spectrosc. Radiat. Trans, 110 (9-10), 533-572.
- [68] NASA Goddard Space Flight Center, National Space Science Data Center (2013).
Earth Data Sheet [*Online Data Sheet*].
Retrieved From: <http://nssdc.gsfc.nasa.gov/planetary/factsheet/earthfact.html>
- [69] National Oceanic and Atmospheric Administration & U.S. Air Force (1976).
US standard atmosphere, 1976
NOAA-S/T, 76-1562.
- [70] Slobin, S. D., and Pham, T. T. (2010).
Antenna Positioning, DSN Telecommunications Link Design Handbook 810-005,
Section 302, Rev. B.
NASA Jet Propulsion Laboratory, 810-005.

- [71] Stelzried, C. T., Clauss, R. C., & Petty, S. M. (2003).
Deep Space Network Receiving Systems' Operating Noise Temperature Measurements.
The Interplanetary Network Progress Report 42-154, April–June 2003, 1-7.
- [72] Mastal, E. F. (1991).
Radioisotope Power Systems for the Common Lunar Lander Program.
Lecture taught by Edward F. Mastal, July 1-2, 1991. U.S. Department of Energy, Washington, D.C. Lecture conducted during the Common Lunar Lander Workshop, NASA Johnson Space Center.
- [73] Akin, D. L. (Undated).
Thermal Analysis and Design.
Lecture taught by Dr. David L. Akin, October 23, 2011; ENAE483 - Principles of Space Systems Design, A. James Clark School of Engineering, University of Maryland-College Park.
- [74] Rebernak, C., Carter, D., Conde, J., Martinez, L., Hernandez, J. (2012).
Uranus REBEL: Research Explorer Beyond Extreme Latitudes [*Undergraduate Design Technical Report*].
The University of Texas at Austin, Austin, TX.
- [75] Keesee, J. E. (2003).
Spacecraft Thermal Control Systems.
Lecture taught by Col. John E. Keesee, undated; Course 16-851, Satellite Engineering, School of Engineering, Massachusetts Institute of Technology.

- [76] Akin, D. L. (Undated).
Cost Estimation and Engineering Economics.
Lecture taught by Dr. David L. Akin, September 20, 2011; ENAE483 - Principles of Space Systems Design, A. James Clark School of Engineering, University of Maryland-College Park.
- [77] Hastrup, R. C., Cesarone, R. J., Srinivasan, J. M., & Morabito, D. D. (1999).
Mars Comm/Nav MicroSat Network.
In 13th AIAA/USU Conference on Small Satellites. SSC 99-VII-5.
- [78] Bennett, G. L. (2006).
Space Nuclear Power: opening the final frontier.
In 4th International Energy Conversion Engineering Conference and Exhibit (IECEC) (pp. 26-29).
- [79] EADS Astrium - Space Propulsion (2014).
1 N Hydrazine Thruster.
20 N Hydrazine Thruster. [*Online Data Sheets*]
Retrieved from: <http://cs.astrium.eads.net/sp/spacecraft-propulsion/hydrazine-thrusters/1n-thruster.html>
- [80] Heidt, H., Puig-Suari, J., Moore, A., Nakasuka, S., & Twiggs, R. (2000).
CubeSat: A new generation of picosatellite for education and industry low-cost space experimentation.
In 14th AIAA/USU Conference on Small Satellites. SSC 00-V-5.

[81] Hubbard, W. R. et al. (2010).

Ice Giants Decadal Study [*Technical Report*].

Planetary Science Decadal Survey, Mission Concept Study Final Report, National Aeronautics and Space Administration, 2010.

[82] Arridge, C. S., Agnor, C. B., André, N., Baines, K. H., Fletcher, L. N., Gautier, D., ... & Karatekin, Ö. (2012).

Uranus Pathfinder: exploring the origins and evolution of Ice Giant planets.

Experimental Astronomy, 33(2-3), 753-791.

Vita

Jason Yunhe Lu was born in Xi'an, Shaanxi Province, China, on June 30, 1989. He and his Mother and Father moved to the United States in 1998, settling in Philadelphia, Pennsylvania. He would move to Columbus, Ohio in 1999; and then to Ellicott City, Maryland in 2003. He graduated from Mount Hebron High School in 2007. He graduated from the University of Maryland-College Park in 2012 with a B.S. in Aerospace Engineering. He completed the Aerospace Engineering Honors Program under Dr. Norman M. Wereley. He earned his most significant award to date at the 2012 NIA RASCAL-Forum, co-presenting his senior undergraduate design project supervised by Dr. David L. Akin. He studied one semester at the City University of Hong Kong in 2010, as part of the International Engineering Study Abroad Program. He participated in four sessions of the NASA Langley Research Summer Scholars (LARSS) Program, working under Dr. Jirong Yu. He is working to earn his Master's of Science degree from the University of Texas at Austin, under the guidance of Dr. Wallace T. Fowler.

Permanent address: 3329 Sonia Trail

Ellicott City, Maryland 21043

This report was typed by the author.